Title
The structure-function relationships of the dentino-enamel junction

Author
Gallagher, Richard R

Publication Date
2004

Peer reviewed|Thesis/dissertation

The Structure-Function Relationships of the Dentino-Enamel Junction

by

Richard R. Gallagher

DISSERTATION

Submitted in partial satisfaction of the requirements for the degree of

DOCTOR OF PHILOSOPHY

in

Bioengineering

in the

GRADUATE DIVISIONS

of the

UNIVERSITY OF CALIFORNIA SAN FRANCISCO

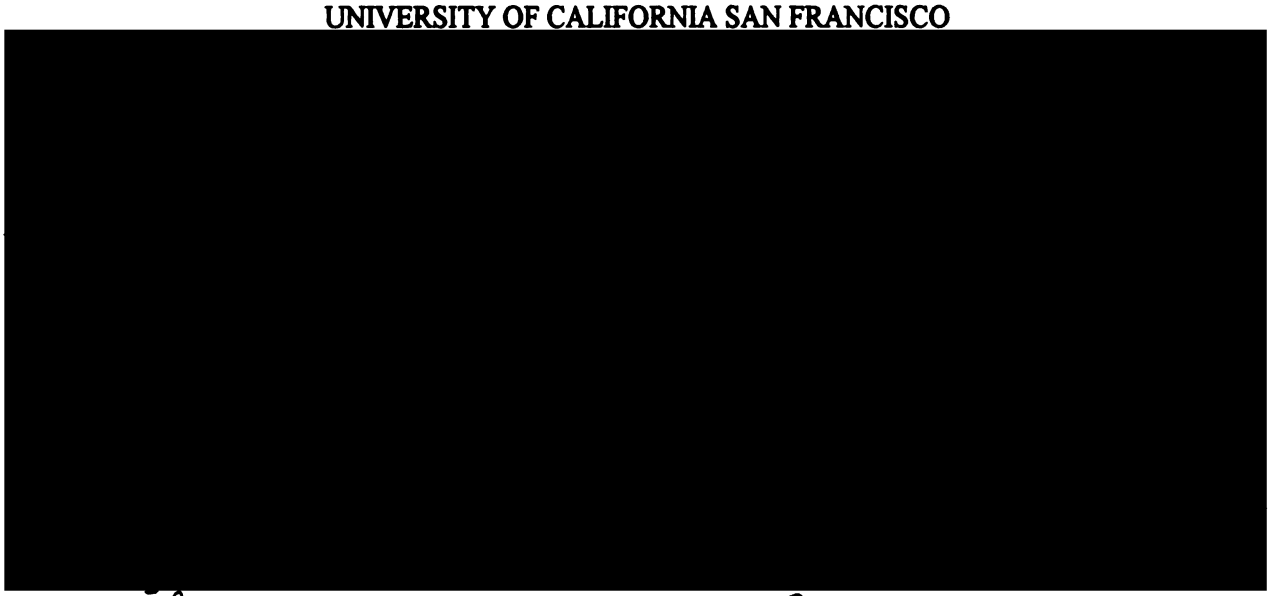

April 2005 .....

Date

.....

University Librarian

Degree Conferred: .....

Dedicated to my wife, daughter and instructors.

ACKNOWLEDGEMENTS

In marked contrast to the tumultuous post-911 world in which this manuscript was written, the time that I have spent performing research to improve our knowledge of the dentino-enamel junction (DEJ) has been one of the greatest challenges and learning experiences in my life. I shall always be deeply indebted and thankful for the support, guidance and devotion of those who have helped me to complete this endeavor. In particular, I would like to thank my advisor, Dr. Grayson W. Marshall and his wife and co-advisor Dr. Sally Marshall for the guidance and support that they have given me. Without their assistance I would have been unable to complete this work.

I am also indebted to Dr. Sheldon Baumrind. It was Dr. Baumrind who inspired my interest in pursuing a career in academic research, and in whose footsteps I would like to someday follow. Dr. Baumrind provided me with a template, the direction and the background to investigate questions of critical interest in the fields of dentistry, engineering and orthodontics. For his leadership, guidance and vision I will always be grateful.

I would like to thank the researchers at Lawrence Livermore National Laboratory with whom I have had the pleasure to work. They include: Michael Staggs and Drs. Mehdi Balooch and Stavros Demos. They challenged my resolve, provided me with insights and direction as to the mechanics of solving complex problems, and became my friends. For their knowledge, direction and assistance I am grateful. It was a very

humbling and rewarding experience to work with people who are among the best in the world at their profession. Thank you.

I would like to thank my teachers and advisors, particularly Drs. Lisa Pruitt, Hari Dharan and Pamela Den Besten. They provided me with an understanding of the research and publication processes, and guided me through the course of my research plan. It was by my interactions with these individuals, and others, that I developed a fuller understanding of what a life in academic research will all be about.

Finally, to my wife, Mari-Anne, and my children Rachael and Brian. Thank you so much for allowing me to take so much time away from you and my housekeeping responsibilities to pursue this quest. It has been a very long time and I hope that I will be able to make it up to you. I have missed a lot of birthday parties, family picnics, vacations and interactions with you. Thank you for affording me with the time and the support to pursue my dream. Thank you for your support, love and friendship. I am eternally indebted.

The text of Chapter 2 of this dissertation, Mechanical Properties of the Dentionenamel Junction: AFM Studies of Nanohardness, Elastic Modulus, and Fracture, is a reprint of the material as it appears in the Journal of Biomedical Materials Research. Additional information was included to better explain the bioinstrumentation techniques employed. The coauthors listed in this publication directed and supervised the research which forms the basis for this chapter.

Chapter 3, Optical Spectroscopy and Imaging of the Dentin-Enamel Junction in Human Third Molars, is contained in this dissertation in order to provide a tenant for understanding of the materials that constitute a tooth, optical spectroscopy theory, and to provide us with our first estimate of DEJ thickness. The text of Chapter 3 of this dissertation is a reprint of the material as it appears in The Journal of Biomedical Research. The coauthors listed in this publication directed and supervised the research plan which forms the basis for this chapter.

The text of Chapter 4 of this dissertation, A Coupled Nano-Mechanical and Micro-Raman Spectroscopic Investigation of Human Third Molar DEJ, represents a research paper that is intended for publication. Additional information was included in Chapter 4 to better explain the rationale and bioinstrumentation techniques that were employed. The coauthors listed in this publication directed and supervised the research plan which formed the basis for this chapter.

The text of Chapter 5, the Dentin-Enamel Junction-A Natural Multilevel Interface, is a reprint of the material as it appears in the Journal of the American Ceramic Society. This chapter is included to provide us with an understanding of the composition, geometry, and dimensionality of the tissues of the DEJ and the near DEJ region. The mechanical properties and behavior of this region is described, as are its fracture properties. The coauthors listed in this publication directed and supervised the research which forms the basis for this chapter.

ABSTRACT

The dentino-enamel junction (DEJ) is a calcified dental tissue interface that connects two dental tissues having widely dissimilar material behaviors, compositions and architectures. This interfacial tissue acts to bind a thin shell of hard and brittle enamel covering the occlusal surface of a tooth, with a thicker layer of tough and soft dentin that makes up the remaining bulk of the tooth. The DEJ binds these materials in such a manner that the resistance of the tooth to catastrophic fracture is ultimately increased. As such, the DEJ is considered to be an interphase, which is defined as a region of distinct or functionally graded properties existing between two or more phases.

To this point, studies employing a variety of imaging and bioinstrumentation assets have been unable to determine the uniqueness of this tissue, or to define its composition, functional width or behaviors. It has been observed that the DEJ is remarkable in that it is able to transfer load from the overlying layer of enamel to dentin in such a manner that cracks or fracture planes that are formed in enamel are rarely propagated across the DEJ into dentin. This makes the DEJ a damage tolerant structure. Using AFM and Raman microspectroscopy we found the DEJ to exist as a zone that exhibits a functional gradation of physical and compositional properties, varying from those exhibited by dentin to those exhibited by enamel. We were unable to define properties, behaviors or compositional characteristics indicating the uniqueness of the DEJ.

A better understanding of the DEJ may allow development of improved dental restorative materials and may have implications to enhance bonding between other materials having widely dissimilar behaviors. This study sought to determine the factors governing the biomechanical performance of this tissue interface by studying its

properties, morphology, composition and width. An understanding of the functional variations in the mechanical and optical properties of the DEJ could afford insight into its composition, and the manner in which the composition affects its physical behavior.

TABLE OF CONTENTS

CHAPTER ONE – INTRODUCTION

1.0 Overview

A tooth is principally composed of two calcified tissues, enamel and dentin. Each of these dental tissues is composed of differing amounts of proteins and minerals. Enamel is a hard, brittle biomaterial that forms a thin shell approximately 1 to 3 mm in thickness and covers the outer coronal portion of a tooth. Enamel exhibits a range of characteristics including wear resistance, acid resistance[1] and crack propagation resistance.[2,3,4] These characteristics act to protect the tooth by preventing rapid surficial abrasion or dissolution, enabling the tooth with the ability to last a lifetime. Dentin is a strong calcified biomaterial that is also ductile and resilient. This dental tissue functions to transfer the occlusal stresses imparted to the overlying enamel during the mastication process to the underlying alveolar bone. Enamel and dentin are both formed by cells, although of differing origin. Enamel is formed by ameloblasts, while dentin is formed by odontoblasts. During tooth formation, the DEJ is the site where tooth formation is initiated.[5] As part of this process, the ameloblasts move radially outward forming enamel while the odontoblasts move inward to form dentin. When tooth formation is complete, the ameloblasts that lines the external surface covering the crown of the tooth fail to exist following mineralization. The odontoblasts, or the dentin forming cells, end up lining the pulp chamber, and continue living. With time they move radially inward and continue to make dentin throughout the life of the tooth.

Sandwiched between dentin and enamel is the dentino-enamel junction (DEJ). The DEJ is a material whose primary functions following tooth formation include joining enamel with dentin, and increasing the resistance of the tooth to catastrophic fracture by

increasing its fracture toughness. Interfaces between dissimilar materials typically act as stress concentrator surfaces that lead to rapid delamination between them.[6] The DEJ is a remarkable tissue interface in that it is able to prevent pathologic tooth fracture despite being subjected to a lifetime of cyclic masticatory, parafunctional and impact loads.[6] It has been observed that cracks that have been initiated within enamel are usually deflected or terminated upon contact with the DEJ.[2] The composition, origin and uniqueness of this tissue have yet to be determined. Its properties and behaviors are ill defined.

The DEJ is a critical interfacial calcified dental tissue that joins hard, wear resistant and brittle enamel with soft, tough and ductile dentin.[3,4,6,7] It constitutes a structurally unique interphase that marries these two highly dissimilar mineralized tissues that have distinctly different properties and behaviors. However, it has been observed that the DEJ is also remarkable in that it is able to transfer loads from overlying enamel to the supporting dentin in such a manner that cracks or fracture planes in enamel are rarely propagated into dentin, making the DEJ a damage tolerant structure.[2,8] The DEJ is proposed to function as a transitional zone that exhibits a gradation of physical properties, varying from those exhibited by dentin to those exhibited by enamel, and that this zone may reflect its inherent protein expression and mineral content.[6] The functional gradation in mechanical properties may act to afford the tooth with increased fracture resistance in spite of the fact that interfaces between two highly dissimilar materials usually act to concentrate stresses and increase the fracture potential of the total structure.

1.1 Motivation and Objectives

This work was first motivated by the observation that cracks formed and propagated through enamel are blunted or deflected upon contacting the DEJ. This makes

the DEJ the principal protection mechanism against catastrophic tooth fracture. The DEJ is also a remarkable tissue in that it serves as the adhesion surface for joining enamel and dentin, materials that exhibit remarkably different biomechanical properties.

Developing a better understanding of the DEJ's adhesion mechanisms may enable us to develop improved dental restorative materials and adhesives for general industrial uses. We would also like to determine the histiologic uniqueness of this dental tissue. Since different cells that initiate their matrix and biominerization processes at the DEJ form dentin and enamel, it is conceivable that there are unique proteins and properties associated with the DEJ. Further, since mantle dentin is formed earlier and differently than bulk circumferential dentin, its lower mineral content may reflect different apatite mineral characteristics than apatite in either dentin or enamel.

Is the DEJ merely a zone representing an intermingling of enamel and dentin? An additional area of interest is the effect that geometry and width of the DEJ have on the distribution of the mechanical properties and observed behaviors. Does the arrangement of the materials, the undulating nature of the interface and the thickness of this structure effect its behavior?

The objectives of this work were to: 1) characterize the topography and morphology of the DEJ, 2) determine the mechanical properties of the DEJ, enamel and dentin in the near DEJ region, 3) characterize the composition of the DEJ, 4) investigate the fracture characteristics of the DEJ region, and 5) relate the morphology, composition and properties to the behaviors observed.

1.2 Tooth Development, Anatomy and Composition of the Dentin-Enamel Junction

Developmentally, dentin and enamel share a common starting point, the DEJ. The DEJ has been modeled as being an evolutionary conserved tissue that plays critical roles as the initiation surface for ameloblastic (enamel forming cells) and odontoblastic (dentin forming cells) activity during tooth formation.[5] In the early stages of tooth development, and prior to the dental calcification processes, a thin membrane that is believed to be the future DEJ separates the inner dental epithelium from the dental papilla. It is from this common interfacial zone that the ameloblasts and odontoblasts begin to move. The ameloblasts travel outward from the DEJ to form enamel, while the odontoblasts move inward and form dentin. As the ameloblasts and odontoblasts move away from the DEJ they form their respective proteinous extracellular matrices. These proteinous templates subsequently calcify, forming enamel and dentin respectively. The calcification of dentin precedes and controls the calcification of enamel and the DEJ. The biomineralization processes are controlled by cellular activities and signaling.[5,6] The size and shape of the mineralizing crystals of enamel and dentin have been found to be very different from one another, although both crystal types are constituted by carbonated, calcium-deficient apatites, related to hydroxyapatite, $Ca_{10}(PO_4)_6(OH)_2$.

The architecture of the DEJ may contribute to its ability to transfer loads and resist brittle fracture. Scalloping and subscalloping of the interface has been reported. Structurally, the DEJ is usually described as consisting of 25- to 100-μm diameter scallops with convexities directed toward dentin and concavities directed toward enamel.[5,9,10,11,12,13,14,15] The scalloped and sub-scalloped architecture of the DEJ is

believed to increase the surface area, surface energy and interfacial bonding.[2] The scallops are further subdivided by microscallops and finer level structures.[16] Little information presently exists regarding the width and variability of these structures.[17]

High resolution scanning electron microscopy (SEM) utilizing immuno-labeled markers was used to identify the presence of collagen within the DEJ region. Immuno-labeling determined that Type I collagen fibrils exist within the scalloped and micro-scalloped border of the DEJ.[17] The collagen fibrils appeared to emanate within the dentin, combined to form 100 nm diameter fibrils that crossed the DEJ and inserted into the enamel mineral. The scallops have been described as being dissected by microscallops and nanolevel finer structures.[17] Lin reported observing collagen fibrils that spanned the DEJ.[17] He found the collagen fibrils appeared to be oriented parallel to each other and perpendicular to the DEJ. The fibrils also appeared to converge towards enamel.[17] Lin reported that the fibrils appeared to insert directly into the mineral phase of enamel and merged at low insertion angles into the fibrillar plexus of dentin. The reported size of the scallops found most recently in the literature appears to be in the range of 25 to 40 μm.

Possibly the earliest reported morphologic characterization of the DEJ was performed by Fraenkel in 1835.[18] The DEJ was subsequently described as having a festooned or scalloped appearance. Recent studies emphasized the undulating scalloped nature of this interface and postulated that the form of the DEJ may act to enhance adhesion between it and enamel and dentin. No general description of the morphology or function of the scalloped nature of the DEJ has been agreed upon. The composition of the DEJ is not presently known.

1.3 Physical Properties and Width of the Dentin-Enamel Junction

Defining the DEJ as being a unique dental tissue, or determining its bulk mechanical properties have been, to this point, impossible to obtain because of the extremely small scale of the structures of this region. Extraction of discrete bulk sections of the DEJ has not been performed. Micro and nanoindentation results indicate that a gradient in materials properties exists across this interface. The results follow a monotonic relationship, ranging from those approximating enamel to those of dentin. No consensus on the width of the DEJ presently exists.[2,4,6,19] Wide variations in DEJ width estimates have been reported in the literature. The variation in DEJ width estimates may be a function of instrumentation modality and sampling volume. Maps relating material properties and composition indicate that a correlation between them exists, however they may not completely correspond with one another.[20]

No unique hardness or modulus has been determined for the DEJ. The observed gradation in mechanical properties across this interface is believed to contribute to interfacial bonding as well as being an important toughening mechanism.[20] Maps of hardness and modulus have been used to describe the mechanical characteristics of the DEJ region. Lines of Vickers microhardness indentation points placed across the DEJ suggested the existence of a gradation in mechanical properties across this zone.[6] No sharp demarcation in the mechanical properties was found to exist at the optically perceived margins of the DEJ. The micro-level biomechanical zone was estimated to have a width of between 27 and 100 μm in humans.[6] Lin[19] and Lin and Douglas[2] characterized the architecture and mechanical properties of bovine DEJ with scanning electron microscopy, microindentation and conventional fracture mechanics and found

that the mechanical properties of the DEJ region exhibited a graded functional width of between 50 to 100 μm in bovine teeth. They also reported that the functional width appeared to be greater than its optical presentation. Wang and Weiner reported a functional transition zone width on the order of 200 μm using a Moire fringe technique on human teeth.[21]

Optical microscopy has been used to describe the architecture of this interfacial region, and to describe enamel, dentin and DEJ. Light microscopy has described the DEJ as being an abrupt demarcation between dentin and enamel. Micro-radiodensity profiles[22] and scanning electron microscopy[10,16] suggest that the margins of the DEJ are sharply demarcated and that the interfacial width is extremely narrow. Nanoscratch testing indicated DEJ width perhaps on the order of 2 μm. Transmission electron microscopy found that the apatite crystals of dentin, and those of enamel might lie virtually in direct approximation with one another at the DEJ.[2] This fact that may indicate that the DEJ exists as only a functional zone in mature teeth.

The development of AFM based nanoindentation affords a method for determining the mechanical properties of discrete structures while simultaneously mapping surface topography and indentation position.[23,24] This technological advance removed the effects of tubule size and tubule density from earlier microindentation results because the reduction in sample volume associated with the nanoindenter enabled testing entirely within enamel, DEJ and intertubular dentin. Early microindenters used a much larger tip, causing the results to be a mixture of peritubular and intertubular dentin. DEJ width estimates based on nanoindentation testing as small as 11.8 μm were found

during this research project. A sampling volume dependency was also noted for the nanoindentation width estimates.

To date, the mechanical properties of the DEJ have been explored in a largely limited fashion. No unique material properties for the DEJ have been found. Gradations in mechanical properties across this interface exist and are sampling volume dependent. Estimates of the width of the DEJ vary by several orders of magnitude. Studies have indicated that a very narrow interfacial zone, if any, may exist between mantle dentin and enamel. Observations of a broad transitional zone in physical properties stand in contrast to data acquired by high-resolution imaging.

1.4 The Dentin-Enamel Junction as a Fracture Resistant Material

The fracture characteristics of the DEJ have been largely unexplored. Early observations implied that the DEJ might serve a critical role in preserving the physical integrity of a tooth against catastrophic tooth fracture. Cyclic mechanical loads imparted to a tooth during mastication may initiate cracks in enamel and propagate them to the DEJ. Enamel cracks have been observed to terminate or deflect upon entering the DEJ. Collagen fibrils spanning the DEJ may act to blunt the crack tip and improve its fracture toughness. The stress transmission and fracture toughness properties of the DEJ suggest that its behavior may be the result of protein expression and biomineralization.[6] Improving our knowledge of the factors governing the behavior of the DEJ may allow us to develop improved dental restorative materials. This information could also be used to model mechanisms for linking other materials having widely dissimilar properties.

Early work by Rasmussen *et al.*,[25] using a work-of-fracture (W_f) approach determined anisotropic work-of-fracture (W_f).values for enamel and dentin. Using a

similar approach, Rasmussen tested the DEJ region and determined a W_f value of 336 J/m^2 for it. Questions arise as to whether Rasmussen tested the DEJ itself, or whether he tested another tissue, or tissues, in the area. He also tested dentin and reported (W_f) values of 221 and 391 J/m^2 for fracture perpendicular and parallel to the dentinal tubules, respectively.[26] Pioch and Staehle[27] studied the shear strength of bovine and human teeth in the near DEJ region and found that fracturing did not occur right at the DEJ. They proposed this was an indication of the inherent fracture toughness of the DEJ. They also speculated that the extremely small size of the DEJ made it very difficult to produce valid and accurate materials testing results.

Lin *et al.*,[17] found the DEJ to be a micro-structurally distinct and fracture resistant region within a tooth. Lin and Douglas[2] and Lin[19] used microindentation testing and a conventional fracture mechanics approach to investigate the architecture and fracture toughness of the DEJ. They found that cracks initiated within enamel blunted or deflected upon entering the DEJ, preventing catastrophic tooth fracture. They concluded that the DEJ appeared to have a graded functional width of between 50 to 100 μm, and that this width was greater than its optical presentation. Xu *et al.*[28] used microindentation and characterized the mechanical properties and fracture toughness in the near DEJ region. They reported hardness, modulus and toughness values for enamel that appeared to be dependent upon sample orientation. Xu *et al.*[28] also reported hardness and modulus values for dentin, and reported that they were unable to induce fractures within dentin. White *et al.*[6] reported a functionally graded microhardness width for the DEJ of approximately 100 μm, a width that was much greater than its optical presentation.

Recent technological advances in nanomechanical instrumentation have lead to the development of testing equipment that use a dramatically smaller indenter stylus than conventional microhardness testers. Such equipment enables materials characterization with smaller applied loads and finer spatial resolution. In addition, nanoindenters are capable of recording the load-displacement behavior, enabling calculation of Young's modulus according to relationships derived by Doerner and Nix.[29] Coupling the nanoindenter with an atomic force microscope (AFM) allowed pre- and post-indentation sample imaging to determine indentation validity and location. Relationships have been derived to calculate fracture toughness using nanoindentation based on radial crack generation.[30,31,32] These developments afford first-order mechanisms for analyzing the fracture characteristic of the DEJ.

1.5 Outline of the Thesis

This thesis is organized into a series of Chapters. Each Chapter is arranged to address a subject of research significance intended to improve our knowledge and understanding of the DEJ. As described in the Abstract, the Chapters represent rewritten and expanded versions of previously published or submitted papers. These papers have been supplemented by additional unpublished research that is intended to provide additional supporting information. The Chapters also provide additional supportive information and analyses.

1.6 References

1 Tramini P, Pelissier B, Valcarcel J, Bonnet B, Maury L. A Raman spectroscopic investigation of dentin and enamel structures modified by lactic acid. Cares Res 2000;34:233-240.

2 Lin CP, Douglas WH. Structure-property relations and crack resistance at the bovine dentin-enamel junction. J Dent Res 1994;73:1072-1078.

3 Fong H, Sarikaya M, White SN, Snead ML. Nano-mechanical properties profiles across dentin-enamel junction of human incisor teeth. Mater Sci Eng 2000;C7:72-79.

4 Marshall GW, Balooch M, Gallagher RR, Gansky SA, Marshall SJ. Mechanical properties of the dentinoenamel junction: AFM studies of nanohardness, elastic modulus and fracture. J Biomed Mater Res 2001;54:87-95.

5 Ten Cate AR Oral Histology: Development, Structure and Function, 4th ed. Mosby, St. Louis 1994.

6 White SN, Paine ML, Luo W, Sarikaya M, Fong H, Yu A, Li ZC, Snead ML. The dentino-enamel junction is a broad transitional zone uniting dissimilar bioceramic composites. J Am Ceram Soc 2000; 83:238-240.

7 UrabeI, Nakajima M, Sano H, Tagami J. Physical properties of the dentin-enamel junction region. Am J Dent 2000;13:129-135.

8 Elliott JC, Anderson P, Gao XJ, Wong FSL, Davis GR, Dowker SEP. Application of scanning microradiography and x-ray microradiography and x-ray microtomography to studies of bones and teeth. X-Ray Sci Technol 1994;4:102-117.

9 Arsenault AL, Robinson BW. The dentino-enamel junction: A structural and microanalytical study of early mineralization. Calcif Tissue Int 1989;45:111-121.

10 Hayashi Y. High resolution electron microscopy in the dentino-enamel junction. J Electron Microsc 1992;41:387-391.

11 Lustman J. Dentinoenamel junction area in primary teeth affected by Morquio's syndrome. J Dent Res 1978;57:475-479.

12 Rywkind AW. So-called scalloped appearance of the dentino-enamel junction. J Am Dent Assoc 1931;18:1103-1110.

13 Scott JH, Symons NBBB. Introduction to Dental Anatomy, 6th ed. Livingstone, Edinburgh 1971.

14 Sela J, Sela M, Lustman J, Ulmansky M. Dentinoenamel junction area of a resorbing permanent incisor studied by means of scanning electron microscopy. J Dent Res 1975;54:110-113.

15 Whittaker DK The enamel-dentine junction of human and Macaca Irus teeth: A light and electron microscope study. *J Anat* 1978;125:323-335.

16 Bodecker CFW. The distribution of living matter in human dentin, cementum and enamel. Dent Cosmos 1957;20:582-590.

17 Lin CP, Douglas WH, Erlandsen SL. Scanning electron microscopy of Type I collagen at the dentin-enamel junction of human teeth. J Histochem Cytochem 1993; 41:381-388.

18 Fraenkel L. De penitiori dentium humanorum structura observationis. Diss Vratislaviae, Pressburg. 1835.

19 Lin CP. Structure-function property relationships in the dentin-enamel complex and tooth restoration interface. [PhD thesis], University of Minnesota 1993.

20 Gallagher RR, Balooch M, Balooch G, Wilson RS, , Marshall SJ, Marshall GW. A Coupled Nano-Mechanical and Micro Raman Spectroscopic Investigation of Human Third Molar DEJ Calcif Tiss Int

21 Wang RZ, Weiner S. Strain-structure relations in human teeth using Moire fringes. *J Biomech* 1998;31(2):135-141.

22 Elliot JC, Anderson P, Gao XJ, Wong FSL, Davis GR, Dowker SEP. Application of scanning microradiography and X-ray microtomography to studies of teeth and bone. J X-Ray Sci Technol 1994;4:102-117.

23 Van Meerbeck B, Willems G, Celis JP, Roos JR, Brahem M, Lambrechts P, Vanherle G. Assessment by nano-indentation of the hardness and elasticity of the resin-dentin bonding area. *J Dent Res* 1993;72:1434-1442.

24 Willems G, Celis JP, Lambrechts P, Braem M, Vanherle G. Hardness and Young's m odulus d etermined by nanoindentation technique of filler particles of dental restorative materials compared with human enamel *J B iomed M ater R es* 1 993;27:747-755.

25 Rasmussen ST, Patchin RE, Scott DB, Heuer AH. Fracture properties of human enamel and dentin. J Dent Res 1976;55:154-164.

26 Rasmussen ST. Fracture properties of human teeth in proximity to the dentinoenamel junction. J Dent Res 1984;63:1279-1283.

27 Pioch T, Staehle HJ. Experimentational investigation of the shear strengths of teeth in the region of the dentinoenamel junction. Quintessence Int 1996; 27:711-714.

28 Xu HHK, Smith DT, Jahanmir S, Romberg E, Kelly JR, Thompson VP, Rekow ED. Indentation damage and mechanical properties of human enamel and dentin. J Dent Res 1998;77:472-480.

29 Doerner MF, Nix WD. A method for interpreting the data from depth-sensing indentation instruments. J Mater Res 1986;1:601-609.

30 Lawn BR, Wilshaw TR. Indentation fracture: Principles and applications. J Mater Sci 1975;10:1049-1081.

31 Lawn BR, Marshall D, Bradt RC, Hasselman DPH, Lange FF, editors. Fracture mechanics of ceramics. Vol. 3. New York: Plenum; 1978. p. 205-229.

32 Lawn BR, Evans AG, Marshall DB. Elastic/plastic indentation damage in ceramics: The median/radial crack system. J Am Ceram Soc 1980;63:574-581.

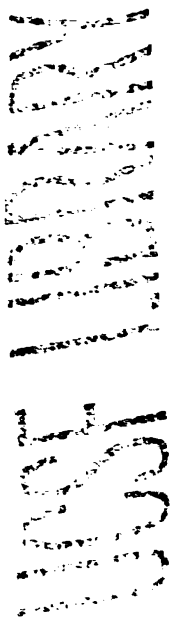

Chapter 2

The following Chapter is based on a previously published research paper. The work has been expanded to include additional data, illustrations, and information intended to improve understanding of the body of research. The citation for the published research document is:

Marshall GW, Balooch M, Gallagher RR, Gansky SA, Marshall SJ. Mechanical properties of the dentinoenamel junction: AFM studies of nanohardness, elastic modulus and fracture. J Biomed Res 2000;54.1:87-95.

CHAPTER TWO - Mechanical Properties of the Dentinoenamel Junction: AFM Studies of Nanohardness, Elastic Modulus and Fracture

2.1 Summary

The dentin-enamel junction (DEJ) is a thin complex calcified dental tissue uniting an overlying layer of brittle enamel covering the outer surface of the tooth to dentin that makes up the remaining bulk of the tooth. The DEJ is a critical interface that joins these tissues and confers fracture toughness and crack deflection properties. AFM based nano-mechanical instrumentation was used to characterize the morphology, width and the nano-mechanical properties of the DEJ region. Nanomechanical testing determined the reduced elastic modulus and hardness of enamel, dentin and DEJ along three lines of indentation points. The lines of indentation points sampled at 1-2 μm intervals across the DEJ on dry, polished sagittal samples that were extracted from three human non-carious third molars. Nanohardness and elastic modulus rose linearly across the interface from dentin to enamel. DEJ width was estimated by local polynomial regression fits for each sample and location using the nanomechanical data, and gave a mean width estimate for the DEJ of 11.8 μm. The width estimate did not display significant intra-tooth or inter-tooth variation. Nanoindentation was also used to initiate cracks in enamel. The fracture toughness of enamel was estimated at 06.-0.9 $MPa \bullet m^{1/2}$. This was in good agreement with microindentation fracture results. Crack formation was difficult to initiate in dentin or DEJ. Cracks initiated in enamel terminated or deflected in the DEJ. The results suggest that the tissues of the DEJ region display gradients in structure and properties, and that nanoinstrumentation methods show promise for allowing us to understand its structure and function.

2.2 Introduction

The DEJ is a thin, complex undulating interfacial structure uniting hard and brittle enamel with tougher and softer dentin. The DEJ plays a critical role as the initiation surface for ameloblastic and odontoblastic activity during tooth formation,[1] and enhances the biomechanical integrity of a tooth[2] by increasing its resistance to catastrophic fracture. Structurally, the DEJ is generally described as being scalloped, with convexities directed towards dentin and concavities directed towards enamel.[3] The undulating nature of this interface is thought to contribute to bonding between dentin and enamel. Little information exists on the size and variability of the structures comprising the DEJ. Intra-tooth, inter-tooth and inter-species variation may be considerable.[4-6] Lin *et al.*[7] found that the scallops are subdivided by sub-scallops and type I collagen fibrils. The collagen fibrils appeared to emanate from dentin. They coalesced to form thick fibrils that crossed the DEJ and inserted into the enamel. Micrographs have been published showing the possible existence of finer level structures. Thus, the DEJ appears to form a three-level architecture: scallops of varying size that may vary with location, micro-scallops contained within each scallop and finer nano-level structures within each micro-scallop.

As Lin *et al.*[7] observed, the DEJ may be a distinct and tougher portion of the tooth that acts to bind dentin to enamel. The DEJ is believed to be critical in preventing enamel cracks from propagating into dentin and from causing catastrophic tooth fracture. Recently, Pioch and Staechle[8] examined the shear strength of human and bovine teeth in the DEJ region and reported that fractures did not occur at the DEJ. This observation is a possible indication of the DEJ's toughness and the difficulty associated with accurately

measuring its mechanical properties. This observation and the small size of the DEJ suggested the need to develop additional methods to instrument the interface.

One approach was to use fracture mechanics rather than simple tests of tensile or shear strength. Rasmussen[9] and Rasmussen *et al.*[10] used work-of-fracture (W_f) approaches to determine the fracture characteristics of dentin and enamel. They determined W_f values for dentin, enamel and DEJ. They reported W_f values of 336 J/m^2 for the DEJ region compared to anisotropic values of 221 to 391 J/m^2 for fracture perpendicular or parallel to the dentinal tubules, respectively.[10] It should be noted that uncertainty exists regarding the tissue, or tissues, instrumented by Rasmussen for their W_f for the DEJ region. They concluded that W_f increases at the DEJ and that minimal fracture occurred there.

Lin[11] and Lin and Douglas[2] conducted extensive fracture and morphologic studies of the DEJ and concluded that the DEJ had a functional width, based on its fracture characteristics, of between 50 and 100 μm. They noted that the functional width was greater than its optical presentation, and that the zone probably underwent plastic deformation during failure. Based on these observations they concluded that the DEJ likely served as a crack deflector to prevent catastrophic tooth fracture. Lin[11] and Lin and Douglas[2] also reported significantly higher values for fracture toughness, K_{IC}, and fracture energy, G_{IC}, for bovine DEJ than for bovine dentin or enamel (see Table 2.1 for literature values of the mechanical properties[2,10,12,13,14,15,16,17,18,19,20,21,22,23,24,25]). Their work supported the contention that the DEJ region has unique characteristics.

Xu *et al.*[12] evaluated the hardness, modulus and fracture toughness of dentin and enamel in the DEJ region using microindentation testing. They reported values for

enamel hardness that ranged from 3.0-3.6 GPa and 0.57 GPa for dentin. The modulus for enamel ranged from 80-94 GPa and was 20 GPa for dentin. They were unable to induce cracks or fractures in dentin, but found fracture toughness for enamel ranged from 0.5-1.3 MPa • $m^{1/2}$, dependent upon sample orientation and the tooth tested. White *et al.*[26] found a microhardness variation existed across the DEJ region in which the mechanical properties increased from dentin to enamel. They estimated a functional DEJ width of 100 μm that appeared to be wider than its optical presentation.

Advances in technology have led to the development of indentation instruments capable of determining modulus and hardness at the nano-level.[14,15] The principle advantage to nanoindentation is that the indenter tip, and the corresponding sampling volume, is significantly smaller than that used in conventional microhardness testing. This allows us to test smaller sampling areas, to shallower sampling depths, allowing us to remove the confounding effects of sampling multiple small structures. Nanoindenters are also capable of determining Young's modulus[27] by using the initial elastic unloading portion of the load-displacement curve to calculate the reduced elastic modulus. In addition to static behavior, the dynamic response of a material can be determined.[28] Conventional nanoindenters are incapable of precisely positioning the indenter tip over a feature of interest since positioning the indenter tip requires the use of an optical microscope. To overcome this limitation, an atomic force microscope (AFM) was modified by coupling it with a nanoindenter to perform site-specific indentations along with pre- and post-indentation topographic surficial mapping. This allowed site-specific hardness values for hydrated intertubular dentin (0.5 ± 0.1 GPa) and peritubular dentin (2.3 ± 0.23 GPa) to be measured.[15,16] The hardness of hydrated enamel was similarly

measured at 3.1 GPa. Recent modifications allow sequential AFM imaging and the production of load-displacement curves at selected sites with loads as low as 1 μN while detecting displacements of up to 35 μm. This method has been used to image and determine the mechanical properties of fully demineralized dentin,[28] as well as across the resin-dentin hybrid zone in dentin bonding.[29]

The DEJ is a region having an extremely small size and a highly variable geometry. These features make study of this region using conventional mechanical testing techniques an extremely difficult, if not impossible, process. The extreme scale and complexity of this region could result in the generation of imprecise and non-uniform stress distributions. The development of nanoindenters coupled to atomic force microscopes allows near simultaneous sample imaging and testing, allowing us to observe the area sampled and determine the validity of the sampling point. This development enabled us to perform hardness and modulus mapping of human third molars using a modified AFM system and to investigate the fracture characteristics of this region.

2.3 Materials and Methods

2.3.1 Sample preparation

Three recently extracted non-carious human third molars were removed from research subjects requiring third molar extractions as part of their normal dental treatment. All subjects who were enrolled in this research responded to an informed consent protocol previously approved by the University of California at San Francisco's Institutional Committee on Human Research. Immediately following extraction, each tooth was stored in purified water at 4°C and later gamma radiation sterilized according

to a standard protocol.[30] Each tooth that was included in this research program was sagittally sectioned parallel to its buccal-lingual surface with a water-cooled diamond saw and hand-polished through a graded series of abrasive papers to a final polishing with 0.05 μm alumina paste. Each sample was subjected to ultrasonic vibrations between successive polishings to clean the sample and eliminate the possibility of cross contamination and scratching between polishings. Following sample final polishing, each sample was affixed to a magnetic backing plate with cyanoacrylate cement. Samples were then air dried by blasts with clean, dry compressed air until all surface moisture was removed. The sample was then placed on the testing platen of the AFM for testing.

2.3.2 Nano-indentation testing

An AFM-Triboscope system was used to perform imaging and nano-mechanical testing. The AFM-Triboscope system consisted of a Nanoscope III (Veeco Probes, Santa Barbara, CA) that had been modified by having its standard head replaced with a Triboscope capacitive sensor indenter system (Hysitron Inc., Minneapolis, MN).[28] The coupled AFM-Triboscope system is a force generating and depth-sensing instrument, that is also capable of performing pre- and post-testing imaging. The instrument is capable of producing load-displacement curves at precisely selected locations in either dry or liquid environments. The coupled AFM-Triboscope consists of a three-plate capacitive force/displacement transducer in which a sharp cube corner diamond tip is attached via a central drive post to the moveable middle plate. The outer two fixed electrode plates (drive plates) are driven by alternating current (AC) signals that are 180 degrees out of phase relative to one another. The central, or pick up electrode is suspended between the outer drive plates by a series of springs. The narrow space between the drive plates

allows changes in the electric field to vary linearly across this space from one electrode to the other. Accordingly, the electric field potential is a maximum at the drive plates and zero at the middle between the two drive plates. The central pick up electrode assumes the potential of the space between the two drive plates. The bipolar output signal is an indication of the pick up electrode's position. During sample imaging this signal is used to provide feedback that is used to maintain a constant contact imaging force. During nanomechanical indentation testing, the contact current is cut off and a voltage ramp is applied to the lower drive plate. This applied voltage ramp produces an electrostatic force between the central pick up electrode and the outer drive plates that is proportional to the applied voltage. The driving force is used to push the indenter tip into the sample's surface. The applied indenter force is:

$$F = k_e V^2 ,$$

where: k_e is the electrostatic force constant and V is the applied voltage. The applied indenter voltage can be varied and controlled to produce triangular, trapezoidal or square sample loading profiles. Sample indentations can be placed into either dry samples (air dried) or fluids (liquids). For dry samples, force is applied to the sample via a diamond tip that is glued to a tapped polymer holder. The tapped polymer holder is attached to the central pick up electrode by a small screw. For wet samples, the diamond tip is glued to a tungsten rod having a large aspect ratio. The long tungsten rod is fixed to the tapped polymer holder and screwed into the central drive plate. For wet sampling the diamond tip, and a portion of the tungsten rod are immersed in the liquid, producing a meniscus force that remains relatively constant even as the liquid height changes with vaporization. The dry and wet sample probe forces are taken into account during calibration procedures

that were performed prior to sample testing. It should be noted that during wet sampling, if the liquid volume surrounding the sample is freely exposed to the atmosphere, evaporation and air conditioning could produce local convective air currents that may affect indenter force readings.

During imaging, the minimum contact force that can be applied to the surface of the sample is approximately 1 μN. Loads up to 30,000 μN can be applied during nanoindentation testing. In this experiment, a diamond cube corner indenter tip having a curvature radius of approximately 20 nm was used for sample imaging and testing. The same cube corner tip was also used to determine the fracture toughness of enamel, dentin and the DEJ.

Prior to nanomechanical testing, the sample's surface was viewed using an optical microscope to define general areas of interest. Once an area of interest had been identified, the sample was positioned and oriented to facilitate imaging with the coupled AFM-Triboscope system. The indenter tip was then lowered into contact with the surface of the sample. An iterative process of sample imaging, repositioning and reorienting occurred until areas of specific interest for nanomechanical testing were identified. Areas that were clearly enamel and dentin were identified and subjected to nanoindentation testing. The results were used to define characteristic modulus and hardness values for these tissues.

Following enamel and dentin characterization, the sample was re-imaged to define the apparent limits of the DEJ. Finite adjustments in sample orientation and position were made to allow lines of nanoindentation points to be placed perpendicularly across the optically apparent DEJ. The center of each indenter line was oriented to

coincide with the middle of the apparent DEJ. Hardness (H) and reduced elastic modulus (E_r) were measured at 1 to 2 μm intervals along lines oriented to intersect the DEJ at a 90-degree angle. Sampling lines were at least 50 μm in length to ensure that baseline hardness (H) and reduced elastic modulus (E_r) levels in dentin and enamel were achieved. Hardness and modulus were calculated as:[27,31]

$$H = F_{max}/\mathbf{a},$$

$$E_r = [(\pi/\mathbf{a})]^{1/2} \bullet S/2$$

According to these equations, F_{max} is the maximum applied indenter force, and **a** is the projected contact area of the indenter tip. E_r is defined as the reduced elastic modulus. E_r is calculated using the contact stiffness, S, which is defined as the slope of the initial linear-elastic unloading portion of the force-displacement curve in the vicinity of F_{max}.[27,31] Three areas of the tooth were tested: (1) along a central line under the central pit extending from the occlusal surface toward the pulp chamber, (2) from the cusp tip toward the pulp horn, and (3) along a central line in a mesial-distal direction at a proximal contact.

2.3.3 Fracture toughness

The small-scale fracture patterns of ceramic materials can be related to their inherent mechanical properties. Sharp indenter tips can produce elastic/plastic stress fields producing localized material fracture. The fracture pattern produced by an indenter tip can be related to the sample's material properties including fracture toughness, K_c, hardness, H, and modulus, E.[32,33,34]

Indentation crack patterns were classified by Lawn *et al.*[34] into two primary systems: cracks forming symmetric median planes that contain the axially applied axial

load and cracks forming laterally on planes parallel to the sample's surface. In this study, crack forming symmetric medial planes were considered as analytical methods for analyzing these cracks that have been developed.

Palmqvist[35] demonstrated empirically that fracture toughness was related to radial crack development. Lawn and Wilshaw[32] used a fracture mechanics approach based on elastic theory to develop relationships governing radial crack propagation. Lawn *et al.*[34] developed fracture mechanics relationships that included elastic and plastic fields governing radial crack development. Figure 2.1 demonstrates the basic components involved in the formulation of the fracture toughness estimate. These relationships were based on the inherent material properties K_c, H and E. According to these relationships, a median sub-surface crack is formed in a material when a critical load, P, is applied. Upon unloading, radial cracks form in response to residual tensile stresses at the indenter tip. The stress intensity factor can be calculated as:

$$K_R = (\chi P_{ind})/c^{3/2}$$

where: χ is the material constant that is dependent upon the elastic modulus, E, and hardness, H, according to :

$$\chi = \alpha(E/H)^{1/2}$$

where α is the material independent constant that is dependent upon the indenter tip geometry. This is an empirically derived parameter that is determined from the slope of $K_c (H/E)^{1/2}C^{3/2}$ versus load for a known material. Values of 0.016[36] and 0.0535[37] have been reported for Vickers and cube corner indenter tips, respectively. Table 2.2 lists typical values reported in the literature for engineering materials using this method.[36,37,38]

In these experiments, a cube corner indenter tip was used for fracture characterization testing. The cube corner tip displaces a greater volume than either a Berkovich or a Vickers tip under the same applied load. Such a tip produces greater and more extensive crack formation, at a lower crack initiation threshold. Fracture testing in these experiments was performed in air under dry conditions. Hardness and modulus measurements were made across the DEJ prior to fracture testing. Modulus and hardness were found to be 10-20% greater in enamel and dentin for teeth tested under dry conditions as opposed to hydrated conditions. Since the mechanical properties of teeth exhibit a dependence on immersion time,[39] it was considered best to conduct the fracture studies under air-dry conditions.

2.3.4 Statistical analyses

Estimates of the nanomechanical functional width were made using local polynomial regression (loess) with 95% confidence limits[40] for each sample and location. Loess is a nonparametric, minimal assumption smoother (proc loess, SAS Institute, Cary, NC). Linear local curve fitting and a smoothing parameter of 0.175 were used. DEJ width was determined from the intersection of the transition data confidence bounds with the values for dentin and enamel; the functional DEJ width was estimated as being the mean from the hardness and modulus derived width estimates. Bootstrap resampling[41] with 10000 resamples (S-PLUS, MathSoft, Seattle, WA) was used to estimate mean width and the lower and upper 2.5% empirical percentiles for the independent samples. An exact Friedman's test was used to compare DEJ widths among locations within samples (StatXact, Cytel, Inc, Cambridge, MA). Exact 2-factor repeated measures (mixed) modes[42] were used to assess differences among locations within samples for 13 serial

measurements 2 μm apart near the DEJ. The location x distance interaction was also assessed (Xpro, X-Techniques, Inc, Millington, NJ).

2.4 Results

2.4.1 Hardness and modulus

Figure 2.2 shows a line nanoindentation points placed to cross the DEJ at a perpendicular angle. The middle of the line of indentations was placed at the optically apparent middle of the DEJ. An additional line of indentation points, made at a glancing angle to the DEJ, is shown in Figure 2.2. This second line of indenter points was placed to evaluate the effect of interception angle on DEJ width estimation. No difference in DEJ width estimation was noted. Typical curves illustrating the hardness and modulus distribution across the DEJ are shown in Figures 2.3a and 2.3b. These curves represent the hardness and modulus levels graphed at their respective locations along the lines of nanoindentation points. Baseline levels of hardness and modulus for bulk enamel and bulk dentin were achieved beyond 10 μm of the DEJ. Once baseline levels were achieved only minor perturbations in their values were observed. Characteristic hardness and modulus values for bulk enamel were found to be 3.5 GPa and 65 GPa, respectively. Likewise, hardness and modulus levels characteristic of bulk intertubular dentin were found to be 0.7 GPa and 20 GPa, respectively.

The lines of nanoindentation points that were placed across the DEJ were used to define the distribution in the mechanical properties across this interface. Hardness and modulus were observed to increase monotonically from those of bulk dentin to those of bulk enamel. Figures 2.3a and2.3b shows the typical hardness and modulus distribution

across the DEJ. No characteristic or unique hardness or modulus values were determined for the DEJ.

To estimate the functional DEJ width, based on the nanoindenter data, a previously described local polynomial regression (loess) statistical method was used.[40] A mean functional DEJ width of 11.8 μm was estimated according to the loess model with 2.5% and 97.5% bootstrap percentiles: 10.3-12.7 μm. The variation in hardness and modulus for the areas of the tooth that were tested are contained in Table 2.3. No significant differences among the locations were found using the exact Friedman's test (p = 0.944). No significant differences among locations (p = 0.324) or in the distance pattern among locations (i.e., location x distance; p = 0.995) were detected with the exact mixed models.

2.4.2 Fracture toughness

No cracks were generated in dentin using the AFM-based nanoindenter, even under the maximal load of the instrument (30,000 μN). Considerable load pile up and debris was generated under these loads. It was possible that such debris could have prevented the visualization of any cracks that were generated, and any contorted or tortuous cracks that were generated could not be used to calculate fracture toughness. We were consistently able to generate cracks in enamel, even in the near vicinity of the DEJ, using the nanoindenter. The maximum indenter load required to induce enamel cracks was in the range of 6,000 to 8,000 μN for testing parallel to the long axis of the enamel rod (parallel to the occlusal surface of the tooth). Figure 2.4 shows such a condition. In this figure, a nanoindentation was made into enamel in the near DEJ region and produced radial cracks. Subsequent AFM mapping produced Figure 2.4 and was used to determine

the length of the cracks. Crack length was used to calculate fracture toughness. Estimates of fracture toughness parallel to the long axis of the enamel rod were made using averaged enamel hardness and modulus values. Axial enamel fracture toughness ranged from 0.6 to 0.9 $MPa \bullet m^{1/2}$. Figure 2.4 shows a typical post-indentation image scan of cracks induced into enamel in the near DEJ region. It should be noted that some indentations produced torturous crack paths and localized delamination along the DEJ. Figure 2.5 illustrates such a condition. In this figure, an irregular crack was generated in enamel close to the DEJ. The crack approached the DEJ but deflected and propagated in enamel. None of the cracks that were initiated in enamel were observed to cross the DEJ. Attempts to initiate cracks in DEJ were unsuccessful, even up to the maximum load of the instrument (30,000 μN).

2.5 Discussion

This research represents one of the earliest attempts to characterize the mechanical properties (hardness and modulus) of the DEJ region using a nanoindenter. The ability to determine material properties characteristic of the DEJ required development of an instrument such as the coupled AFM-Triboscope system. This instrument's ability to perform mechanical testing at an incredibly small scale provided sampling volumes small enough to fit entirely within the DEJ. This allowed direct sampling and testing of the tissue of interest.

For indentation testing, sampling volume is a function of indentation load, sample surface smoothness and tip sharpness (tip curvature radius). In our case, indentation depth averaged 0.3 μm. The coupled AFM-Triboscope system was used to allow site-specific mechanical property measurements to be made. This system had the additional advantage

of performing sample imaging based on the sample's surficial topography. Pre-indentation imaging enabled features of interest to be selected prior to testing. Post-indentation imaging provided the ability to observe the structure or tissue that had been tested. It also proved helpful in checking the validity of the results by viewing the form of the indentation that was made and the amount or degree of debris pile up generated.

The mechanical property results for enamel and dentin agree well and are within the range of values reported in the literature. This is shown in Table 2.1. It should be noted that a wide range of values has been reported. The results on dentin agree well with values suggested by Kinney *et al.*[43,44] They reported average modulus and hardness values for dry dentin of 23.9 GPa and 0.83 GPa, and wet values of 20.2 GPa and 0.85 GPa, respectively. The results are also in agreement with results on dentin reported by Xu *et al.*,[12] as well as microhardness results reported by White *et al.*[26] The results for enamel were in line with, but somewhat lower than, reported values for sagittally sectioned bulk enamel.

A smooth and relatively linear gradient in mechanical properties was observed across the DEJ. This transition appeared to follow an increasing monotonic relationship from dentin to enamel. No single or unique modulus or hardness value was noted. No substructures were detected. The DEJ appeared to be a linearly graded interface serving to unite two dissimilar calcified dental tissues. This implies that linear gradients in mineral and protein contents may exist across this region, since mineral contents have been related to mechanical properties in calcified tissues.[45]

Estimates of DEJ width reported in the literature have been variable, and appear dependent upon instrument modality and sampling volume. White *et al.*[26] used

microindentation and reported a functional DEJ width based on microhardness of 100 μm. In contrast, Hayashi used high-resolution transition electron microscopy (TEM) on rat DEJ and reported that the apatite crystals of enamel and dentin were in direct contact to each other.[46] Lin[11] and Lin and Douglas[2] investigated the architecture, mechanical properties and fracture toughness of bovine DEJ using SEM, microindentation and conventional fracture mechanics approaches. They determined a functional DEJ width of between 50 to 100 μm in bovine teeth. They also reported that the functional width appeared to be greater than its optical appearance.

In this experiment, we estimated a functional DEJ width, based on the nanomechanical properties, of 11.8 μm. Fong *et al.*, used a Berkovich nanoindenter and estimated the functional DEJ width at between 15 and 25 μm.[47] This represents a significant refinement in the functional DEJ width based on hardness than that reported by White *et al.*[26] This is likely the result of a reduction in sampling volume, decreased inter-sampling spacing and the undulating and variable nature of the DEJ. Microindentation samples a greater volume than nanoindentation; producing a wider DEJ width estimate as the result of sample mixing that includes contributions from dentin, enamel and DEJ. White *et al.*[26] found considerable variability in enamel in the near DEJ region, a possible result of sample mixing caused by a greater sampling volumes.

In transmission electron microscopy (TEM), sample thickness is reduced to the point that electrons are allowed to pass through the sample where they are collected and later analyzed. TEM sample thickness can be as thin as 30 to 100 nm. As a result, it is possible that TEM sample preparation could remove the three-dimensional variability of

the DEJ, producing a further reduction in the DEJ width estimate as compared with that derived using nanomechanical testing.

Our fracture results are in line with previous work. The results indicated that it is extremely difficult to initiate cracks in dentin, or to propagate cracks into dentin that were initiated in enamel. Xu *et al.*[12] reported fracture toughness values for sagittal sections that varied from 0.52 $MPa \bullet m^{1/2}$ parallel to the enamel rods to 1.3 $MPa \bullet m^{1/2}$ when perpendicular to it. These were in line with values reported by Hassan *et al.*[48] using microindentation. Therefore, nanoindentation is a tool that can be used to improve our understanding of dental material properties at finer spatial levels than microindentation.

It is also noted that caution should be used when interpreting the results of this study. Only three third molars were evaluated in this study, and there is an extremely narrow width between the baseline hardness and modulus levels in dentin and enamel. This only allowed a limited number of sample points to be placed within the junction. Additional studies should be performed to confirm or elucidate the effects of sample size, intra-tooth location, inter-tooth variability and nanoindenter tip size.

2.6 Conclusion

No characteristic or unique mechanical or fracture properties were determined for the DEJ. Lines of nano-indentation points placed across the DEJ showed a monotonic increase in hardness and modulus from bulk dentin to bulk enamel. A functional DEJ width estimate of 11.8 μm was made based on inflections in the graphed nano-mechanical data, in accordance with the loess statistical model used. The DEJ width estimate did not display intra-tooth or inter-tooth variation, although sample size was too small to allow tests of statistical significance. Crack initiation was not observed to occur

in dentin. Cracks were initiated in enamel, but the cracks were not observed to cross the DEJ and extend into dentin. Fracture toughness for enamel in the near DEJ region was found to range from 0.6 to 0.9 $MPa \bullet m^{1/2}$. Further studies involving larger sample sizes could improve our understanding of this material interface. The results are in line with earlier work,[36] and may improve our knowledge of binding materials having widely dissimilar behaviors.

2.7 References

1. Ten Cate AR. Oral Histology: Development, structure, and function. 4th Ed., St. Louis: Mosby; 1994. p. 184-185.
2. Lin CP, Douglas WH. Structure-property relations and crack resistance at the bovine dentin-enamel junction. *J Dent Res* 1994; 73:1072-1078.
3. Bhaskar SN, editor. Orban's oral histology and embryology. 11th Ed. Chicago: Mosby year Book; 1990. p 70-71.
4. Jones SJ, Boyde A. In: Dentin and dentinogenesis Vol II. Linde A, Editor. Boca Raton: CRC Press; 1984. p. 5-97.
5. Scott JH, Symons. NBB. Introduction to dental anatomy. 6th ed, Edinburgh,: Livingstone; 1971: p. 448.
6. Whittaker DK. The enamel-dentine junction of human and Macaca Irus teeth: A light and electron microscope study. *J Anat* 1978;125:323-335.
7. Lin CP, Douglas WH, Erlandsen SL. Scanning electron microscopy of type I collagen at the dentin-enamel junction of human teeth. *J Histochem Cytochem* 1993;41:381-388.
8. Pioch T, Staehle HJ. Experimental investigation of the shear strengths of teeth in the region of the dentinoenamel junction. *Quintessence Int* 1996;27:711-714.
9. Rasmussen ST. Fracture properties of human teeth in proximity to the dentinoenamel junction. *J Dent Res* 1984;63:1279-1283.
10. Rasmussen ST, Patchin RE, Scott DB, Heuer AH. Fracture properties of human enamel and dentin. *J Dent Res* 1976;55:154-164.

11. Lin CP. Structure-function property relationships in the dentin-enamel complex and tooth restoration interface. PhD thesis, University of Minnesota 1993.

12. Xu HHK, Smith DT, Jahanmir S, Romberg E, Kelly JR, Thompson VP, Rekow ED. Initiation damage and mechanical properties of human enamel and dentin. *J Dent Res* 1998;77:472-480.

13. Van Meerbeck B, Willems G, Celis JP, Roos JR, Brahem M, Lambrechts P, Vanherle G. Assessment by nano-indentation of the hardness and elasticity of the resin-dentin bonding area. *J Dent Res* 1993;72:1434-1442.

14. Willems G, Celis JP, Lambrechts P, Braem M, Vanherle G. Hardness and Young's modulus determined by nanoindentation technique of filler particles of dental restorative materials compared with human enamel *J Biomed Mater Res* 1993;27:747-755.

15. Kinney JH, Balooch M, Marshall SJ, Marshall GW, Weihs TP. Atomic force microscope measurements of the hardness and elasticity of peritubular and intertubular dentin. *J Biomech Eng* 1996;118:133-135.

16. Kinney JH, Balooch M, Marshall SJ, Marshall GW, Weihs TP. Hardness and Young's modulus of human peritubular and intertubular dentine. *Arch Oral Biol* 1996;41:913.

17. Bowen RL, Rodriguez. Tensile strength and modulus of elasticity of tooth structure and several restorative materials. *J Am Dent Assoc* 1962;64:378-387.

18. Braden M. Biophysics of the tooth. Kawamura Y, editor. Frontiers of oral physiology. Vol 2: Physiology of oral tissues. Basel: Karger; 1976. p 1-37.

19. Waters NE. Some mechanical and physical properties of teeth. Vincent JFV, Currey JD, editors. The mechanical properties of biologic materials. Cambridge: Cambridge University; 1980. p 99-136.

20. Duck FA. Physical properties of tissue. London: Academic; 1990. p 137-165.

21. Craig RG, Peyton FA. Elastic and mechanical properties of human dentin. *J Dent Res* 1958;37:710-718.

22. Sano H, Ciucchi B, Matthews WG, Pashley DH. Tensile properties of mineralized and demineralized human and bovine dentin. *J Dent Res* 1994;73:1205-1211.

23. Watanabe L, Marshall GW, Marshall SJ. Dentin shear strength: Effects of tubule orientation and intratooth location. *Dent Mater* 1996;12:109-115.

24. El Mowafy OM, Watts DC. Fracture toughness of human dentin. *J Dent Res* 1986;65:677-681.

25. Rasmussen ST. Fracture properties of human teeth in proximity to the dentinoenamel junction. *J Dent Res* 1984;63:1279-1283.

26. White SN, Paine ML, Luo W, Sarikaya M, Fong H, Yu A, Li ZC, Snead ML. The dentino-enamel junction is a broad transitional zone uniting dissimilar bioceramic composites. *J Am Ceram Soc* 2000;83:238-240.

27. Doerner MF, Nix WD. A method for interpreting the data from depth-sensing indentation instruments. *J Mater Res* 1986;1:601-609.

28. Balooch M, Wu-Magidi, IC, Lundkvist AS, Balazs, Marshall SJ, Marshall GW , WJ Seikhaus, Kinney JH. Viscolelastic properties of demineralized

human dentin in water with atomic force microscopy (AFM)-based indentation, *J Biomed Mater Res* 1998;40:539-544.

29. Marshall SJ, Balooch M, Breunig T, Kinney JH, Tomsia AT, Inai N, Watanabe LG, Wu-Magidi IC, Marshall GW. Human dentin and the dentin-resin adhesive interface. *Acta Mater* 1998;46:2529-2539.

30. White JM, Goodis HE, Marshall SJ, Marshall GW. Sterilization of teeth by gamma radiation. *J Dent Res* 1994; 73:1560-1567.

31. Harding DS, Oliver WC, Phar GM. Cracking during nanoindentation and its use in the measurement of fracture toughness. *Mater Res Soc Symp Proc*1995;356:663-668.

32. Lawn BR,Wilshaw TR. Indentation fracture: principles and applications. *J Mater Sci* 1975;10:1049-1081.

33. Lawn BR, Marshall D. In: Fracture mechanics of ceramics, Vol 3, Bradt RC, Hasselman DPH and Lange FF, Editors, New York: Plenum; 1978:205-209.

34. Lawn BR, Evans AG, Marshall DB. Elastic/plastic indentation damage in ceramics: the median radial crack system. *J Am Ceram Soc* 1980;63:574-81.

35. Palmqvist S. Occurrence of crack formation during Vickers indentation as a measure of the toughness of hard materials. *Arch Eisenhuettenwes* 1962;33:629-633.

36. Anstis GR, Chantikul P, Lawn BR, Marshall DB. Critical evaluation of indentation techniques for measuring fracture toughness: I. Direct crack measurements. *J AM Ceram Soc* 1981;64:533-538.

37. Scharf TW, Deng H, Barnard JA. Mechanical and fracture toughness studies of amorphous SiC-N hard coating using nanoindentation, *J Vac Sci Technol* 1997;A15:963-967.

38. Ritchie RO, Dauskardt RH, Gerberich WW, Strojny A, Lilleodden E. Fracture, fatigue and indentation behavior of pyrolytic carbon for biomedical applications. D rory MD, Donley MS, Bogy D, Field JE, editors. MRS Sym Proc 383. 1995. p 229-254.

39. Kinney JH, Balooch M, Marshall GW, Marshall SJ. A micromechanics model of the elastic properties of human dentin. *Arch Oral Biol* 1999;44:813-822.

40. Cleveland WS, Devlin SJ, Grosse E. Regression by local fitting. *J Econometrics* 1988;37:87-114.

41. Efron B, Tibshirani RJ. An introduction to the bootstrap. San Francisco: Chapman & Hall; 1993. p. 436.

42. Weerahandi S. Exact statistical methods for data analysis, New York:Springer-Verlag; 1994. p. 328.

43. Kinney JH, Habelitz, S, Marshall SJ, Marshall GW. The importance of intrafibrillar mineralization of collagen on the mechanical properties of dentin. *J Dent Res* 2003;82(12):957-961.

44. Kinney JH, Marshall SJ, Marshall GW. The mechanical properties of human dentin: a critical review and re-evaluation of the dental literature. *Crit Rev Oral Biol Med* 2003;14(1):13-29.

45. Currey JD, Brear K. Hardness, Young's modulus and yield stress in mammalian mineralized tissues. *J Mat Sci in Med* 1990;1:14-20.

46. Hayashi Y. High resolution electron microscopy in the dentino-enamel junction. *J Electron Microsc* 1992;41:387-391.

47. Fong H, Sarikaya M, White SN, Snead ML. Nano-mechanical properties profiles across dentin-enamel junction of human incisor teeth. Mat Sci Engr C, Biomim Supramol Sys 2000; C7:119-128.

48. Hassan R, Caputo AA, Bunshah RF. Fracture toughness of human enamel. *J Dent Res* 1981;60:820-827.

49. Lawn BR, Evans AG, Marshall DB. Elastic/plastic indentation damage in ceramics. The median/radial crack system. *J Am Ceram Soc* 1980;63:574-581.

2.8 Tables and Figures

Tables:

Figures:

TABLE 2.1
The Mechanical Properties of Dentin, Enamel and the DEJ[a]

Material Parameter	Enamel	Dentin	Peritubular Dentin	Intertubular Dentin	DEJ
Compressive Strength (MPa)	95-140	230-370			
Young's Modulus (GPa)	9-90	11-20	31	16.3	
Shear Strength (MPa)	90.2	36-138			
Tensile Strength (MPa)	8-35	31-104			
Microhardness (GPa)	3.2-4.4	0.25-0.8			
Nanohardness (GPa)	3.1-3.4		1.6-2.5	0.13-0.58	
Work of Fracture (J/m^2)	200[b]	270[b]			
	13[c]	550[c]			336
	1.1[b]	2.6[b]			
K_{IC}	0.52[c]	2.8-3.1[c]			
K_{IC} ($MPa \bullet m^{1/2}$)	1.3[b]	2.8[b]			3.38[b]
G_{IC} 560		669-742[c]			988[b]
(J/m^2)	23[d]	750[d]			695[c]

[a] Compiled from Bowen and Rodriguez;[38] Braden;[39] Waters;[40] Duck;[41] Van Meerbeck et al;[14] Craig and Peyton;[42] Sano et al;[43] Willems et al;[15] Kinney et al;[18-19] Watanabe et al[44]; Rasmussen et al;[9] Rasmussen;[10] El Mowafy and Watts;[45] Lin and Douglas;[2] Lin;[11] Xu et al.[12]

[b] Perpendicular to prisms or tubules. [c] parallel to prisms or tubules. [d] bovine.

TABLE 2.2

Mechanical Properties and Fracture Toughness Values Obtained by Indentation Technique for Some Selected Brittle Materials[a]

Material Parameter	Soda-Lime Glass[46]	Silicon[46]	SiC Hard Coating[27]	Polycrystalline Graphite[47]
Hardness, (H)	5.5 (GPa)	9 (GPa)	29 (GPa)	50-120 (DPH)
Elastic Modulus (E)	70 (GPa)	168 (GPa)	330 (GPa)	4-12 (GPa)
Fracture Toughness (K_{IC})	0.7 MPa•$m^{1/2}$	0.75 MPa•$m^{1/2}$	2.97 MPa•$m^{1/2}$	1.5 MPa•$m^{1/2}$

[a](Data for soda-lime glass and Si from Lawn et al.,[46] SiC from Anstis et al.,[27] and graphite from Ritchie et al.[47]

TABLE 2.3
Young's Modulus and Hardness Values from Nanoindentation for Enamel and Intertubular Dentin Adjacent to the DEJ (with 95% Confidence Intervals)

Material Parameter	Enamel	Dentin
Modulus (GPa)	63.55 (62.09,65.02)	19.65 (18.61, 20.69)
Hardness (GPa)	3.51 (3.38, 3.63)	0.83 (0.74, 0.92)

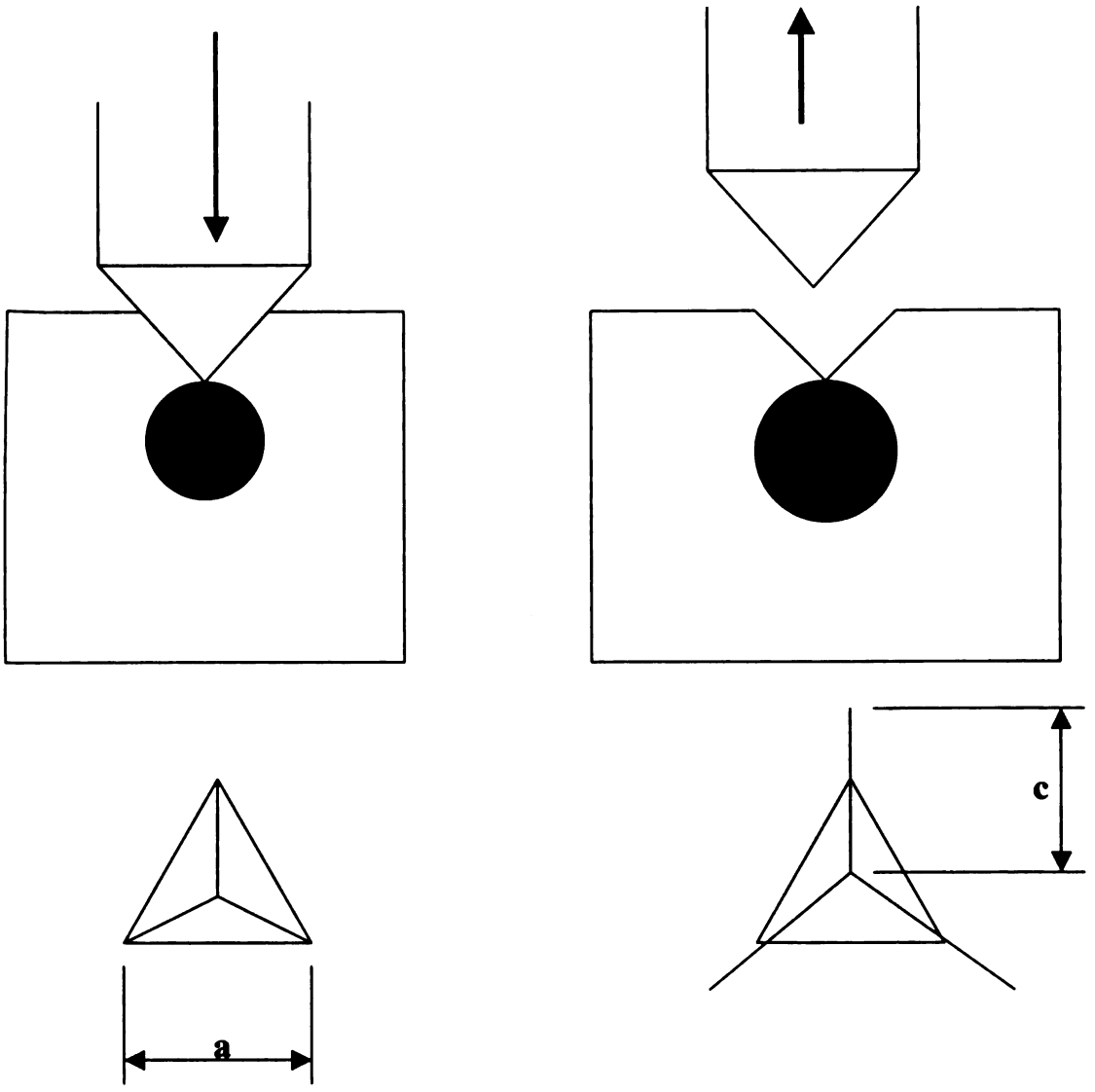

Figure 2.1. Schematic diagram illustrating the indentation process. At the critical indentation load, P (left), a median subsurface crack is generated under the cube corner indentation tip of width, **a**, due to tensile stress and is the characteristic size for the three-sided indenter. Upon unloading (right), the median cracks become unstable and radial cracks of length, **c**, form in response to the indenter residual stress field.

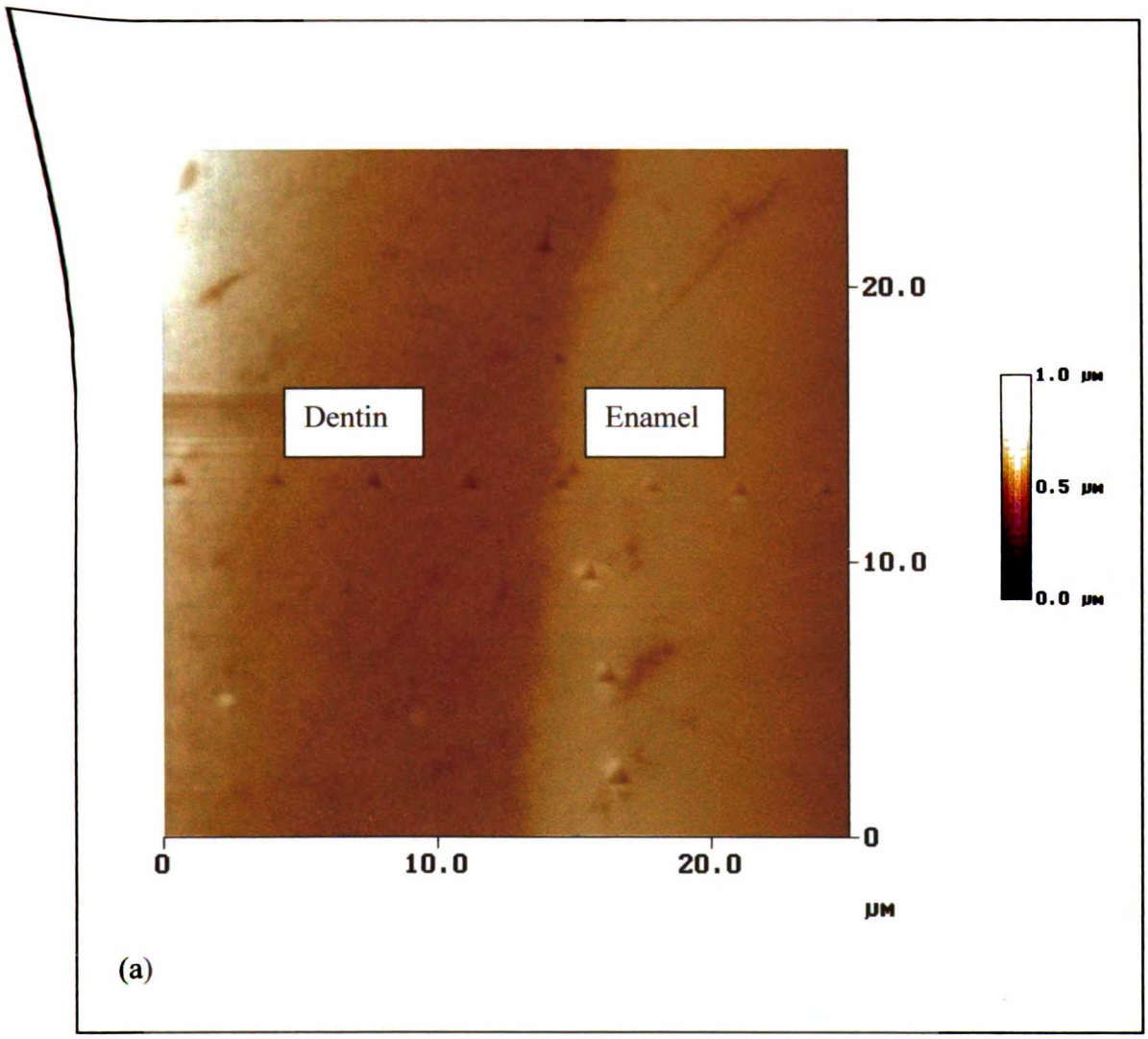

Figure 2.2 An AFM image of nanoindents placed perpendicularly across the DEJ. Indents were also placed at a glancing angle to study the effect of interception angle. No effect on DEJ width estimation was found.

a)

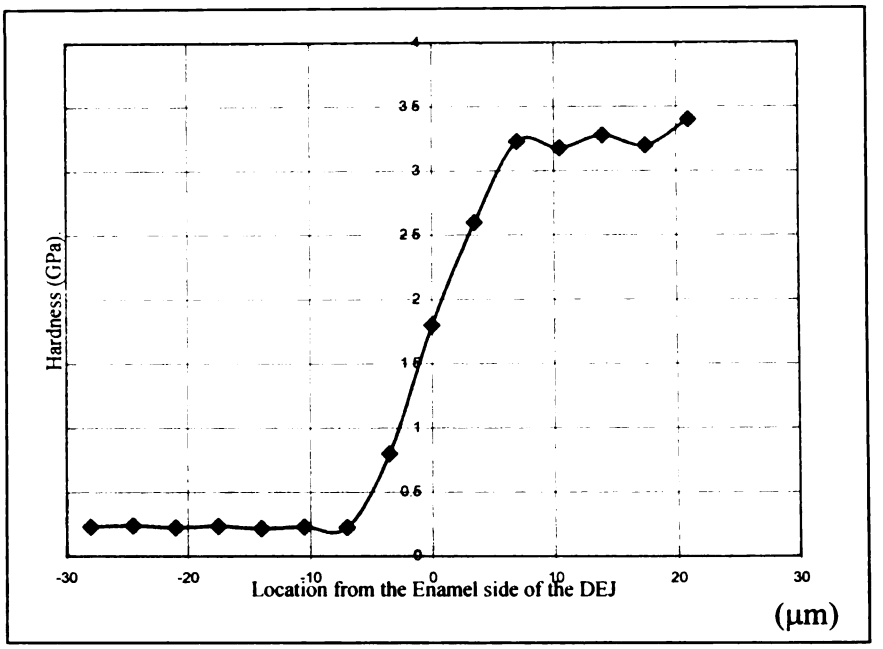

b)

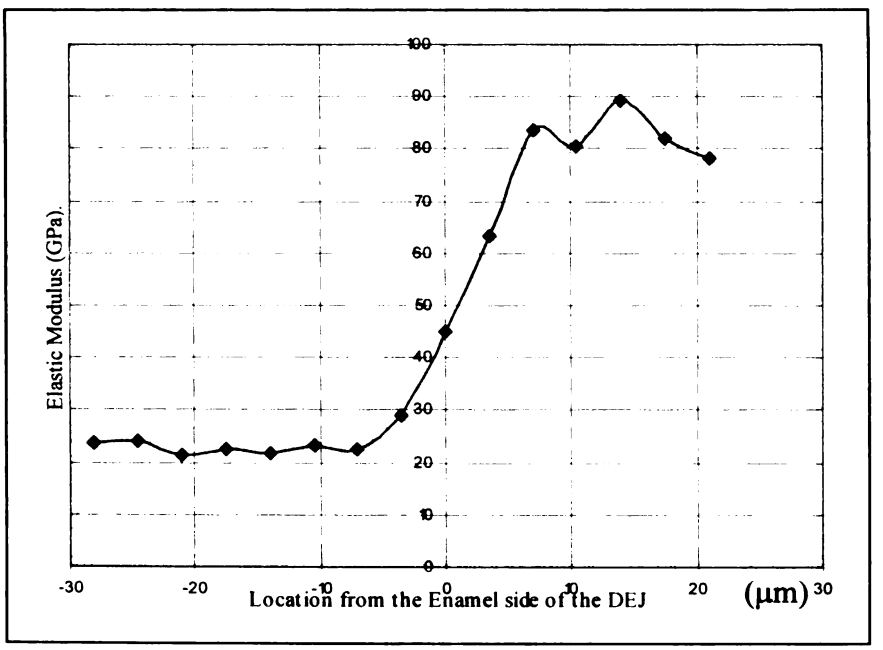

Figure 2.3 Graphs showing the variation in a) hardness and b) elastic modulus across this region. Estimates of the width of the DEJ were made using deviations from linear models of the material properties.

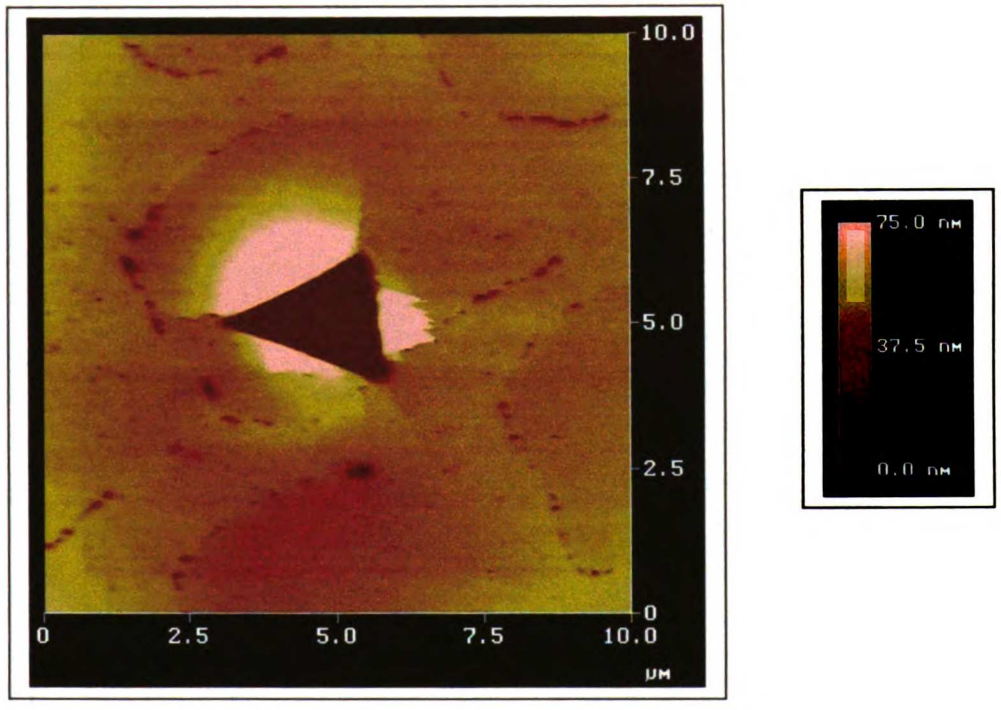

Figure 2.4 A nanoindentation placed into enamel in the near DEJ region under an applied load of 6,000 μN. Radial cracks were generated and used to estimate the fracture toughness of enamel. Based on knowledge of the crack length, and using local average modulus and hardness values, an estimated fracture toughness of 0.7 MPa•$m^{1/2}$ was determined.

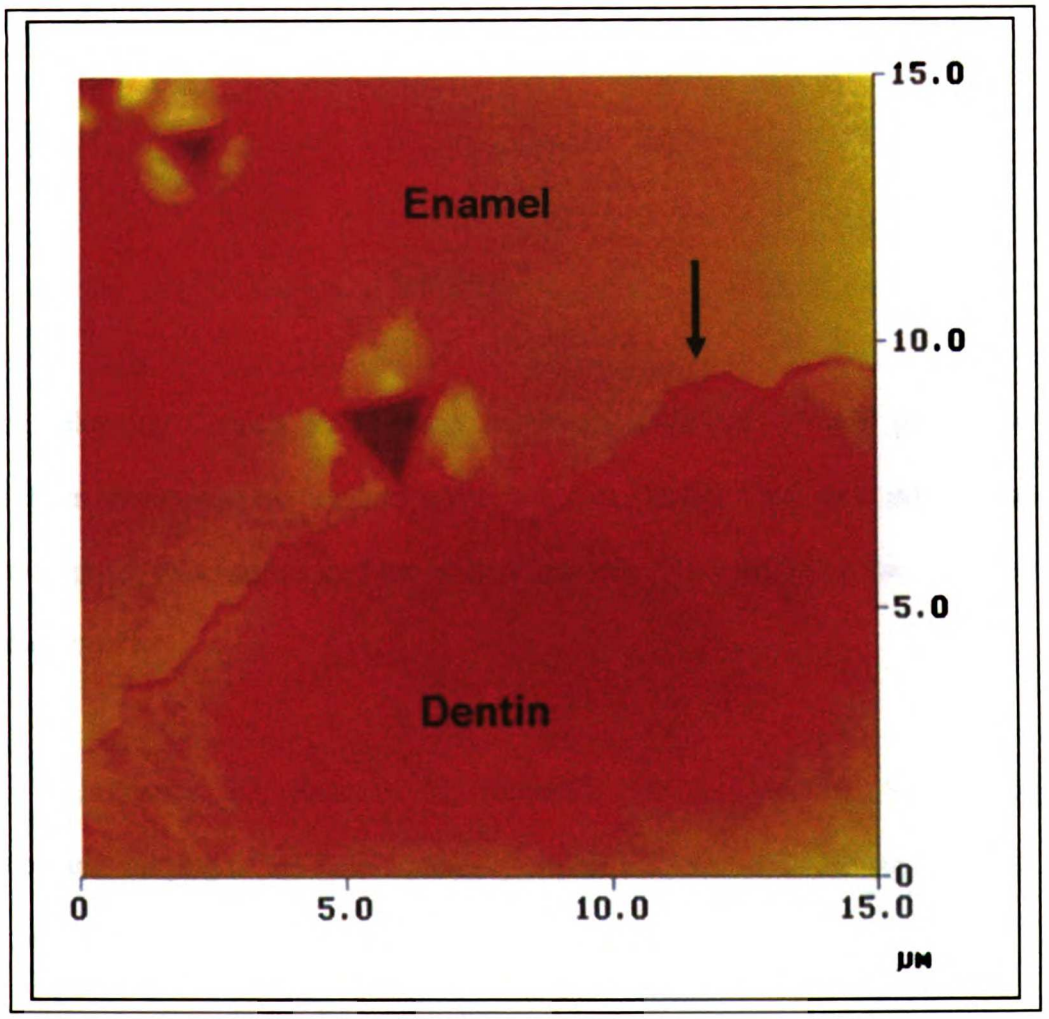

Figure 2.5 An irregular crack introduced into the near-DEJ region using a nanoindenter. The crack was initiated into enamel and approached the DEJ but deflected and propagated in enamel.

Chapter 3

The following Chapter represents a previously published research paper. The work has been expounded to include additional data, illustrations, and information intended to improve understanding of the body of research. The citation for the published research document is:

Gallagher RR, Demos SG, Balooch M, Marshall GW Jr, Marshall SJ. Optical spectroscopy and imaging of the dentin-enamel junction in human third molars, J Biomed Res 2003;64A:372-377.

CHAPTER THREE – Optical Spectroscopy and Imaging of the Dentin-Enamel Junction in Human Third Molars

3.1 Summary

A 351-nm laser excitation source was used to perform autofluorescence microscopy of dentin, enamel and the dentino-enamel junction (DEJ) to obtain information regarding their morphology and spectral characteristics. The emission spectra of these calcified dental tissues were found to be different from one another, enabling the DEJ to be imaged and the width to be determined. The DEJ was observed to display sharp and clearly delineated borders at both its enamel and dentin margins. The dentinal tubules and the enamel prisms appeared to terminate abruptly at their respective borders with the DEJ. The median DEJ width was found to be 10-μm, ranged from 7-μm to 14-μm, and did not appear to be dependent on intra-tooth position.

3.2 Introduction

The DEJ is a critical interface that functions to join hard, brittle enamel with softer and tough dentin.[1] During tooth formation, the DEJ serves as the initiation surface for amelogenesis and odontogenesis. In these processes, enamel forms radially outward from the DEJ, while dentin forms inward from this interface. The DEJ has been described as having a scalloped topography, with concavities directed toward the enamel and convexities directed toward the dentin.[2,3] The scallops are subdivided by micro-scallops and finer submicroscopic structures, forming a three level microstructure. The geometry and composition of the DEJ is believed to enhance bonding between dentin and enamel,

and mitigate the effects of crack propagation between these tissues. Little information presently exists regarding the width, composition and variability of these structures.[4,5]

Whittaker examined 162 deciduous and permanent teeth that were extracted from monkeys and humans and found considerable variability in the form and width of the DEJ.[5] In monkey's teeth, scalloping was not observed, but 5 μm depressions near the ends of the enamel prisms were usually seen. In humans, Whittaker observed scallops on the order of 25 to 100 μm, and noted that the proximal surfaces displayed greater scalloping than either the buccal or lingual surfaces.[5] Scott and Symons reported increased scalloping under the cusps,[6] while Schour found more scalloping in the gingival third of the tooth.[7]

Lin et al. used high resolution scanning electron microscopy (SEM) and immuno-labeling to identify the type and orientation of collagen present in human DEJ.[3] They found type I collagen fibrils were present in the scalloped and micro-scalloped areas. They reported that the collagen fibrils appeared to emanate from the dentin and coalesced to form coarse fibrils approximately 100 nm in diameter that traversed the DEJ before inserting into the enamel mineral. Habelitz et al.[8] found the diameter of most dentin collagen was on the order of 100 nm diameter., implying that collagen fibrils traversed the DEJ and inserted directly into the enamel mineral. *Lin* et al. also observed scalloping that was on the order of 25 to 40 μm.[3] They postulated that the DEJ is a tough, distinct dental tissue essential to joining dentin and enamel, and that the DEJ functions to prevent catastrophic tooth fracture by blunting or deflecting the crack and absorbing its driving energy. Lin[3] and Lin and Douglas[9] investigated the architecture, mechanical properties and fracture toughness of bovine DEJ using SEM and conventional fracture mechanics

approaches. They determined that the mechanical properties of the DEJ appeared to have a graded functional width of between 50 to 100 μm in bovine teeth, and reported that the functional width appeared to be greater than its optical appearance. They were unable to find any clear demarcation of the borders of the DEJ, and were unable to correlate the mechanical and optical properties.

White *et al.* used a microindenter to study the variation in mechanical properties across the DEJ.[10] Microindentations were placed across the tooth surface at a perpendicular angle to the DEJ. They found a 100 μm wide region in which the microhardness values increased from dentin to enamel. White *et al*[10]. noted that this functional width appeared to be greater than the optical appearance of this junction. Elliot *et al.* performed a microradiodensity survey across the DEJ and reported a profile consistent with White's microindentation results.[11] Common features included the graded transition from dentin to enamel, the small peak on the enamel side near the DEJ, and a dip on the dentin side.

Marshall *et al.* used nano-mechanical testing and local polynomial regression fits of reduced modulus data and estimated the functional width of the DEJ at 11.8 μm.[12] They reported that this value did not display significant inter-tooth or intra-tooth variability, although the results were not statistically significant because of the limited sample size used. Balooch *et al.* used laser induced fluorescence spectroscopy to study the architecture and composition of human dentin.[13] They employed the use a 351 nm Argon-ion laser source to illuminate dry polished samples of human third molars, and determined emission spectra for normal and transparent dentin. They provided an initial

estimate the width of the DEJ, based on fluorescence spectroscopy, of between 10 and 20 μm.[14]

In 1911, Stubell[15] introduced optical spectroscopy into the field of dental research when he reported the presence of tooth fluorescence under ultraviolet photoexcitation. Eisenberg[16] reported the presence of tooth fluorescence under excitation from blue or violet light. Alfano and Yao[17] conducted the first published systematic spectroscopic investigation on teeth. They used spectroscopy to compare carious and non-carious teeth nearly 50 years after its introduction to the field. Additional work has been conducted and published in the area that better defined the effects of dental caries.[17,18,19] Utilization of optical spectroscopy in this field has grown to include its use for the detection of dental caries.[20,21]

This chapter represents a research effort to determine the width, morphology and fluorescence spectra of human third molar DEJ using optical spectroscopy. A 351 nm laser source was used to determine emission spectra and emission ratios for enamel, dentin and DEJ. The width and morphology of the DEJ were determined using differences in the fluorescence characteristics of these dental tissue components.

3.3 Materials and Methods

3.3.1 Sample preparation

Human third molars were collected from research subjects requiring third molar extractions as part of their dental treatment plan. All subjects enrolled in this study responded positively to an Informed Consent protocol, previously approved by the UCSF Institutional Committee on Human Research. Following extraction, all teeth were immediately stored in filtered and purified water at 4°C. They were sterilized by gamma

irradiation shortly thereafter in accordance with a standard protocol prior to sample preparation.[4] Five teeth were sagittally sectioned across the center of the tooth to prepare 1 mm thick slabs containing enamel, dentin and DEJ. The surface of each slab was metallographically polished through a series of silicon carbide abrasive papers down to 4000 mesh. The samples were then successively polished with alumina powder slurries of 1 μm, 0.3 μm, and 0.05 μm. All samples were ultrasonically cleaned in filtered and purified water at the end of each polishing step to remove polishing agents as well as any residual smear layer. Following sample preparation, each sample was air dried for 24 hours prior to optical spectroscopic imaging.

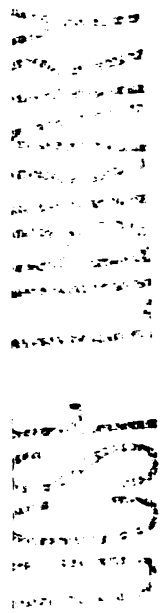

3.3.2 Laser induced fluorescence microscopy

The experimental arrangement for the laser induced fluorescence microscope system used in this research is illustrated in Figure 3.1, and has been previously described.[13] The system consists of a continuous wave argon-ion laser that operates at 351 nm. It was used to excite five sagittally sectioned and polished 1 mm thick human third molar samples as shown in Figure 3.1. The laser excitation source was oriented to strike the surface of each sample at an incident angle of approximately 45 degrees. This condition also produced an illumination field approximately 10 mm in diameter. The laser intensity within the illumination field was considered to be relatively uniform. The fluorescence microscope collected light that had been back radiated from the sample. This microscope consisted of a long working length objective lens connected in series with a 5-power zoom lens. This assembly was used to image the center of the illumination field, and transmitted the captured signal to a charge coupling device (CCD) detector following passage through a narrow pass filter. The image was then captured

with a liquid nitrogen cooled CCD detector. Spatial resolution of the system was on the order of 1 μm. The entire apparatus was constructed on an isolation table to mitigate the effects of vibration.

The construction of response spectra required the use of a series of 10 nm wide narrow-band interference filters. These filters covered the range from 400 nm to 850 nm. The fluorescence microscope captured the signal return emitted from the illuminated sample at each 10 nm wide narrow pass filter. All images were taken with the same perspective and magnification. In addition, each image was of the same portion of each tooth. This allowed image data sets to be super-imposed following image processing.

Following system calibration, spectral construction was initiated by collection of the 400 nm narrow pass filter image data. This consisted of inserting the 400 nm narrow pass filter into the filter holder, illuminating the sample with the 351 nm Argon-ion laser excitation source, and capturing the filtered and fluoresced signal with the charge coupling device (CCD) detector. Following successful capture, the 400 nm filter was removed and replaced by a 410 nm filter. This sequence was continued until the 850 nm filter was reached. In this way a set of 45 super-imposable fluorescence microscope images were recorded for each sample. Each image represented the captured emission signal that was filtered by a corresponding filter.

Image processing was performed post-experimentation. This consisted of a series of sharpening and contrast enhancement operations. The sharpening operations were intended to improve image quality and resolution. Contrast enhancement operations included pixel-by-pixel inter-image processing of the digitized intensity maps that enabled differences in the spectral characteristics of the DEJ to be distinguished from

those of dentin and enamel. To accentuate these differences, the displayed image intensity maps were viewed to identify representative areas of enamel, dentin and DEJ. The pixel coordinates ascribed to each of these tissues of interest were identified from the base image intensity map. Since the maps were super-imposable, the pixel coordinates of the tissues of interest identified from the base image intensity map were used on the subsequent maps to identify the same tissues or areas of interest. The emitted intensity ascribed to the pixel coordinates of the tissue of interest at each narrow pass filter was recorded. Spectral construction used this information that was collected from the 45 image intensity maps to construct a spectrum of each tissue. These operations allowed these dental tissues to be characterized and enabled chemical composition and mineralization changes to be studied by comparing their spectra.

3.4 Results

Figure 3.2 is a fluorescence microscope image taken across the dentino-enamel interface of a human third molar. The image was obtained using a 510-nm narrow pass filter. No inter-image operations were performed to increase tissue contrast on this sample. The image shows a distinct band at the interface between dentin and enamel. The dentinal tubules and the enamel prisms appear to terminate from their respective sides of this band. The band is shown to display relatively uniform emission intensity, and therefore appears to be compositionally more homogenous than either enamel or dentin. The width of this band, which apparently corresponded to the dentin-enamel junction, was 7 μm in this sample. The width of the DEJ was measured at 10 μm using the same approach in three other samples. The width did not appear to vary with intra-tooth

position in any of the samples. The morphology of the DEJ in this, and all samples imaged, appeared to follow a scalloped and sub-scalloped pattern.

Emission intensities from enamel, dentin and the DEJ were observed to vary from sample to sample. Some of these variations were subtle, making it difficult to distinguish DEJ from enamel and dentin without resorting to image processing operations to enhance the DEJ's visibility. An example of this condition is illustrated in Figure 3.3. In this image, dentin and enamel are clearly visible but the presence of the DEJ is not readily apparent. To address this condition, the collected and filtered emission intensities were subjected to image processing operations to enhance differences in the data.

Emission spectra were constructed for characteristic regions of enamel, dentin and DEJ. A 351 nm argon-ion laser excitation source and 45 super-imposable fluorescence images were used to construct spectra as described previously. Figure 3.4 shows the emission spectra normalized to peak intensity and vertically translated to facilitate comparison. Enamel was further broken down into being either bulk or tuft enamel. In general, spectra for enamel, dentin and DEJ were found to be similar. An emission band centered at 450 nm was found to be common to each tissue. In dentin, a second emission band was found to be centered at 490 nm. This is consistent with previously reported emission spectra from dentin under 351 nm excitation.[13] Enamel showed a second emission band that was broader than that in dentin and was located at a longer wavelength, approximately 530 nm. This was observed to occur in both bulk and tuft enamel. For the DEJ, the second band was found to be broad, as is that of enamel, but the peak was centered at 490 nm.

To better delineate these spectral differences, emission spectra ratios were calculated for the sample, and they are shown in Figure 3.5. An emission spectra ratio is an image processing operation calculated as the pixel-by-pixel emission intensity collected for one condition divided by the emission intensity collected for another condition. The dentin/DEJ emission ratio is such a pixel-by-pixel operation comparing the dentin and DEJ intensities. This operation suggested that dentin is relatively more emissive at shorter wavelengths than is the DEJ. The enamel/DEJ emission ratio indicated that the DEJ is relatively more emissive at shorter wavelengths than enamel. Finally, the dentin/enamel emission ratio indicated enamel increased its emissivity at longer wavelengths. The results indicate that the majority of the relative changes in the emission spectra take place within the 400- to 600-nm range.

To further enhance the visibility of the DEJ, differences in the fluorescence image intensity maps were used. Image processing operations were conducted on a pixel-by-pixel basis to increase tissue contrast differences. Inter-image emission spectra ratio processing operations using the 600 nm and 410 nm image intensity maps were performed. The resulting image is shown in Figure 3.6. In this image, the DEJ is visible as a strip between dentin and enamel. Counting the number of pixels between the respective borders of the DEJ, and applying the corresponding scaling factors allowed us to estimate the with of the DEJ. The width of the DEJ in this sample using this method was estimated at 15 μm.

3.5 Discussion

To this point, information on the width and architecture of the DEJ has been conflicting and confusing. Various instrumentation modalities have been employed in an

attempt to delineate the width and morphology of the DEJ. Lin and Douglas determined that a graded functional width, based on micro-mechanical testing of bovine teeth, was on the order of 50 to 100 μm.[9] They noted that this width, which they termed a "functional width" appeared to be greater than its optical appearance. White *et al.* estimated the functional width of human DEJ at 100 μm, based on microhardness testing.[10] They noted that this width also appeared to be greater than the optical width, which they estimated as being less than 2 μm. In a preliminary study, Demos *et al.* (2000)[13] used laser induced fluorescence spectroscopy and estimated the width of the DEJ at 10 to 20 μm.

Our results indicate that the DEJ appears to exhibit distinct and clearly defined borders with 351 nm argon-ion laser-induced fluorescence imaging. Using this instrument we estimated its median width at 10 μm. For teeth where the enamel, dentin and DEJ emission intensities were similar, inter-image emission ratio operations were performed to accentuate tissue contrast. Using this approach a DEJ width estimate of 15 μm was determined for a specimen where no optically apparent DEJ appeared to exist. DEJ width was estimated in four specimens where the emission intensities displayed sufficient tissue contrast differences to clearly define the borders of the DEJ. For these specimens, no additional inter-image processing operations were performed. DEJ width for these samples was estimated to range from 7 μm to 10 μm. The DEJ width was not observed to vary with intra-tooth position in any of the teeth tested, although it should be noted that all testing was performed on dry, human third molars. DEJ width was determined at three points in each sagittally sectioned tooth, under the central pit and at the approximate mesial and distal inter-tooth contact points.

Our estimates of DEJ width are within the range of values reported in the literature. Marshall *et al.*[12] reported a mean functional DEJ width estimate of 11.8 μm, based on inflections in the graphed hardness and modulus variation of nanoindentation points placed to cross the DEJ perpendicularly. It represents a wider DEJ width estimate than that described in Chapter 4, which combines Raman microspectroscopic and nano-mechanical approaches. This method determined a mean functional DEJ width was estimate of 4.7 (± 1.2) μm to 6.1 (± 1.9) μm based on hardness and 4.9 (± 1.1) μm to 6.9 (± 1.9) μm based on modulus. Mean compositional DEJ width was estimated from Raman peak intensity variations to be in the range of 8.0 (± 3.2) μm to 8.5 (± 3.1) μm based on the phosphate peak, and 7.6 (± 3.2) μm to 8.0 (± 2.6) μm for C-H stretching mode. These width estimates were wider than the 2.0 ± 1.1 μm width estimate reported by Habelitz *et al.*[8] determined from changes in friction coefficient linearity using a AFM-based nanoscratching machine. Recently, Balooch *et al*[22] used an AFM-based force modulation system to map the dynamic viscoelastic properties of the DEJ region. Their data suggested a 2-3 μm wide functional DEJ width existed. This width is considerably narrowed than our nanoindenter estimate. This result may be related to an improvement in spatial resolution resulting from continuous monitoring of the dynamic and spatial responses.

In addition, we found that the emission spectra of enamel, dentin and the DEJ as a result of 351 nm laser excitation were similar. The first emission peak of each tissue was found to be located at 450 nm. This peak suggests that these materials might have, in general, a similar composition. This is as expected since they contain similar apatite phases. Differences in the emission spectra were principally related to the location and

character of the second peak. These differences, and differences in the emission ratios, may be best explained by the compositional differences of these tissues. Dentin contains a larger percentage of organic matter than enamel, while enamel contains a greater amount of mineral. Although fluorescence under a 351 nm excitation source may be due to both organic and inorganic matter, emission from organic matter is much more intense in the 400 to 500 nm region. This results in dentin being "blue shifted", or relatively more emissive than enamel at lower wavelengths. The second peak of dentin is narrow and located at 490 nm. On the other hand, enamel exhibits stronger emission at longer wavelengths that may be attributed to the emission characteristics of the mineral fraction. This results in a broadening of the second spectral band and a "red shift" of the second peak to 530 nm. This result is in line with the experimental results of Emami *et al.*[23]

The emission spectrum of the DEJ contains a broad second emission band that extends toward longer wavelengths, similar in character to that seen in enamel. This suggests that the DEJ contains a significant mineral fraction. The second peak is positioned at 490 nm, the same second peak location exhibited by dentin. This suggests that the DEJ is also composed of a large amount of organics, similar to dentin, and that the organics are responsible for the position of the second emission peak at 490 nm. It is the position and character of the second peak that defines differences in the calcified dental tissues. Other analytical techniques may be required to clarify this point.

3.6 Conclusion

Laser induced auto-fluorescence or emission spectroscopy can be used to characterize enamel, dentin and the DEJ. Using this technique, the DEJ was found to be a

spectroscopically distinct tissue from either enamel or dentin. This property was exploited using microscopic autofluorescence imaging, allowing for the delineation of the margins of the different tissue types. The width of the DEJ was estimated to be in the range of 7 μm to 15 μm, with a median width estimate of 10 μm. DEJ width was found to be independent of intra-tooth position. The first emission peaks of dentin, enamel and DEJ were located at 450 nm. The second peaks of dentin and the DEJ were located at 490 nm. This peak was narrow for dentin and broad for DEJ. Enamel exhibited a broad second peak at 530 nm.

The emission spectroscopy results suggest that the DEJ is composed of large amounts of organic and mineral matter, and that the width is usually well defined and uniform under 351 nm Argon-ion laser excitation. Future instrumentation with other analytical methods could be used to improve our understanding of the composition of the DEJ.

3.7 References

1. Marshall GW. Dentin: Microstructure and characterization. Quintessence Int 1993;24:606-617.

2. Bhaskaar SN, editor. Orban's oral histology and embryology. Chicago: Mosby 1990.

3. Lin CP Structure-function property relationships in the dentin-enamel complex and tooth restoration interface. [PhD thesis]. University of Minnesota, Minneapolis, MN; 1993.

4. White JM, Goodis HE, Marshall SJ, Marshall GW. Sterilization of teeth by gamma radiation. J Dent Res 1984;73:1560-7.

5. Whittaker DK The enamel-dentine junction of human and Macaca Irus teeth: A light and electron microscope study. *J Anat* 1978;125:323-335.

6. Scott JH, Symons NBB. Introduction to dental anatomy. Edinburgh: Churchill Livingstone; 1971.

7. Schour I. Noyes oral histology and embryology. London: Kimpton; 1960.

8 Habelitz S, Marshall SJ, Marshall GW, Jr., Balooch M. The functional width of the dentino-enamel junction determined by AFM- based nanoscratching. J Struct Biol 2001; 135:294-301.

9. Lin CP, Douglas WH. Structure-property relations and crack resistance at the bovine dentin-enamel junction. J Dent Res 1994;73:1072-1078.

10. White SN, Paine ML, Luo W, Sarikaya M, Fong H, Yu A, Li ZC, Snead ML. The dentino-enamel junction is a broad transitional zone uniting dissimilar bioceramic composites. J Am Ceram Soc 2000; 83:238-240.

11. Elliot JC, Anderson P, Gao XJ, Wong FSL, Davis GR, Dowker SEP. Application of scanning microradiography and X-ray microtomography to studies of teeth and bone. J X-Ray Sci Technol 1994;4:102-117.

12. Marshall GW, Balooch M, Gallagher RR, Gansky SA, Marshall SJ. Mechanical properties of the dentinoenamel junction: AFM studies of nanohardness, elastic modulus, and fracture. J Biomed Mater Res 2001;54:87-95.

13. Balooch M, Demos SG, Kinney JH , Marshall GW, Balooch G, Marshall SJ. Local mechanical and optical properties of healthy and transparent root dentin. J Mater Sci Med 2001;12:507-514.

14. Demos SG, Balooch M, Marshall GW, Marshall SJ, Gallagher RR. Optical spectroscopy of transparent non-carious human dentin and dentin-enamel junction. In: Featherstone JD, Rechmann P, Fried D, editors. Lasers in dentistry. Bellingham, WA: SPIE-The International Society for Optical Engineering; 1999. Vol. 6, p 102-105.

15. Stubel H. Die fluoreszone tierische gewebe in ultra-violettum licht. Pflingers Arch Ges Physiol 1911;141:1.

16. Eisenberg J. Phenomena observed by subjecting dental tissues to ultra-violet rays corresponding to approximately 3590AU. Dent Cosmos 1933;5:284.

17. Alfano RR, Yao SS. Human teeth with and without dental caries studied by laser scattering, fluorescence and adsorption spectroscopy. IEEE J Quantum Electron 1984;20:1512.

18 Bjelkhagen H, Sundstrom F, Angmar-Manson B, Ryden H. Early detection of enamel caries by luminescence excited by visible laser light. Swed Dent J 1982;6:1.

19. Sundstrom F, Fredriksson K, Montan S, Hafstrom-Bjorkman U, Strom J. Laser induced fluorescence from sound and carious tooth substance: Spectroscopic studies. Swed Dent J 1985;9:71.

20. Lussi A, Imwinkelried S, Pitts NB, Longbottom C, Reich E. Performance and reproducibility of a laser fluorescence system for detection of occlusal caries in vitro. Caries Res 1999;33:295.

21. Hibst R, Paulus R. Caries detection by red excited fluorescence: investigations of fluorophores. Caries Res 1999;33:295.

22. Balooch G, Marshall GW, Marshall SJ, Warren OL, Asif SAS, Balooch M. Evaluation of a new modulus mapping technique to investigate microstructural features of human teeth. *J Biomech* 2004;37:1223-1232.

23 Emami Z, Al-Khateeb S, de Josselin de Jong E, Sundstrom F, Trollsas K, Angmar-Mansson B. Mineral loss in incipient caries lesions quantified with laser fluorescence and longitudinal microradiography. Acta Odontol Scand 1996;54:8.

3.8 Tables and Figures

Figures:

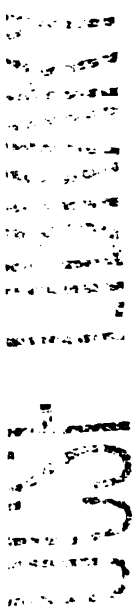

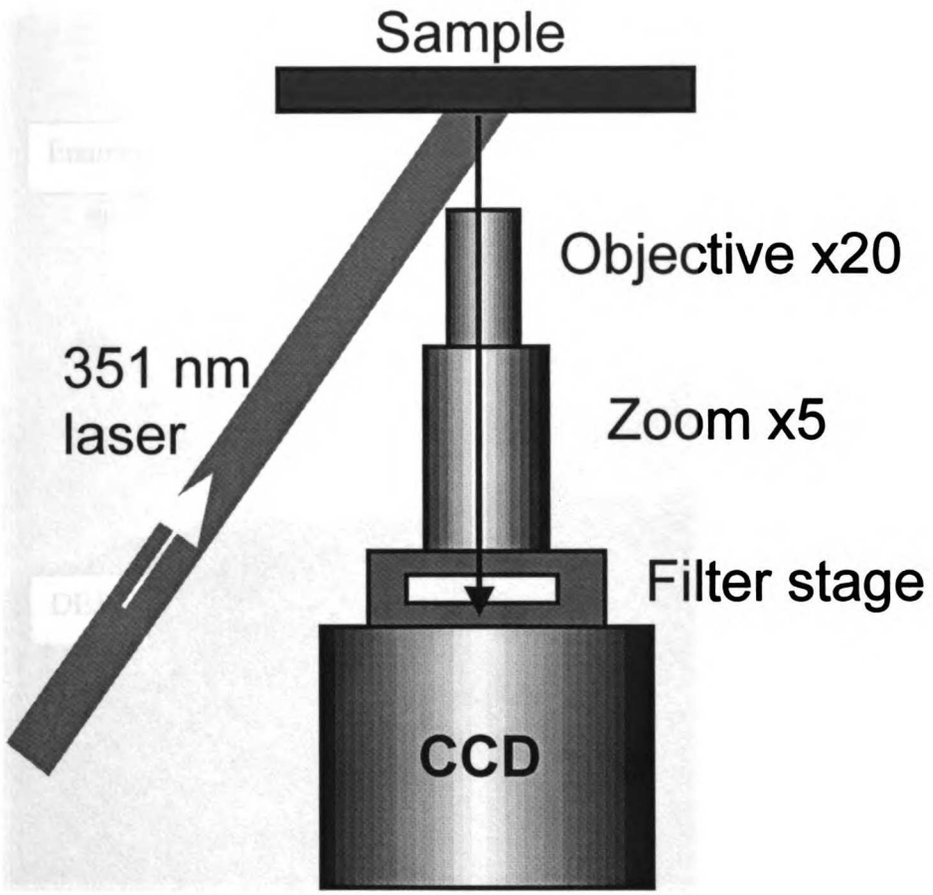

Figure 3.1 Autofluorescence microscopy experimental set up. A 351-nm continuous wave argon-ion laser was used to excite the sample. Fluoresced light was collected by a series of lenses and passed through a filter before collection by the CCD detector.

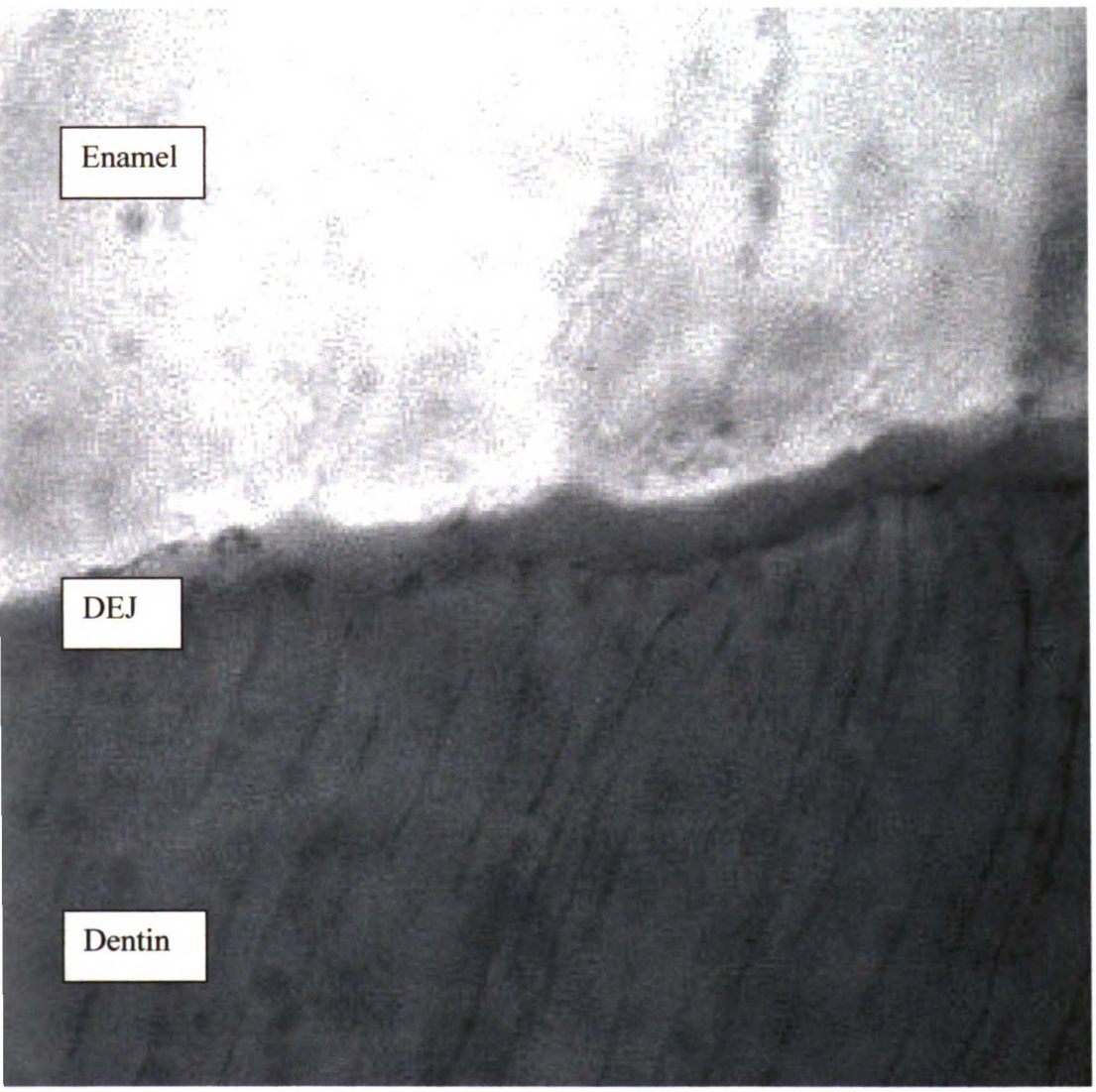

gure 3.2 150 μm by 150 μm fluorescence microscope image of human DEJ. The dth of the DEJ in this sample was estimated at 7 μm.

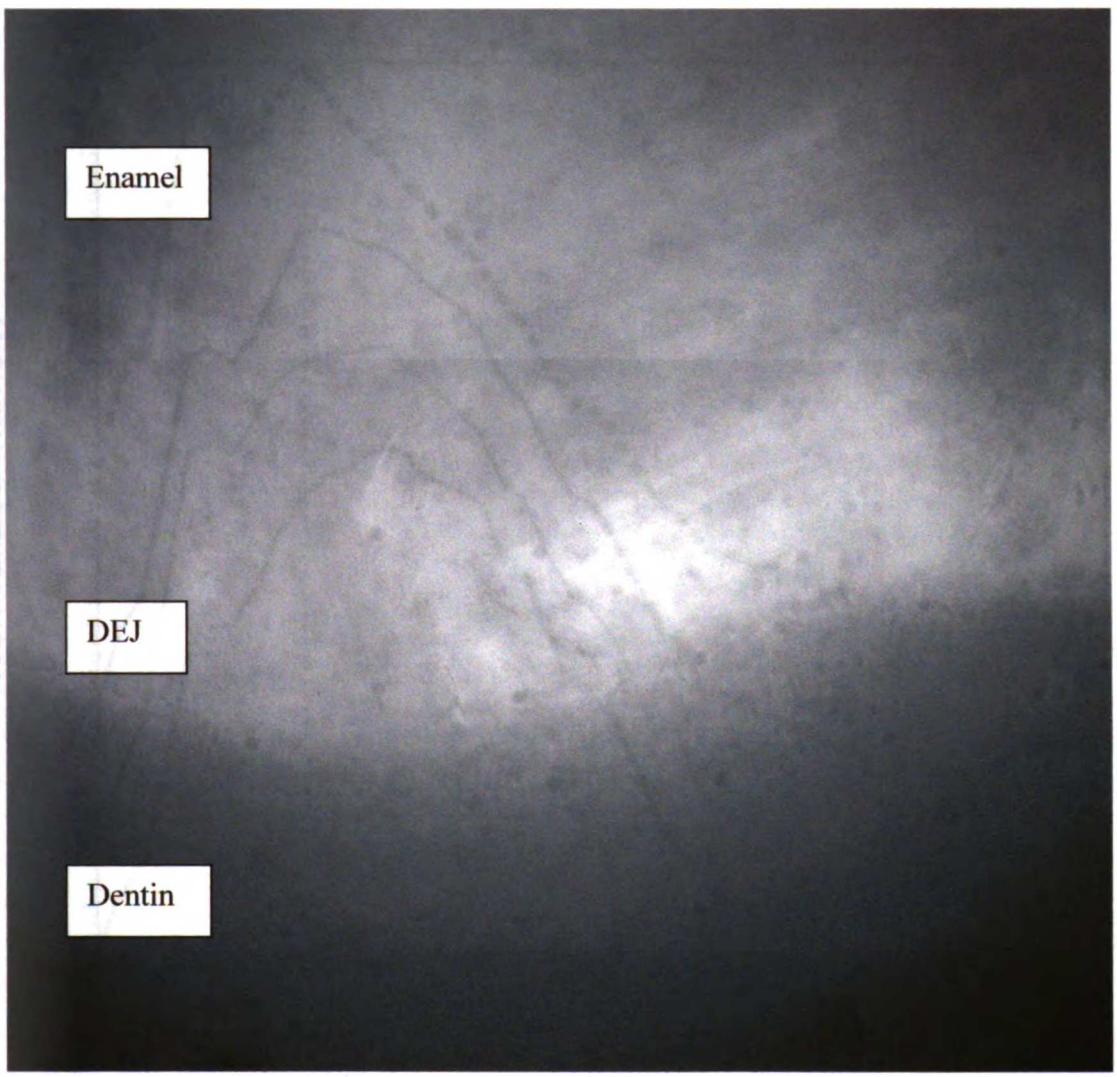

gure 3.3 A 880 μm by 860 μm fluorescence microscope image of the human DEJ gion taken with a 600 nm filter.

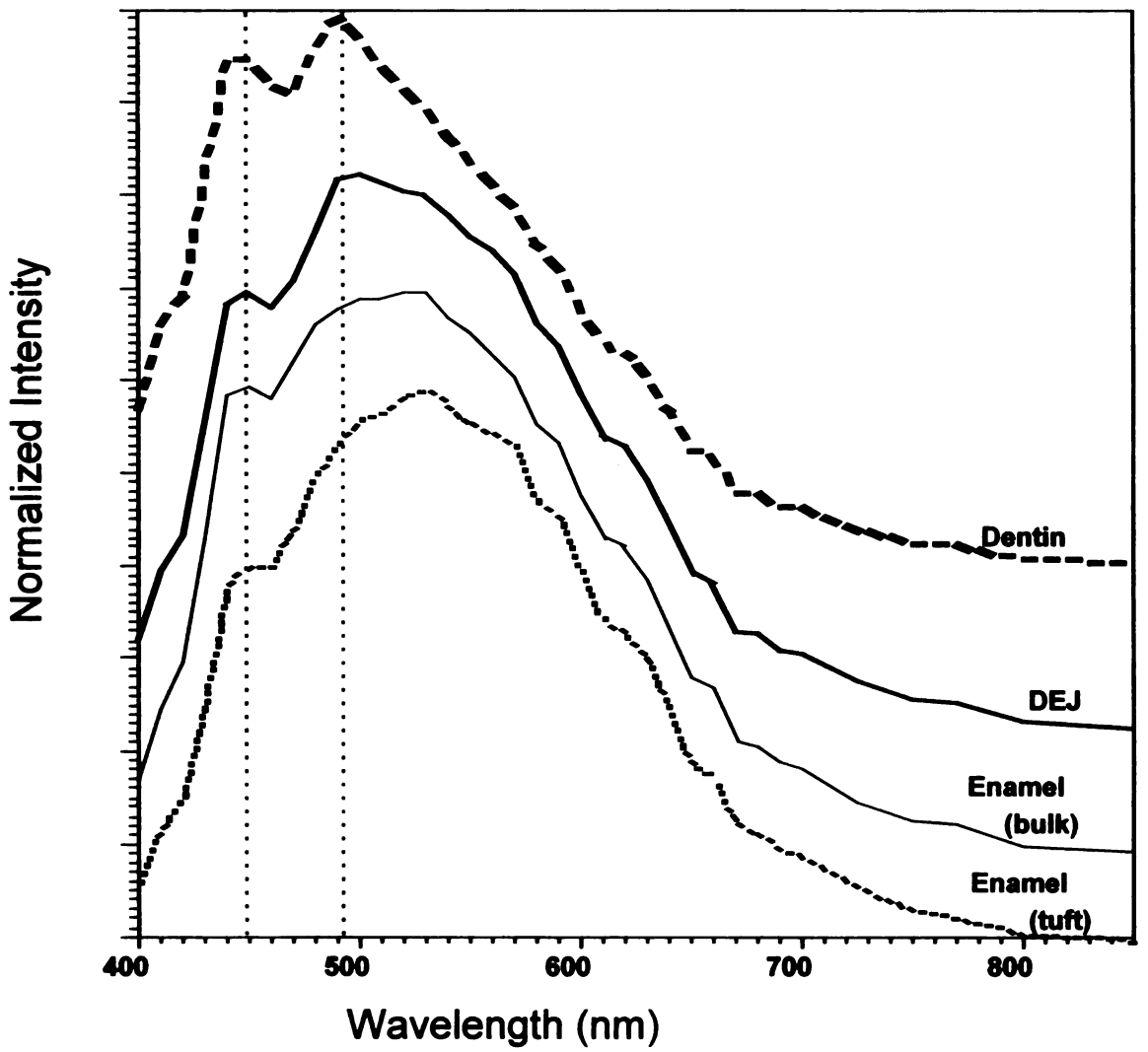

Figure 3.4 Tissue specific spectra under 351 nm argon-ion excitation.

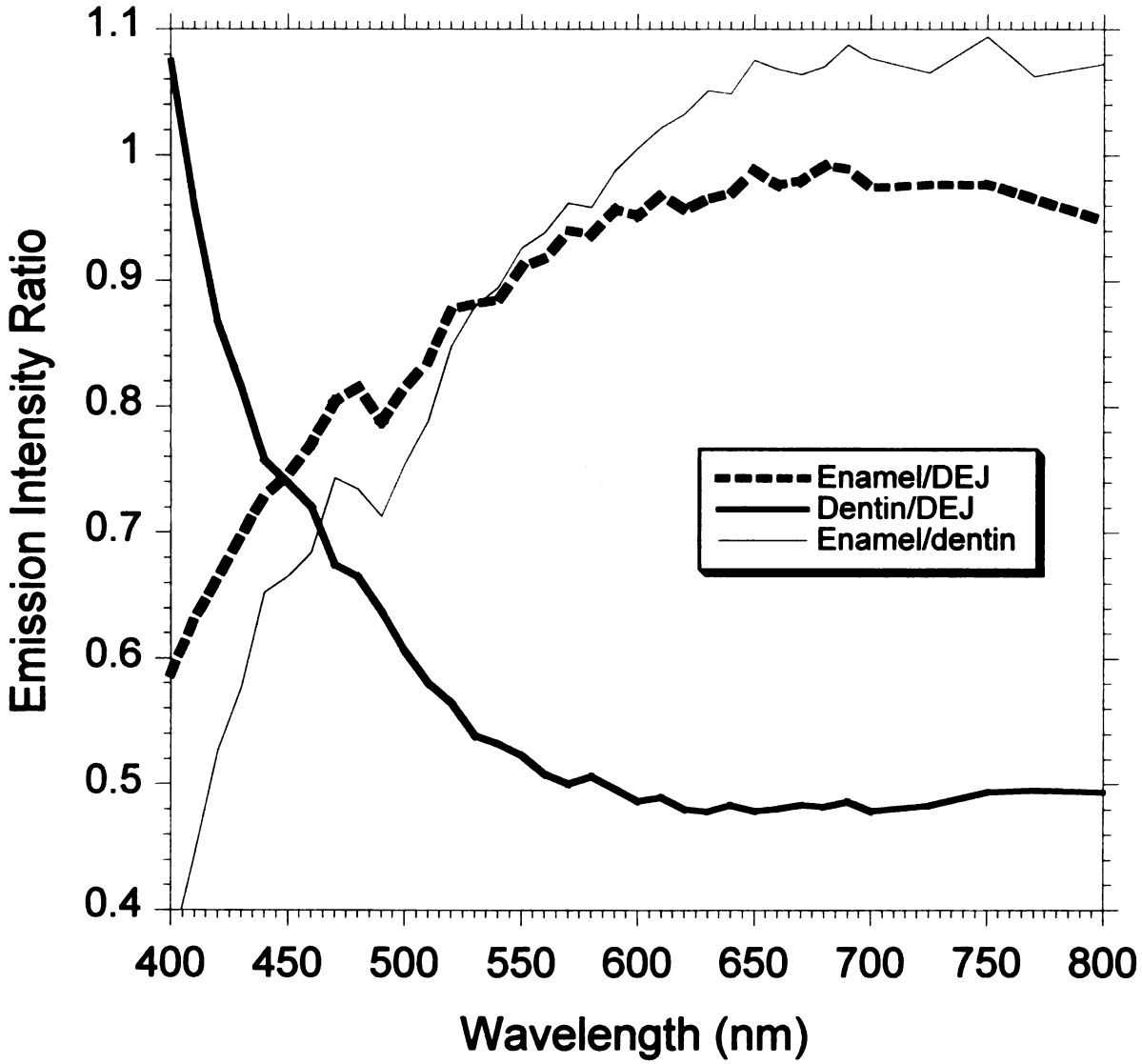

Figure 3.5 Emission ratios.

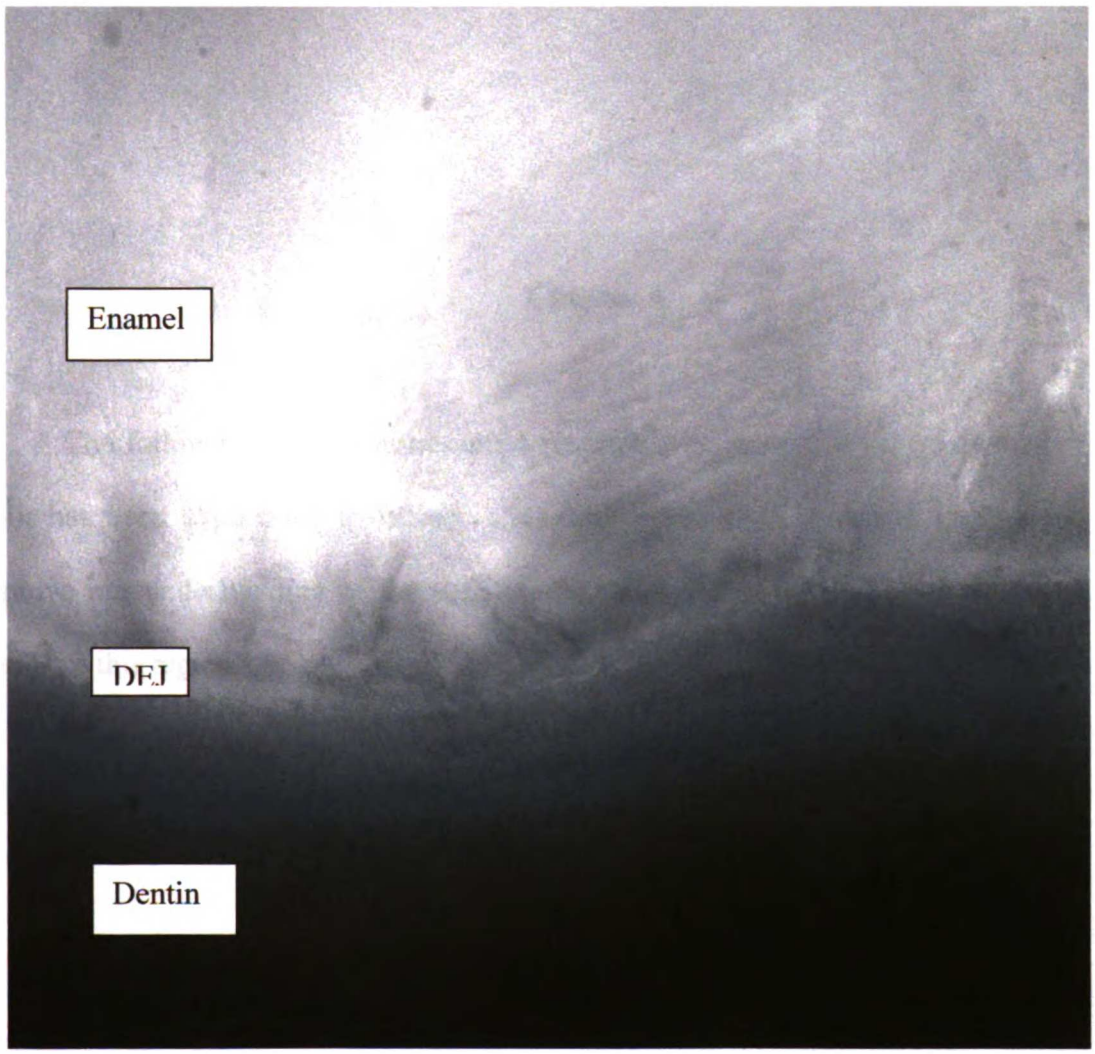

Figure 3.6. 600 nm/410 nm emission ratio. Width of the DEJ in this sample was estimated at 15 μm.

Chapter 4

The following Chapter represents a research paper intended for publication. The work has been expounded to include additional information, data and illustrations to improve our understanding of the structure-function relationships existing between the tissues of this region.

CHAPTER FOUR - A Coupled Nano-Mechanical and Micro Raman Spectroscopic Investigation of Human Third Molar DEJ

4.1 Summary

The dentino-enamel junction (DEJ) is an interfacial calcified dental tissue connecting a thin shell of enamel that covers the outer coronal surface of a tooth, to an underlying and thicker layer of dentin. The DEJ appears to be a critical dental tissue interface that permits joining these two materials whose mechanical properties exhibit widely dissimilar behaviors. AFM based nano-mechanical instrumentation and Raman microspectroscopy were used to define the width, composition and behavior of dry human third molar DEJ. Nano- mechanical testing was used to determine the elastic modulus and hardness of enamel, dentin and DEJ along lines of indentation points at 2 μm intervals that were oriented to cross the DEJ perpendicularly. The initial and final two indentation points were placed using maximal loads, producing microscopically visible orientation markers. Lines of Raman spectroscopy points at 1 μm intervals were placed across the DEJ and used the large nanoindentations as their orientation points. Functional DEJ width estimates were made based on results from nano-mechanical instrumentation and Raman microspectroscopy. Two statistical methods were used to estimate DEJ width. Mean functional DEJ width was estimated to range from 4.7 (± 1.2) μm to 6.1 (± 1.9) μm based on hardness and 4.9 (± 1.1) μm to 6.9 (± 1.9) μm based on modulus. Mean compositional DEJ width was estimated from Raman peak intensity variations to be in the range of 8.0 (± 3.2) μm to 8.5 (± 3.1) μm based on the phosphate peak, and 7.6 (±

3.2) μm to 8.0 (± 2.6) μm for C-H stretching mode. These estimates are within the range of reported DEJ width estimates using nanoindentation.

4.2 Introduction

The DEJ is a complex interfacial zone that joins two highly dissimilar calcified dental tissues, enamel and dentin. Enamel covers the coronal portion of a tooth and is primarily composed of a defective carbonate rich apatite that is arrayed in rods or prisms 4-5 μm in diameter. These rods are oriented to intersect the DEJ almost perpendicularly, and contain highly oriented and long apatite crystals.[1,2] Dentin is a calcified tissue that is compositionally similar to bone. In dentin, a calcium phosphate mineral that does not remodel following mineralization, acts to reinforce a collagen rich structural matrix. Dentin underlies enamel, and contains a series of dentinal tubules approximately 1 μm in diameter. These tubules contain dentinal fluid and odontoblastic cellular processes that are surrounded by columnar-like cylinders of peritubular dentin approximately 0.5-1 μm in thickness. The mineral component of peritubular dentin contains randomly oriented apatite crystallites.[3] The dentinal tubules are embedded within a collagen matrix-apatite reinforced composite and are the tracks of the retreating odontoblastic cells that act to form dentin during odontogenesis. The mechanical behavior of dentin is dominated by the behavior of intertubular dentin.[4]

The DEJ is the initiation surface for ameloblastic and odontoblastic activity during tooth formation[1] and is believed to play a critical role in enhancing the biomechanical integrity and resistance of a mature tooth to catastrophic fracture.[5] It has been found that the DEJ is more resistant to acid attacks[6] and crack propagation than is enamel.[5,7,8] The DEJ also has been observed to display a remarkable ability to transfer

loads between enamel and dentin such that cracks or fracture planes that are formed within enamel rarely propagate across the DEJ into the underlying dentin.[5]

In 1835, Fraenkel provided one of the earliest morphological descriptions of the DEJ.[9] The DEJ usually has been described as consisting of a series of 25-100 μm wide scallops, whose convexities are directed towards dentin.[1,2,10] These scallops are further subdivided into a series of smaller micro-scallops, which contain finer structures.[11] Little information exists on the size and variability of the scallops and subscallops, and considerable variability between and within a given tooth may exist.[10,12] This three-leveled architecture of the DEJ is believed to be responsible for the smooth gradient in the mechanical properties across this zone. It is also believed to contribute to reducing stress concentrations along this interface, providing a toughening mechanism to prevent catastrophic fracture.

Large variations in width estimates of the DEJ have been reported in the literature. A variety of mechanical testing equipment, with increasingly smaller sampling sizes, has been used to estimate the functional DEJ width based on its mechanical properties. Microhardness indentation profiles across the DEJ suggest that a broad gradation in mechanical properties exists.[5] Studies using Vickers microhardness measurements estimated the width of this interface as being between 27 to 100 μm.[13] Lin[14] and Lin and Douglas[5] determined a functional DEJ width in the range of 50 to 100 μm using microhardness and a conventional fracture mechanics approach. They reported that their functional width estimate was considerably wider than its optical presentation. The apparent discrepancy between these measurements may reflect a graded functional transition zone indicative of the DEJ region. Wang and Weiner reported a functional

transition zone width on the order of 200 μm using a Moiré fringe technique on human teeth.[15] Nanoindentation testing has been used to produce narrower DEJ width estimates. Fong *et al.*[8] employed a Berkovich nanoindenter and reported DEJ width estimates in the range of 15 to 25 μm, while Marshall *et al.* [7] used similar technology fitted with a cube corner indenter tip and estimated a functional DEJ width of 11 to 13 μm. Habelitz *et al.*[16] employed a nanoscratch technique and reported a very narrow, linearly varying transitional zone of 1-3 μm. Balooch *et al.*[17] used AFM based force modulation to measure the dynamic viscoelastic properties of the DEJ region and estimated DEJ width at 2 to 3 μm.

The observations that the mechanical properties of the DEJ exhibit a broad transitional behavior stand in contrast with data acquired from high-resolution imaging sources. Studies have indicated that a very narrow interfacial zone, if any, exists between mantle dentin and enamel.[18,19] Data derived from light microscopy, microradiodensity profiles and scanning electron microscopy suggest the margins of the DEJ are sharply demarcated and that the interface is very narrow, perhaps on the order of 2 μm.[5,7,11,20,21] Gallagher *et al.*[22] used a 351 nm laser excitation source to perform autofluorescence microscopy of human third molars and reported a 10 μm median DEJ width. Transmission electron microscopy of the DEJ found that the apatite crystals of dentin, and those of enamel might lay virtually in direct approximation to one another. This infers that the DEJ may not exist, and may simply represents a meeting surface between these materials. Observations of the fracture characteristics of a tooth indicate that the properties of the DEJ differ significantly from either enamel or dentin.[5] Observations of

the DEJ have also found that cracks formed in enamel become blunted or terminate upon entering the DEJ.

To this point, the mechanical properties of the DEJ have been explored in a limited fashion, and often from implied data. The very small size of the DEJ, coupled with our inability to isolate this material, have made it a difficult tissue to study using conventional mechanical testing techniques. To date, bulk property measurements of the DEJ have been impossible to obtain because conventional tensile, compressive and shear testing of the extremely small samples could produce complex geometries and non-uniform stress distributions. In addition, it could be extremely difficult to extract DEJ as there are indications that the tissue simply may not exist. Pioch and Staehle (1996) examined the shear strength of human and bovine teeth in the region of the DEJ and reported mean values of 39 MPa and 37.4 MPa, respectively.[23] They reported that fractures that occurred within dentin were not observed to occur at the DEJ, an indication of the scaling difficulties associated in working with this material.

Conventional morphologic studies of the DEJ[21] lack the ability to obtain chemically related information. Raman microspectroscopy is a technique to characterize the spatial distributions of organic and inorganic functional groups with resolution on the order of 1 μm.[24] The Raman spectrum of enamel is dominated by peaks or bands attributed to its mineral apatite at 591, 961 and 1071 cm^{-1}. The Raman spectrum of dentin indicates the presence of a larger proportion of organic compounds. C-H stretching bands at 2940 and 2880 cm^{-1} are more intense than those found in enamel. Amide I and III bands at 1670 and 1243 cm^{-1} have also been identified. These bands are similar to those

found in the Fourier transformation (FT) Raman spectra of bone and suggest a similar protein composition.[25]

The aims of this study were: 1) to obtain estimates of the functional and compositional widths of the DEJ using nano-mechanical testing and Raman microspectroscopy; and 2) compare and correlate the information to provide a better understanding of the structure-function relationships existing within the DEJ.

4.3 Materials and Methods

4.3.1 Sample preparation

Five recently extracted non-carious human third molars were collected from the UCSF Oral Surgery clinic according to a protocol previously approved by the UCSF Institutional Committee on Human Research. Immediately following extraction, each tooth was placed into physiologic saline solution (Hanks BSS) and maintained in a hydrated condition. The teeth were gamma radiation sterilized according to a standard protocol.[26] Each tooth was sagittally sectioned parallel to its buccal-lingual surface with a water-cooled diamond saw and hand-polished through a graded series of abrasive papers to a final polishing with 0.05 μm alumina paste. Each sample was subjected to ultrasonic cleaning between successive polishings to eliminate the possibility of cross contamination and surface scratching. Following final polishing, each sample was affixed to a magnetic backing plate with cyanoacrylate cement. The samples were then air dried by blasts with clean, dry compressed air until all surface moisture was removed. Each sample was then positioned on the testing platen of the relevant testing machine. Nano-indentation testing and Raman microspectroscopy imaging were subsequently performed across the same section of the DEJ of each tooth, in the region of its central pit.

Orientation makers were placed into the sample's surface to orient and position the sample so that the microRaman and nanoindentation testing lines occurred at virtually the same location.

4.3.2 Nano-indentation testing

An AFM-Triboscope system was used for imaging, nano-mechanical testing and placing optically visible sample orientation markers. The AFM-Triboscope system consisted of a Nanoscope III (Veeco Probes, Santa Barbara, CA) with its standard scanner head replaced by a Triboscope indenter system (Hysitron Inc., Minneapolis, MN). The coupled AFM-Triboscope system is a force generating and depth-sensing instrument.[7,27] It is capable of imaging the area of testing before and following sampling. The AFM Triboscope system consists of a three-plate capacitive force/displacement transducer in which a cube corner diamond tip is affixed via a central drive post to the middle plate. A voltage applied between the middle and the outer drive plates was used to generate an indentation force proportional to the square of the applied voltage. A feedback capacitive sensor determined indentation depth by sampling the feedback voltage. The system was capable of producing load-displacement curves at precisely selected locations with indentation loads ranging from 1 to 15,000 μN. A 90°-cube corner diamond tip was used for all indentations. This tip was calibrated before and after testing. A triangular force loading profile with load adjustments to ensure measurement validity as the mechanical properties changed from those of dentin to those of enamel along each line of nanoindentations was used for each measurement. Trial indentations were placed across the DEJ prior to experimentation to determine typical operational measurements for valid testing points. The most important parameters monitored were indenter force

and vertical indenter tip displacement. The indenter load was adjusted with trial indentations until the smallest load capable of producing valid indenter points could be determined for enamel and dentin. These loads produced relatively constant vertical indenter displacements and sampling volumes. The corresponding indenter loads were then applied when clearly in enamel or dentin. The indenter loads were adjusted when crossing the DEJ to maintain a relatively constant vertical indenter displacement in the range of 300 to 400.nm.

Each indentation produced a load-deformation curve from which the reduced elastic modulus was calculated using the unloading portion of the curve. Hardness was calculated as the maximum force divided by the projected contact area between the tip and the sample under maximum load, in accordance with the methods of Doerner and Nix.[28] The same tip was used for imaging, nano-mechanical testing and placing optically visible sample orientation markers. These markers were subsequently used to relocate and reorient the sample following its removal from the Triboscope and its placement on the Raman microspectroscope's pedestal.

In three of the samples, a single line of nano-indentation points, each having a length of at least 50 μm, was placed across the DEJ at 2 μm intervals to prevent interference between adjacent indentations. In the remaining two samples, two parallel lines of nano-indentation points, each with a length of at least 50 μm, were placed across the DEJ in opposite directions. All lines were made perpendicular to the DEJ and were oriented so that their midpoint was roughly coincident with the expected middle of the DEJ. Trial indentation lines of greater overall lengths were placed across the DEJ to ensure baseline modulus and hardness levels were achieved in both enamel and dentin. At

the start of each indentation line, two indentation points were placed under the maximum indentation load. A single indentation point was similarly placed at the end of each line. These terminal points were used as orientation markers as they were visible with the optical microscopes of both the AFM-Triboscope and the Raman microspectroscope. Along each indentation line, nano-indentations were made at 2 μm intervals to prevent interference with adjacent indentations. In three of the samples, a single line of nano-indentation points, each having a length of at least 50 μm, was placed across the DEJ. In the remaining two samples, two parallel lines of nano-indentation points, each with a length of at least 50 μm, were placed across the DEJ in opposite directions. These lines were offset from one another by 2 to 3 μm. All lines were made perpendicular to the DEJ, and oriented so that their midpoint was roughly coincident with the expected middle of the DEJ. Trial indentation lines having greater overall lengths were placed across the DEJ to ensure baseline modulus and hardness levels were achieved in both enamel and dentin. Plots of hardness and modulus versus location were made. An estimate of the functional width of the DEJ was then made for each indentation line according to the statistical methods described below.

4.3.3 Raman microspectroscopy

Raman microspectroscopy was used to characterize the mineralized matrix of dentin. This is a non-contact, non-destructive technique that identifies and quantifies the functional groups that are present in a sample being tested. An HR-800 Raman micro-spectrophotometer (Jobin Yvon, Horiba, France) was used to define the Raman spectra of enamel, dentin and DEJ. This instrument also provided an estimate of the compositional width of the DEJ based on mineral and organic content differences. The HR-800 Raman

micro-spectrophotometer uses monochromatic radiation emitted by a He-Ne laser having a wavelength of 632.8 nm and operating at 20 mW of power before entrance optics. The spot size of the HR-800 is on the order of 0.5 μm. Spectra were measured at 1 μm increments along lines across the DEJ in the same manner as for nano-indentation testing, yielding compositional information at half the sampling incremental distance of the nano-indentation study.

Raman microspectroscope imaging lines were oriented parallel to the orientation points previously placed in the sample by the AFM-Triboscope using the microspectroscope's 50x objective lens. The line of Raman spectra was laterally offset by 5 μm to avoid disturbances that might arise from the plastic deformation induced by the nanoindents. The sample was scanned using a 30 second acquisition time for each Raman measurement point. Spectra were acquired for the phosphate (PO_4^{3-}) band at 960 cm^{-1} and the C-H stretching mode at 2900 cm^{-1} in three of the samples. These constituted characteristic functional groups from the mineral (phosphate) and organic constituents, respectively. In one sample, spectra were acquired for only the phosphate band. One sample that received nano-mechanical testing was not examined by Raman spectroscopy because of technical difficulties. Plots of PO_4^{3-} and C-H stretch intensity versus location were made. An estimate of the compositional width of the DEJ was then determined for each imaging line using the statistical methods described below. The results were then compared to each other and to the nano-mechanical results.

4.3.4 Statistical analyses

To avoid the arbitrariness of estimating DEJ width by simply viewing graphed data, two statistical methods were developed using the SAS programming language. For

each method, an algorithm was developed to select data inflection points based on deviations from linear models of the nano-mechanical and Raman response of dentin and enamel. An inflection point was defined as being the first data point encountered that varied significantly from the linearly modeled response. Inflection points defined the dentin-DEJ and DEJ-enamel borders. DEJ width was defined as the distance between these inflection points.

According to the first statistical method, a multiplier, K, was used to obtain statistical cut points. The multiplier, K, was used to modify the value of the standard deviation calculated for the series points under consideration. Values of K were determined by trial and error, and were uniformly applied according to Table 4.1. Eyeball methods were used to replace some of the outlying values supplied by the algorithm. This was most evident in enamel close to the DEJ where data could sometimes vary significantly between successive instrumentation points. The first and last nine points of each series were used to determine a mean and standard deviation for that series. The mean and standard deviation provided a cut point, computed as: mean +/- (K * standard deviation). The nano-indenter and Raman microspectroscopy data for dentin and enamel were defined to behave as linear models. To detect the dentin-DEJ junction, the algorithm was defined to begin at the dentin end of the line of data points and move inward towards the DEJ. Each point was considered in turn beginning with the fourth data point. For each point considered, the algorithm determined if that point, and the preceding three points were less than the value of the prior cut point, and if the following three points exceeded the value of the post cut point. The first such point under consideration that detected a difference was considered the dentin-DEJ inflection point. The DEJ-enamel inflection

point, or where the junction 'ends' and enamel 'begins', was similarly determined. The first and last nine points of each series were used to estimate the mean and standard deviation of, respectively, the dentin and enamel measurements for that series.

The second method for estimating DEJ width was based on detecting differences from linear models describing the DEJ's nano-mechanical and Raman behaviors. In this approach, mean values for the response of dentin and enamel were initially determined for each data line. These values were used to identify the construction midpoint of the DEJ. The construction midpoint was calculated as the middle of the difference between the mean response values of dentin and enamel. The data points located immediately on each side of the construction midpoint were then identified. These three (eleven for Raman) points were used to fit a linear model describing the DEJ's behavior.

The linear model of the DEJ's behavior was used for statistical testing to estimate the dentin-DEJ and DEJ-enamel borders. In this approach, each point was sequentially examined to determine if it was within the eighty percent confidence interval of the predicted value. The first points moving outward from the construction midpoint that deviated from the linear DEJ model defined the inflection points between the DEJ and dentin or the DEJ and enamel. The width of the DEJ was calculated as the distance between these inflection points.

4.4 Results

Typical curves for the normalized hardness, modulus, C-H stretch and phosphate band intensities are shown in Figures 4.1 and 4.2. Mineral content was found to increase monotonically from dentin to enamel, while organic content decreased monotonically.

Functional and compositional DEJ width estimates are tabulated in Table 4.2. DEJ width estimates based on hardness were 6.1 (± 1.9) μm according to statistical method 1 and 4.7 (± 1.2) μm according to statistical method 2. DEJ modulus based width estimates were 6.9 (± 1.9) μm for method 1 and 4.9 (± 1.1) μm for method 2, respectively. Tests of statistical difference between the mean widths as estimated by either indentation method for each statistical method indicated that the indenter results for hardness and modulus yielded similar and consistent estimates of the functional DEJ width. Since no statistical difference between the results was noted, we combined the indentation width estimates into a single "technique" width estimate of 6.4 (Standard Error ± 0.63, 95% confidence interval: 4-9) μm according to method 1 and 4.6 (Standard Error ± 0.60, 95% confidence interval: 2-7) μm for method 2. These estimates that were obtained from combined methods were provided by a general linear model. The general linear model contained adjustments for multiple measures made on the same tooth, and are contained in Table 4.3.

The DEJ functional width estimates based on Raman-microspectroscopy yielded a phosphate band estimate of 8.0 (± 3.2) μm according to method 1 and 8.5 (± 3.1) μm according to method 2. The C-H stretching mode width estimates were 7.6 (± 3.2) μm for method 1 and 8.0 (± 2.6) μm for method 2. Tests of statistical difference between mean DEJ width estimates for the two Raman methods showed no significant difference. As with the indentation data, we combined the two Raman estimates into a single microspectroscopy estimate of 7.8 (Standard Error .± 0.86) μm with a 95% confidence interval of 4-11 μm according to method 1. The combined estimate (Table 4.3) provided

by method 2 was 8.3 (Standard Error ± 0.74) μm with a 95% confidence interval of 5-12 μm.

The DEJ width estimates based on the two types of measurements, nano-indenter and Raman microspectroscopy, did not show a statistically significant difference according to method 1. However, they did show a statistically significant difference according to method 2 (p-value = 0.035 from SAS proc mixed). Taking the lower 95% confidence interval of the smallest estimate and the upper 95% confidence interval of the largest estimate gave a conservative estimate of the width of the DEJ for each instrumentation method based on multiple measurements. For the indenter data, this range was 2-9 μm; for the Raman data it was 4-12 μm.

4.5 Discussion

In the present study, we characterized the chemical composition and the nanomechanical behavior of the same region of the DEJ using Raman microspectroscopy and nano-indentation testing. The Raman microspectroscope provided information concerning the mineral and protein variations across this interface. The coupled AFM-Triboscope system allowed site-specific mechanical property measurements to be made, affording estimates of the functional DEJ width by spatially mapping the nano-mechanical response across the junction. Since for most samples both instruments tested the same areas of each sample, we were able to monitor the variation in mechanical properties and chemical composition across this interface and compare the results to each other.

This research found consistent mean functional DEJ width estimates using hardness and modulus of between 4.7 and 6.1 μm. The nanoindentation DEJ width

estimates based on hardness data were somewhat narrower than estimates obtained using modulus data, although the difference was not statistically significant. Hardness and modulus were found to vary linearly across the DEJ, and were highest in enamel. This observation was in agreement with earlier work.[5,7] The nano-mechanical results represent a refinement in the functional width estimates from previous nano-indentation results.[7,8] This may result from the use of an extremely sharp cube corner tip that allowed shallower indentation depths and smaller sampling volumes to be made. In our study, we also used the nanoindenter to place optically visible sample orientation markers that allowed the same area of the DEJ to be sampled by the nanoindenter and the Raman microspectroscope.

No unique or constant Raman signature was observed for the DEJ using either the C-H stretching mode or the phosphate peak data. Relatively linear variations in the Raman profiles for the phosphate and C-H stretching mode peaks were observed across the DEJ from those of dentin to those of enamel. The phosphate peak, an indication of the mineral content present, was found to be highest in enamel and lowest in dentin. The converse was observed for the C-H stretching mode, an indication of the protein content variation across this region. These observations were in accordance with conventional theories. No characteristic phosphate or C-H stretching mode peak or peak shift was observed for the DEJ.

Estimates of DEJ width based on Raman microspectroscopy produced results that were consistent and greater (by approximately 1 μm) than those determined from nano-mechanical property profiles. The variance of the Raman microspectroscopy width estimates was roughly twice that found using nano-mechanical testing. The effect of

testing direction was not determined for micro-Raman width estimates due to insufficient data. Raman microspectroscopy measurements were made at 1 μm intervals. The distance between successive nano-mechanical measurement points was on the order of 2 μm. Thus, the Raman data was twice as variable as the nanoindentation data, yet its sampling distance was half that obtained from nanoindentation testing.

The use of maximal load terminal indentation points as optically visible sample orientation markers allowed us to sample the same areas of the same teeth using both nanoindentation and Raman-microspectroscopy. The nano-mechanical and micro-Raman data lines were made parallel to one another, but with approximately 5 μm of lateral offset parallel to the DEJ in order to prevent possible interaction effects. The results indicate that the nano-mechanical DEJ width estimates were narrower and less variable than those that used Raman microspectroscopy.

The Raman and indentation results showed monotonic spectroscopic and mechanical property variations across the DEJ. While it is possible that the observed variation in properties across the DEJ could represent the actual mechanical and chemical properties, it is more likely that what we observed is actually a superimposition or averaging of the properties of dentin and enamel within this region.

The DEJ is a highly irregular and undulating junction. It has a three-level structure consisting of 25-100 μm scallops that are subdivided by 2-5 μm microscallops and smaller scale structures. Indentations and spectroscopy performed on such a three-dimensional structure may sample varying mixtures of the constituents bordering each side of the interface since sampling occurs over a finite volume. The greater the sampling volume, the higher the probability that sample mixing is occurring and the greater the

variability in the results seen. Sample volumes consisting of two or more phases produce property measurements different from those of the bordering materials. Testing modalities that minimize sampling depth, width and volume produce more accurate material property measurements having greater spatial resolution. For indentation testing, narrower DEJ width estimates were dependent upon minimizing indentation depth via the use of sharper indentation tips since they lead to decreased sample mixing and narrower step widths.

In this study, we attempted to control the effects of the undulating scalloped architecture of the DEJ by orienting the sampling lines to cross the DEJ at a perpendicular angle. It is likely that sampling lines also crossed the scalloped DEJ at other angles, leading to increases in the size and variability of the functional DEJ width estimates. Additionally, since approximately 5 μm of lateral offset between paired indentation and spectroscopic sampling lines were made; the material sampled by each method was slightly different. Nanoindentations were performed prior to Raman microspectroscopy because we needed to place optically visible sample orientation points that allowed us to coordinate data from the different testing modalities. These points were placed using the maximum indentation load. A single maximal load indentation point was placed to denote the starting point for the line of indentations. Two maximal load indentations were placed to denote the end of the indentation line. The maximum load indenter points were placed across the middle of the scallop. Each line of indentation points was then placed directly between these optically visible orientation points or markers. Raman microspectroscopy was subsequently performed along a line parallel to, but with approximately 5 μm of lateral offset. Such a condition would naturally result in

a greater DEJ width estimate for Raman microspectroscopy simply because a line crossing the curved DEJ is not perpendicular there.

Differences in sampling volume also exist between Raman microspectroscopy and nano-indentation testing. The sampling volume we used for Raman microspectroscopy was on the order of 1 μm^3. This is 4 to 20 times greater than the nano-indentation sampling volumes that were used. The Raman sampling volume was also less defined than the plastically deformed zone indicative of nano-mechanical testing. The Raman sampling depth was also ill defined. Such conditions made it much easier for sample mixing to occur with Raman microspectroscopy. These differences help explain the greater variability observed in the spectroscopy results. Coupling the increased sampling volumes for Raman imaging with the size of the DEJ's microscallops it is evident that sample mixing was occurring more often with Raman microspectroscopy than for nanoindentation testing. It is likely that this may also be responsible for the wider DEJ width estimates obtained using Raman microscopy. Further, minute changes in composition can produce significant changes in mechanical properties. Therefore, indentation testing may be more sensitive to detecting differences than alterations in composition. These factors can help explain the greater DEJ width estimates obtained with Raman microspectroscopy.

4.6 Conclusion

No characteristic mechanical or spectroscopic properties were noted for the DEJ. DEJ width estimates of 6.1 to 6.9 μm based on nano-mechanical testing, and 7.6 to 8.5 μm based on micro-Raman spectroscopic mapping were found for either statistical method that was used to analyze the results. The DEJ width estimates were found to be

essentially independent of the statistical techniques employed. It is probable that the DEJ's undulating three-leveled architecture is responsible for many of the observed behaviors. Further studies involving larger sample sizes could improve our understanding of this variability. Since this study was performed using only human third molars, studies should be performed to determine the coupled mechanical and spectroscopic behaviors across the DEJ region for other tooth types and for other species. Our results are in line with earlier work,[29] and represent a mechanism for linking the observed physical properties to their underlying composition.

4.7 References

1. Ten Cate AR (1994) Oral Histology: Development, Structure, and Function. 4th Ed., St. Louis: Mosby.

2. Bhaskar SN, editor. Orban's oral histology and embryology. 11th Ed. Chicago: Mosby year Book; 1990. p 70-71.

3. Marshall GW. Dentin: Microstructure and characterization. *Quintessence Int* 1993;24:606-617.

4. Kinney JH, Balooch M, Marshall GW, Marshall SJ. A micromechanics model of the elastic properties of human dentine. Arch Oral Biol; 1999;44:813-822.

5. Lin CP, Douglas WH. Structure-Property Relations and Crack Resistance at the Bovine Dentin-Enamel Junction. J Dent Res 1994; 73:1072-1078.

6. Tramini P, Pelissier B, Valcarcel J, Bonnet B, Maury L. A Raman spectroscopic investigation of dentin and enamel structures modified by lactic acid. Caries Res 2000; 34:233-40.

7. Marshall GW, Jr., Balooch M, Gallagher RR, Gansky SA, Marshall SJ. Mechanical properties of the dentinoenamel junction: AFM studies of nanohardness, elastic modulus, and fracture. J Biomed Mater Res 2001; 54:87-95.

8 Fong H, Sarikaya M, White SN, Snead ML. Nano-mechanical properties profiles across dentin-enamel junction of human incisor teeth. Mat Sci Engi C, Biomim Supramol Sys 2000; C7:119-28.

9. Fraenkel L. De penitiori dentium humanorum structura observationis. Diss Vratislaviae, Pressburg. 1835.

10. Whittaker DK The enamel-dentine junction of human and Macaca irus teeth: A light and electron microscope study. *J Anat* 1978;83:323-335.

11. Bodecker C FW. T he d istribution of living matter in human dentin, cement and enamel. Dent Cosmos 1957; 20:582-590.

12. Scott JH, Symons NBB. Introduction to dental anatomy. 6th ed, Edinburgh,: Livingstone; 1971:448.

13. White SN, Paine ML, Luo W, Sarikaya M, Fong H, Yu ZK, Li ZC, Snead ML. The d entino-enamel j unction i s a b road t ransitional z one u niting dissimilar bioceramic composites. J Am Ceram Soc 2000; 83:238-240.

14. Lin CP (1993). Structure-function property relationships in the dentin-enamel complex and tooth restoration interface. PhD thesis, University of Minnesota.

15. Wang RZ, Weiner S. Strain-structure relations in human teeth using Moire fringes. *J Biomech* 1998;31(2):135-141.

16. Habelitz S, Marshall SJ, Marshall GW, Jr., Balooch M. The functional width of the dentino-enamel junction determined by AFM- based nanoscratching. J Struct Biol 2001; 135:294-301.

17. Balooch G, Marshall GW, Marshall SJ, Warren OL, Asif SAS, Balooch M. Evaluation of a new modulus mapping technique to investigate microstructural features of human teeth. J Biomech 2004;37:1223-1232.

18. Bencz L. Befunde an der Dentinzement Grenze. Z Stomat 1927; 5:877-896.

19. Blackwood HJJ. Intermediate cementum. Brit dent J 1957; 102:345-350.

20. Brear K, Currey JD, Pond CM, Ramsay MA. The mechanical properties of the dentine and cement of the tusk of the narwhal Monodon monoceros compared with those of other mineralized tissues. Arch Oral Biol 1990; 35:615-21.

21. Yamamoto T, Domon T, Takahashi S, Islam MN, Suzuki R. The fibrillar structure of the cemento-dentinal junction in different kinds of human teeth. J Periodontal Res 2001; 36:317-321.

22. Gallagher RR, Balooch M, Balooch G, Wilson RS, Marshall SJ, Marshall GW. A Coupled Nano-Mechanical and Micro Raman Spectroscopic Investigation of Human Third Molar DEJ.

23. Pioch T, Staehle HJ. Experimental investigation of the shear strengths of teeth in the region of the dentinoenamel junction. Quintessence Int 1996;27:711-714.

24. Pelletier M, Pelletier MJ. Analytical applications of Raman spectroscopy, Malden, MA: Blackwell Science; 1999:478.

25. Hendra P, Jones C, Warnes G. Fourier transform Raman spectroscopy: instrumentation and chemical applications. Ellis Horwood series in analytical chemistry, New York: Ellis Horwood; 1991:311.

26. White JM, Goodis HE, Marshall SJ, Marshall GW. Sterilization of teeth by gamma radiation. J Dent Res 1994; 73:1560-7.

27. Balooch M, Wu-Magidi IC, Lundkvist AS, Balazs, Marshall SJ, Marshall GW, Seikhaus WJ, Kinney JH. Viscoelastic properties of demineralized human dentin in water with AFM-based indentation. J Biomed Mater Res 40:539-544,1998.

28 Doerner MF, Nix WD. A method for interpreting the data from depth-sensing indentation instruments. J Mater Res 1986;1,601-609.

29. Marshall SJ, Balooch M, Habelitz S, Balooch G, Gallagher R, Marshall GW. The dentin-enamel junction-a natural multilevel interface. J European Ceram Soc 2003 23: 2897-2904.

4.8 Tables and Figures

Tables:

Figures:

Instrumentation Modality	Dentin	Enamel
Nano-indenter	8	3
Raman	6	3

Table 4.1: Values of the multiplier, K.

		Statistical Method 1		Statistical Method 2	
Measure	Observations	Mean (μm)	Std Dev (μm)	Mean (μm)	Std Dev (μm)
Hardness	7	6.1	1.9	4.7	1.2
Modulus	7	6.9	1.9	4.9	1.1
Raman 960	4	8.0	3.2	8.5	3.1
Raman 2900	3	7.6	3.2	8.0	2.6

Table 4.2. N ano-indentation and Raman microspectroscopy DEJ width estimates. The DEJ width estimates were derived using different statistical modeling techniques. Statistical Method 1 was derived using linear enamel and dentin models. Method 2 assumed a linear model that described the behavior of the DEJ. The first points that deviated from the linear models defined the inflection points. DEJ width was defined as the distance between these points.

Measure	Method 1 (μm)				Method 2 (μm)			
	Mean	Std. Err.	95% CI	Std. Dev. (1)	Mean	Std. Err.	95% CI	Std. Dev. (1)
Indentation	6.4`	0.63	4 – 9	1.8	4.6	0.60	2 – 7	1.1
Raman	7.8	0.86	4 – 11	2.9	8.3	0.74	5 – 12	2.7

Table 4.3. Summary statistics for combined measures DEJ width estimates. (1) The Standard Deviation (Std. Dev.) was computed using measured DEJ widths. Other measures were computed using width estimates that employed a linear model which adjusted for multiple measurements on same tooth and combined measurements using the same instrumentation device (hardness and modulus or Raman 960 & 2900).

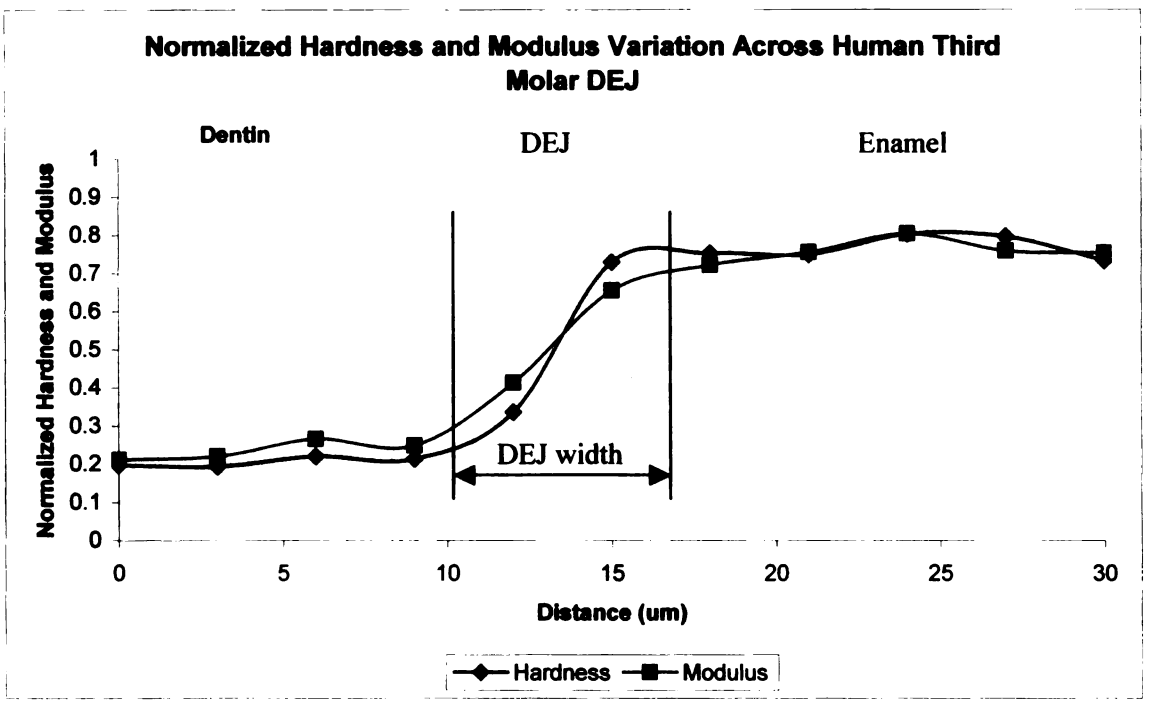

Figure 4.1. Typical normalized hardness and modulus variations along a line oriented to perpendicularly cross the DEJ. The hardness and modulus DEJ width estimates in this sample were both 8 μm. Hardness and modulus exhibit monotonic increases across the DEJ from those of bulk dentin to those of bulk enamel.

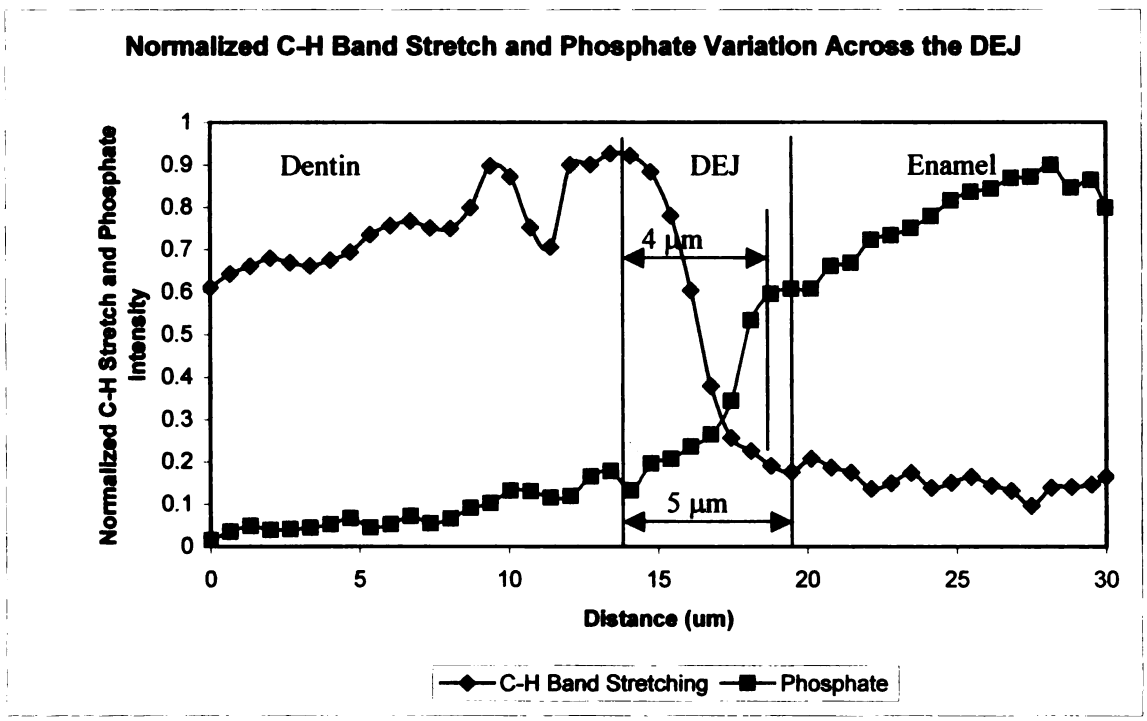

Figure 4.2. Typical normalized Micro-Raman C-H stretch (2900 cm^{-1}) and phosphate bond (960 cm^{-1}) peak intensity variations along a line oriented to cross the DEJ at a perpendicular angle. In this sample, DEJ width was estimated at 4 µm based on the peak phosphate band stretch intensity variation. Peak C-H stretching estimated DEJ width at 5 µm.

Chapter 5

The Chapter is based on a previously published research paper. The work has been expanded to include additional data, illustrations, and information intended to improve understanding of the body of research. The citation for the published research document is:

Marshall SJ, Balooch M, Habelitz, S, Balooch G, Gallagher R, Marshall GW. The dentin-enamel junction-a natural multilevel interface. J European Ceram Soc 2003;23:2897-2904.

CHAPTER FIVE - The Dentin-Enamel Junction-A Natural Multi-Level Interface

5.1 Summary

A tooth is primarily composed of two constituents, enamel and dentin (Figure 5.1). Enamel forms the hard, brittle and abrasion resistant surface layer covering the outer coronal portion of the tooth. Dentin is a softer and tougher biomaterial that underlies enamel and makes up the remaining bulk of the tooth. Dentin acts to distribute the masticatory stresses from enamel to the supporting alveolar bone. These materials are joined to one another by an undulating calcified dental interface known as the dentin-enamel junction, or the DEJ. The DEJ is a critical structure joining these dissimilar dental tissues and functions to prevent the propagation of cracks formed in enamel from extending into dentin (Figure 5.2). The DEJ has been modeled as having a 3-level architecture, 25-100 μm scallops with convexities directed towards dentin, 2-5 μm microscallops lining the inside of the scallops and finer level structures. AFM based functional widths estimates derived from differences in the mechanical properties observed, chemical composition variations and imaging across the DEJ were made. Lines of nanoindentation points estimated a functional DEJ width based on mechanical property differences of 11.8 μm, while AFM based nanoscratching estimated DEJ width at 2.0 μm. The unique architecture of the DEJ may help explain the different functional width estimates based on enamel and dentin phase intermixing. The goal of this research was to develop a biomimetic model that could be used to develop interfaces for joining dissimilar materials and for the development of improved dental restorative materials.

5.2 Introduction

5.2.1 Overview

The dentin-enamel junction (DEJ) is an undulating, multileveled, calcified tissue interface that appears to have unique qualities permitting the joining of calcified dental tissues having highly dissimilar properties. As illustrated in Figure 5.1, the DEJ appears as an interface separating enamel from dentin. Despite considerable research, questions remain regarding the characteristics, properties and functions of the DEJ.[1,2,3,4,5,6,7,8,9] These include the architecture and functional width of the scalloped interface, its mechanical and optical properties, and the resultant fracture resistance of this region. Further, it is not know if the DEJ exists as a unique or histologically distinct tissue. Advances in nanotechnology and AFM based nanomechanical testing allow imaging and characterization of the mechanical properties. Study of the fracture properties and fracture characteristics of the DEJ could suggest mechanisms by which it acts to resist the propagation of cracks initiated in enamel from extending into dentin. Improving our understanding of the architecture and mechanisms of action of the DEJ could be used to develop improved bonding materials for joining materials having widely dissimilar behaviors.

5.2.2 The Architecture of Enamel, Dentin and the DEJ

The DEJ is a calcified dental tissue interface uniting two dental tissues having widely dissimilar properties. The DEJ occupies a thin layer sandwiched between hard and brittle enamel covering the outer occlusal tooth surface, with softer and tougher dentin that comprises the remaining bulk of the tooth. Enamel is primarily comprised of a

carbonate rich defective apatite that is arranged in long rods or prisms 4-5 μm in diameter. The apatite lies virtually perpendicular to the DEJ and contains highly oriented and very long apatite crystals.[10,11] Dentin, compositionally, is similar to bone and is a tougher biological composite than enamel. Dentin makes up the majority of the tooth and exists as a hydrated biomaterial. It is composed largely of nano-crystalline carbonated apatite mineral[12] (approximately 45 percent by volume), type-I collagen fibrils (approximately 30 percent by volume) and fluid (approximately 25 percent by volume). The apatite mineral is organized in the form of 5 nm thick crystallites on a scaffold of 50 to 100 nm diameter collagen fibrils. The apatite is believed to provide structural strength, while the organic component provides improved fracture properties.[13] The fluid component is primarily located within the dentinal tubules (approximately 75 percent), with the remaining 25 percent being distributed throughout the intertubular matrix.[14]

The distinctive feature of dentin is that it is primarily composed of two types of structures, peritubular dentin and intertubular dentin. Peritubular dentin consists of a 1 μm diameter tubule surrounded by a 0.5-1 μm thick cylindrical wall containing randomly oriented apatite crystallites.[15] Contained within the tubules are odontoblastic cell processes. The odontoblasts are vital structures that are responsible for forming dentin. The dentinal tubules represent the formative tracks taken by the odontoblasts during their retreat toward the pulp chamber. With tooth maturation, the odontoblasts reside on the surface of the pulp chamber, and continue to move inward with age, forming secondary dentin throughout life. The cylinders of peritubular dentin are embedded within a collagen matrix-apatite reinforced composite known as intertubular dentin. The mineralized collagen fibrils form a relatively planar and felt-like structure that is oriented

perpendicular to the long axis of the dentinal tubules.[16] Significant variations exist in the morphology, architecture and tubular density of dentin dependent upon the proximity to the pulp chamber.

The DEJ is believed to play critical roles as the initiation surface for ameloblastic and odontoblastic activity during tooth formation,[11] and upon maturity it provides a critical role for the tooth by increasing its resistance to catastrophic fracture.[4] Cracks that have been initiated in enamel can rapidly propagate through it but generally do not cross the DEJ to extend into the underlying dentin (Figure 5.2). Catastrophic tooth fracture occurs when the crack extends through the tooth extending into the pulp chamber or extending into the biologic width of the periodontium. It is widely held that the principle function of the DEJ is to join enamel to dentin, a significantly tougher biologic composite that can absorb and distribute the occlusal stresses

The structure of the DEJ has generally been described as being scalloped with convexities directed towards the dentin and concavities directed towards the enamel (Figures 5.3a and 5.3b). These adaptations are thought to enhance bonding between enamel and dentin. Little information on the size and variability of these structures exists. Considerable variability between animals, between teeth and within a given tooth may exist.[9,17] Whittaker examined 162 deciduous and permanent teeth extracted from humans and monkeys and found considerable variability existed.[9] In human teeth the scallop size was found to vary considerably and frequently appeared to be in the range of 25-100 μm. Each scallop appeared to have a substantial range of microstructure. Whittaker reported the proximal surfaces were more scalloped than the buccal or lingual surfaces.[9] In

contrast, Scott and Symons reported more scalloping in the vicinity of the cusps,[17] while Schour suggested increased scalloping occurred in the gingival third of the tooth.[18]

Lin *et al.* employed high resolution SEM and immuno-labeling to identify collagen in the near DEJ region.[19] They found that the scalloped architecture of the DEJ contained microscallops in addition to type I collagen fibrils. As shown in Figure 5.4, the collagen fibrils, identified by their characteristic 67 nm banding pattern, appeared to emanate from dentin that then coalesced to form 100 nm diameter fibrils. These fibrils crossed the DEJ and inserted directly into the enamel mineral. Habelitz *et al.*[20] found the predominant diameter of dentin collagen was on the order of 100 nm diameter. Lin *et al.*[19] reported variability in the shape and size of the scallops, in the range of 25-40 μm. They reported that contained within each scallop was a series of microscallops. As yet uncharacterized finer level structures have been observed within each micro-scallop. It appears that the DEJ forms a complex interface with at least three architectural levels of structure: scallops, micro-scallops and finer level structures. The scallops forming this interface may vary in size and location. This three-leveled architecture of the DEJ has been described by a model known as the 3LM model.

Although the composition of the DEJ is unknown, it is believed to be less mineralized than enamel or dentin, and contains a higher organic content. It is also believed to be associated with the first formed mantle dentin.[11,19] Mantle dentin is the first dentin formed by the retreating odontoblasts during their transit from the DEJ to the pulp chamber. The composition and architecture of the DEJ may help to make it good at binding materials with dissimilar mechanical properties. The DEJ may help prevent the growth of cracks formed within enamel from extending into dentin.[19] This affords the

tooth with a mechanism for protection against catastrophic fracture and premature tooth loss.

Lin et al.[5] noted that the DEJ may be a microstructurally distinct and mechanically tougher portion of the tooth than either dentin or enamel that functions to prevent enamel cracks from extending through the remainder of the tooth. Clinical examination of teeth commonly reveals the presence of multiple deeply penetrating enamel cracks (Figure 5.2). Such flaws would be expected to propagate across the tooth until catastrophic loss of that portion of the tooth occurs. In spite of this, tooth fracture is a relatively rare occurrence. This is particularly true in non-restored and non-carious teeth. These observations imply that the DEJ may play a critical role in terminating the progression of enamel cracks. The key roles of binding materials having dissimilar mechanical properties and preventing crack propagation across the tooth were subjects that prompted study of this bio-interfacial tissue.

5.2.3 The Mechanical Properties of Enamel, Dentin and the DEJ

Numerous investigators have studied the mechanical properties of enamel and dentin. Bulk property measurements for these biomaterials have been made, although with great variability. To date, the mechanical properties of the DEJ have been poorly studied.[15] No unique or characteristic mechanical property values have been found for the DEJ. The variability in mechanical property measurements for enamel and dentin may be attributed, in part, to their inherent structural variations and to the brittle and anisotropic nature of these bordering dental tissues. Recent advances in nanotechnology have led to the development of AFM based nanomechanical testing equipment. Nanoindentation results suggest that enamel has modulus values ranging from 75-90 GPa, dependent upon

sample orientation.[3] Modulus and hardness values for intertubular dentin are around 20 GPa and 1 GPa respectively. These values are independent of testing direction. Variability in these measures has been observed relative to their degree of hydration.[21]

The DEJ is a complex region of diminutive size and irregular geometry that probably forms a graded interphase. The scale and undulating nature of this interface makes conventional materials characterization testing methods impossible. Our inability to extract this material and obtain bulk samples makes conventional shear, compression and tension testing difficult or impossible because the undulating geometry could generate complex and non-uniform sample stress distributions within the sample. Such conditions could cause premature sample failure and provide erroneous material property measurements.

Pioch and Staehle examined the shear strength of human and bovine teeth in the region of the DEJ and reported mean values of 39 MPa and 37.4 MPa, respectively.[7] They noted that fracturing did not occur at the DEJ, an indication of the toughness of the DEJ and the difficulty associated with accurately measuring its mechanical properties. They reported that all fractures occurred in dentin. The results imply that human and bovine mechanical properties may approximate one another.

Rasmussen *et al.* used a work-of-fracture (W_f) approach to characterize the fracture characteristics of enamel and dentin.[22] Using this approach they found anisotropic W_f values for enamel and dentin. For enamel they found W_f values that were much more resistant to fracture perpendicular to the prisms (200 J/m^2) than parallel to them (13 J/m^2). Dentin was also found to be anisotropic and more resistant to fracture than enamel, with values of 550 J/m^2 parallel to the tubules and 270 J/m^2 perpendicular to

the tubules (see Table 2.1). In 1984 Rasmussen again used a work-of-fracture approach, this time to characterize the fracture properties of the DEJ region.[8] They found a W_f value for the DEJ region of 336 J/m^2 as compared to 221 and 391 J/m2 for fracture perpendicular and parallel to the tubules, respectively. They observed that minimal fracturing occurred at the DEJ, even when the mandrel was positioned within 0.2 mm of the DEJ and concluded that the work-of-fracture increased at the DEJ. This is an indication o f the toughening ability of the DEJ. Rasmussen *et al.*[8,22,23] used a work of fracture approach and determined a directional dependence in these material properties parallel or perpendicular to the long axis of the dentinal tubule. Their work suggested that it was energetically favorable to fracture dentin across the tubules rather than parallel to them. El Mowafy and Watts[1] first attempted to measure fracture toughness, K_{IC}, of coronal dentin using a blunt notch conventional compact tension specimen. They reported a value of 3.08 MPa m$^{1/2}$. They concluded that the fracture toughness was high for a brittle material, and possibly indicated that the collagen fibrils provided a crack bridging or toughening mechanism.

Lin[19] and Lin and Douglas[4] conducted extensive studies to determine the fracture toughness of bovine DEJ. Their work centered on determining if the DEJ functioned as a fracture resistant interface, and therefore might indicate a basic biomechanical design principle. They used microindentation equipment and reported that the DEJ had a wider functional width, estimated to be in the range of 50-100 μm, than its optical appearance. They also postulated that the functional width of the DEJ was probably related to mantle dentin, and that the DEJ probably underwent plastic deformation during crack propagation, a process that acted to increase fracture toughness by serving as a crack

deflection or blunting device. Lin[19] and Lin and Douglas[4] also reported K_{IC} and G_{IC} values for the bovine DEJ that were significantly greater than that of bovine enamel or dentin, and noted that significant plastic deformation occurred when a crack encountered the DEJ. They concluded that the calcified dental tissues were optimized for the stresses and conditions to which they were subjected, and that enamel and dentin along with the DEJ acted as an integrated biomechanical complex. Enamel and dentin were modeled as being optimized to resist the masticatory stresses and transmit them to the supporting alveolar bone. They implied that the DEJ functioned as a moderately mineralized fibril-reinforced composite material that acted as a complex zone capable of undergoing small-scale plastic deformation.[4] In these experiments, Lin and Douglas[4] propagated cracks perpendicular to the DEJ but did not measure crack length. They also did not map or measure the stress distribution as the crack advanced to and thru the DEJ.

More recently, Imbeni *et al.*[24] used sharp cracks to determine bounds on the *in vitro* fracture toughness of human dentin perpendicular to the dentinal tubule long axis. They reported KIC values in simulated body fluid of 1.8 MPa $m^{1/2}$ for an anatomically sharp pre-crack stress concentrator that was generated with fatigue cycling to 2.7 MPa $m^{1/2}$ for identical conditions except that the specimen contained a sharp machine notch, noting an initial stress concentrator size effect on the fracture toughness estimate. Kahler *et al.*[25] noted significant hydration effects on the fracture toughness of bovine dentin, suggesting crack bridging as a fracture toughening mechanism. Kruzic *et al.*[26] used resistance curves (R-curves) to study fracture resistance with increased crack extension on elephant dentin to determine the relevance and significance of any toughening mechanisms that may be present. They used microscopy and X-ray tomography and

identified crack bridging by the uncracked ligaments and hydration as major fracture toughening mechanisms in dentin.

5.3 Areas of Research Focus

5.3.1 Overview

The DEJ is a complex biomechanical interface with an ill-defined and multi-layered microstructure. The organic and mineral contents of the DEJ are unknown. The intra-tooth and inter-tooth variability in width and morphology has not been established. To date, the mechanical properties of the DEJ have been explored in a limited fashion because the very small size and highly variable geometry of this biointerfacial tissue has prevented its extraction. The observed fracture behavior indicates that the DEJ differs significantly from either enamel or dentin. It appears that the DEJ serves to provide the tooth with protection against catastrophic fracture by providing the tooth with a greater fracture toughness. This suggests that the DEJ could serve an important role as a biomimetic model for linking other materials having dissimilar characteristics and properties. Such a junction appears to confer critical properties that allow the tooth to function efficiently. It joins enamel and dentin, two materials having dissimilar properties, while increasing the fracture resistance of the total tooth structure. This suggests that improving our knowledge of the DEJ could be useful in helping to develop models for binding other materials having dissimilar properties. There are many applications that could benefit from such an optimized design. These could include optimizing dental and orthopedic implant design and improving dental restorative and adhesive materials.

5.3.2 Scalloped Microstructure of the DEJ

In an attempt to improve our knowledge of the undulating nature of the interface that is the DEJ, a method was developed to expose the DEJ by removing the enamel.[27] Human incisors and molars were sectioned bucco-lingually and the enamel was ground down to within 1 mm of the DEJ. The remaining enamel was removed with 0.5 M EDTA having a pH of 7.4 until the DEJ became optically apparent. This usually occurred within 7 to 10 days. This occurred when the "chalky" appearance of the EDTA exposed enamel disappeared, an optical indication that the enamel had been removed. The samples were then fixed in gluteraldehyde and dehydrated in a graded ethanol series that was followed by drying in HMDS before the samples were sputter coated and examined in the SEM. Five SEM images were collected at 500x and 2000x from five areas in each vertical third of the tooth. The diameters of each scallop were then measured along three lines, each having 120 degrees of separation between the other lines. Typical images are shown in Figures 5.5a and 5.5b. No significant intratooth scallop differences were noted. Significant scalloping differences were noted between the incisors and the molars. The average scallop size noted in the incisors was 29.4 ± 8.5 μm and 42.3 ± 8.5 μm for the molars (t-test, $P<0.001$).[28]

High-resolution non-invasive imaging of the DEJ was also performed using Synchrotron Radiation Computed Tomography (SRCT). SRCT images were taken of tooth specimens bonded to a composite restorative material using synchrotron beamline 10-2 at Stanford Synchrotron Radiation Laboratory (SSRL). This source has a resolution of 3.33 μm. This allowed for the selected x-ray attenuation level to be displayed. An

SCRT image of the DEJ having an attenuation level corresponding to the DEJ is shown in Figure 5.6. The image illustrates the scalloped nature of the DEJ.

5.3.3 Mechanical Properties and Functional Width

The development of AFM-based nanomechanical instrumentation has allowed us to perform site-specific elastic modulus and hardness mapping. We used a standard AFM head that had been specially modified by incorporating the use of a capacitive sensor that allowed load and vertical displacement measurements during indentation to be made.[6] Indentations were placed along lines that crossed the DEJ perpendicularly. Figure 5.7 shows the typical variation in reduced elastic modulus and hardness across the interface. A 1-2 μm spacing interval was used between successive indentations to avoid interaction effects. Stiffness was obtained from the unloading curve by calculating the reduced elastic modulus, E_r. Hardness was calculated as the maximum force divided by the projected indentation contact area in accordance with relationships derived by Dorner and Nix.[29] The results indicated a consistent monotonic increase in modulus and hardness across the DEJ from dentin to enamel. Modulus increased from 20 GPa in dentin to 70 GPa in enamel.[6] Similarly, hardness increased linearly from approximately 1 GPa in dentin to 3.5 GPa in enamel.

High-resolution imaging of the DEJ by a variety of imaging methods suggests close apposition of the apatite crystals of dentin with the larger apatite crystals of enamel. A high resolution AFM image of the DEJ illustrating this approximation is shown in Figure 5.8. In contrast to the close approximation of the enamel and dentin apatite crystals, the variation in mechanical properties occurs over a much greater distance. The change in mechanical properties across the DEJ has been termed its functional width.

Considerable differences between the anatomic and functional DEJ width estimates exist. Habelitz et al. pointed out that the functional width appears to be dependent upon indenter technique, indenter tip type, and sampling volume.[20] Microindentation based functional DEJ width estimates gave values up to 100 μm wide.[30] Berkovich and cube corner nanoindentation suggested functional width estimates of approximately 25 μm and 12 μm, respectively.[2,6]

To attempt to resolve questions related to the nature of the functional width, a nanoscratching technique was used to continuously measure vertical and lateral friction forces encountered as the indenter tip passes across the DEJ. A small spherical indenter tip attached to the AFM via two capacitive sensors enabled the interface to be "scratched." The modified AFM uses two capacitive sensors to measure force and displacement in vertical and lateral directions. Vertical tip loads in the range of 50 to 600 μN were applied to a spherical diamond indenter tip (r = 10 μm), which was driven across the sample surface perpendicular to the DEJ, recording lateral tip force. A nanoscratch placed to cross the DEJ at a perpendicular angle is shown in Figure 5.9a. Friction coefficients of enamel, dentin and DEJ were measured with the described nanoscratcher attached to the AFM. Pre-scratch imaging facilitated exact positioning and orienting of the scratches. Post-scratching imaging was conducted to ensure the validity of the results obtained and is shown in Figure 5.9b.

Baseline enamel and dentin friction coefficients obtained in the near DEJ region were 0.31 and 0.16, respectively. Additional measurements were made on a number of teeth under a range of loads to estimate the friction coefficient of intertubular dentin. These measurements estimated the friction coefficient of intertubular dentin as 0.31

±0.05, significantly above the coefficient of friction found in enamel (0.14 ±0.02).[20] It should be noted that intertubular dentin is a much softer material than is enamel. This difference may have allowed an indenter tip to be pressed further into dentin than into enamel when subjected to the same indenter load. We propose that this difference is likely the result of the higher protein content, and the consequent lower mineral content, of dentin.

The variation in friction coefficients across the DEJ showed a monotonic decrease from dentin to enamel. This difference allowed us to estimate the functional width of the DEJ, based on its nanoscratch characteristics. The functional width estimate based on nanoscratching was smaller than that based on nanoindentations. Habelitz *et al.*, 2001 reported an average functional DEJ width based on the difference in friction coefficients between dentin and enamel at 2.0 ±1.1 μm.[20] Because the nanoscratching tip had a radius of 10 μm, the actual functional width may be even smaller than the 2 μm determined.

Other bioinstrumentation modalities have been employed in an attempt to characterize the properties of, and estimate the width of the DEJ. Gallagher *et al.*, used a 351-nm continuous Argon-ion laser excitation source to study the DEJ using autofluorescence microscopy and found the median DEJ width was approximately 10 μm.[31] This result was in agreement with previous nanoindentation results.

Mapping variations in material composition across the DEJ could provide a mechanism for determining a composition-based width. Raman microspectroscopy was employed to map the mineral and organic content distributions across the DEJ region.[32] Characteristic peak positions and peak intensities for PO_4^{3-} band and the C-H stretching modes were determined and were used to characterize enamel and dentin. A He-Ne laser

having a 0.5 μm spot size was used to emit monochromatic radiation having a 632.8 nm wavelength. Spectra were measured in 1μm steps along 100 μm long lines that crossed the DEJ perpendicularly. Prior to Raman imaging, a line of nanoindentation points was placed perpendicularly across the DEJ as shown in Figure 5.10a. A single maximum load indent was placed at the enamel end of the line to denote the enamel terminis. Two, or more, indents were similarly placed at the other end to denote the dentin end of the data points. The terminal indents were used as optically visible sample orientation markers as they were visible using the light microscope of each instrument. Hardness and modulus were calculated and plotted relative to their position as shown in Figure 5.10b. Approximately 5 μm of lateral offset between the nanoindent and Raman spectroscopy imaging lines was provided in order to prevent possible instrumentation interaction effects.

The middle of each Raman microspectroscopy imaging line was centered over the middle of the DEJ as viewed with an optical microscope. The line paralleled the nanoindent line, but with 5 μm of lateral offset (Figure 5.11). Peak positions and intensities were then compared among the mineralized tissues. Plots of the peak Raman intensity variations across the DEJ for the PO_4^{3-} band and C-H stretching modes are shown in Figures 5.12a and 5.12b, respectively. The peak intensity of the PO_4^{3-} band is an indication of the mineral content present. C-H stretching mode peak intensity is an indication of the organic content. The mineral content was found to increase monotonically from dentin to enamel (Figure 5.12a), while the organic component decreased monotonically (Figure 5.12b). The composition-based width of the DEJ was then estimated from plots of the intersections of regression lines fit to intensity values of

dentin, enamel and DEJ plotted relative to position. The PO_4^{3-} band estimated a composition-based DEJ width based on Raman microspectroscopy of 7.6 (± 2.8) μm. A composition-based DEJ width estimate of 8.6 (± 3.6) μm was determined using the C-H stretching mode. High-resolution analysis indicated no difference in peak position for the PO_4^{3-} band among the tissues (959 cm^{-1}). Enamel showed a 4.6 cm^{-1} peak shift in the C-H stretching mode as compared to DEJ or dentin, but no unique components could be found in the DEJ.

Regarding the meaning of a functional width, little evidence exists suggesting that the DEJ is a unique tissue or has unique or characteristic properties. Mechanical property and Raman microspectroscopy mappings of the DEJ failed to find a hardness or modulus value that represented DEJ. Likewise, Raman microspectroscopy maps did not reveal a characteristic mineral or organic content for the DEJ. Therefore, the evidence fails to suggest a unique tissue that causes the observed variations in the mechanical properties.

Based on a 3-level scalloped micro-structural model of the DEJ, variations in the properties of the DEJ could be explained based on the relative proportions of enamel and dentin present. Such a model suggests that different estimates of the functional width result from the scalloped morphology of a very narrow junction between enamel and dentin. This conclusion is reinforced by the observed monotonic variation of organic and mineral contents across the junction. In addition, no unique peak shifts were seen across this region. This implies that no unique or characteristic composition properties were found for the DEJ. Thus, it appears that the interdigitation of enamel and dentin expressed at the 3 length scales: scallops, micro-scallops, and finer-level structures

account for the observed variation in the DEJ's mechanical properties, and implies that a unique DEJ tissue does not exist.

5.3.4 Fracture Properties of the DEJ

The fracture characteristics of the DEJ are of particular interest since they impart resistance to catastrophic tooth fracture over the lifetime of an individual. In addition, this bio-interface joins two materials having widely dissimilar mechanical properties, implying that it has excellent adhesion properties. The scale and undulating three-dimensional geometry of this interface have made characterization of its composition, mechanical properties and fracture characteristics difficult to define using conventional instrumentation approaches.

In 1976, Rasmussen first observed that cracks that had been initiated in enamel rarely propagated across the DEJ.[22] Pioch and Staehle (1996) also noted that the DEJ imparted fracture resistance during studies investigating the shear strength of this region.[7] Xu *et al.*,[33] and Marshall *et al.*,[6] used microindentation and nanoindentation, respectively to study the fracture characteristics of the DEJ. A crack initiated in enamel in the near DEJ region using a nanoindenter is shown in Figure 2.4. As illustrated in the picture, the crack propagated to the DEJ but failed to cross it. Upon encountering the DEJ region the crack was deflected and blunted while still in enamel. Attempts to initiate cracks in dentin were unsuccessful using a Triboscope nanoindenter system (Figure 5.13a), even at loads to 30,000 μN. An MTS microindenter was used to attempt to fracture dentin since it can deliver significantly higher loads. Attempts to crack dentin failed using the MTS indenter, even at loads up to 192 mN (Figure 5.13b). It should also be noted that attempts to crack enamel sometimes produced asymmetric and non-radial fractures, or fractures

with significant debris and pile up (Figure 5.14). In light of this, additional study of the fracture characteristics, the composition and the architecture of the DEJ are required. Improving our knowledge of this bio-interface could provide important insights into bonding materials with dissimilar mechanical properties and bonding materials together to improve their resistance to fracture.

5.4 References:

1 El Mowafy OM, Watts DC. Fracture toughness of human dentin. J Dent Res 1986;65:677-681.

2 Fong H, Sarikaya M, White SN, Snead ML. Nano-mechanical properties profiles across dentin-enamel junction of human incisor teeth. Mater Sci Eng 2000;C7:119-128.

3 Habelitz S, Marshall SJ, Marshall GW, Balooch M. Mechanical properties of human dental enamel on the nanometer scale. Arch Oral Biol 2001;46:173-183.

4 Lin CP, Douglas WH. Structure-property relations and crack resistance at the bovine dentin-enamel junction. J Dent Res 1994;73:1072-1078.

5 Lin CP, Douglas WH, Erlandsen SL. Scanning electron microscopy of type I collagen at the dentin-enamel junction of human teeth. J Histochem Cytochem 1993;41:381-388.

6 Marshall GW, Balooch M, Gallagher RR, Gansky SA, Marshall SJ. Mechanical properties of the dentinoenamel junction: AFM studies of nanohardness, elastic modulus and fracture. J Biomed Mater Res 2001;54:87-95, 2001.

7 Pioch T, Staehle HJ. Experimental investigation of the shear strengths of teeth in the region of the dentinoenamel junction. Quintessence Int 1996;27: 711-714.

8 Rasmussen ST. Fracture properties of human teeth in proximity to the dentinoenamel junction. J Dent Res 1984;63:1279-1283.

9 Whittaker DK. The enamel-dentine junction of human and macaca irus teeth: A light and electron microscopic study. J Anat 1978;125:323-335.

10 Bhaskar SN, ed., *Orban's Oral Histology and Embryology 11th Edition*, Mosby Year Book, St. Louis, 1991.

11 Ten Cate AR. Oral histology: development, structure and function. 4th ed. Mosby, St. Louis, 1994.

12 Marshall GW, Marshall SJ, Kinney JH, Balooch M. The dentin substrate: structure and properties related to bonding. *J Dent* 1997;25:441-458.

13 Marshall GW, Balooch M, Tench RJ, Kinney JH, Marshall SJ. Atomic force microscopy of acid effects on dentin. *Dent Mater* 1993;9:265-268.

14 van der Graaf E, Ten Bosch J. The uptake of water by freeze-dried human dentine sections. *Arch Oral Biol* 1990;35:731-739.

15 Marshall GW. Dentin: microstructure and characterization. Quintessence Int 1993;24:606-617.

16 Jones SJ, Boyde A. Ultrastructure of dentin and dentinogenesis, in Dentin and dentinogenesis, Vol. 1 (2). Boca Raton, FL: CRC Press; 1984. p. 81-134.

17 Scott JH, Symons NBB. Introduction to dental anatomy, 6th ed, Churchill Livingstone, Ltd. Edinburgh, Scotland, 1971.

18 Schour, Noyes Oral Histology and Embryology, 8th ed. Kimpton, London, England, 1960.

19 Lin CP. Structure-function property relationships and crack resistance at the bovine dentin-enamel junction. University of Minnesota, 1993.

20 Habelitz S, Marshall SJ, Marshall GW, Balooch M. The functional width of the dentino-enamel junction determined by AFM-based nanoscratching. J Struct Biol 2001;135:294-301.

21 Kinney JH, Habelitz, Marshall SJ, Marshall GW. The importance of intrafibrillar mineralization of collagen on the mechanical properties of dentin. *J Dent Res* 2003;82(12):957-961.

22 Rasmussen ST, Patchin RE, Scott DB, Heuer AH. Fracture properties of human enamel and dentin. J Dent Res 1976;55:154-164.

23 Rassmussen ST, Patchin RE. Fracture properties of human enamel and dentin. *J Dent Res* 1984;63:1362-1368.

24 Imbeni V, Nalla RK, Bosi C, Kinney JH, Ritchie RO. In vitro fracture toughness of human dentin. *J Biomed Mater Res* 2003;1;66A(1):1-9.

25 Kahler B, Swain MV, Moule A. Fracture-toughening mechanisms responsible for differences in work of fracture of hydrated and dehydrated dentine. *J Biomech* 2003;36:229-237.

26 Kruzic JJ, Nalla RK, Kinney JH, Ritchie RO. Crack blunting, crack bridging and resistance-curve fracture mechanics in dentin: effect of hydration. *J Biomater* 2003;24:5209-5221.

27 Le TQ, Habelitz S, Marshall GW, Pugach MK, Marshall SJ. Acid and deproteinization resistance of the DEJ. *J Dent Res* 2001;80,763.

28 Lingg B, Marshall GW, Watanabe LG, Habelitz, S, Ho SP, Marshall SJ. Incisor and molar DEJ scallop size as a function of intratooth location. *J Dent Res* 82A, Abstract 1700.

29 Doerner MF, Nix WD. A method for interpreting the data from depth sensing indentation instruments. J Mater Res 1986;1:601-609.

30 White S, Paine M, Luo W, Sarikaya M, Fong H, Yu Z, Li ZC, Snead M. The dentin-enamel junction is a broad transitional zone uniting dissimilar bioceramic composites. J Am Ceram Soc 2000;64A:372-377.

31 Gallagher RR, Demos SG, Balooch M, Marshall Jr. GW and Marshall SJ. Optical spectroscopy and imaging of the dento-enamel junction in human third molars. J. Biomed Mater Res 2003;64A:372-377.

32 Schulze K, Balooch M, Balooch G, Marshall S, Marshall G. A micro Raman spectroscopic investigation of the dentin-enamel junction and cementum-dentin junction. J Biomed Mater Res (submitted for publication).

33 Xu HH, Smith DT, Jahanmir S, Romberg E, Kelly JR, Thompson VP, Rekow EG. Indentation damage and mechanical properties of human enamel and dentin. J Dent Res 1998;77:472-480.

5.5 Tables and Figures

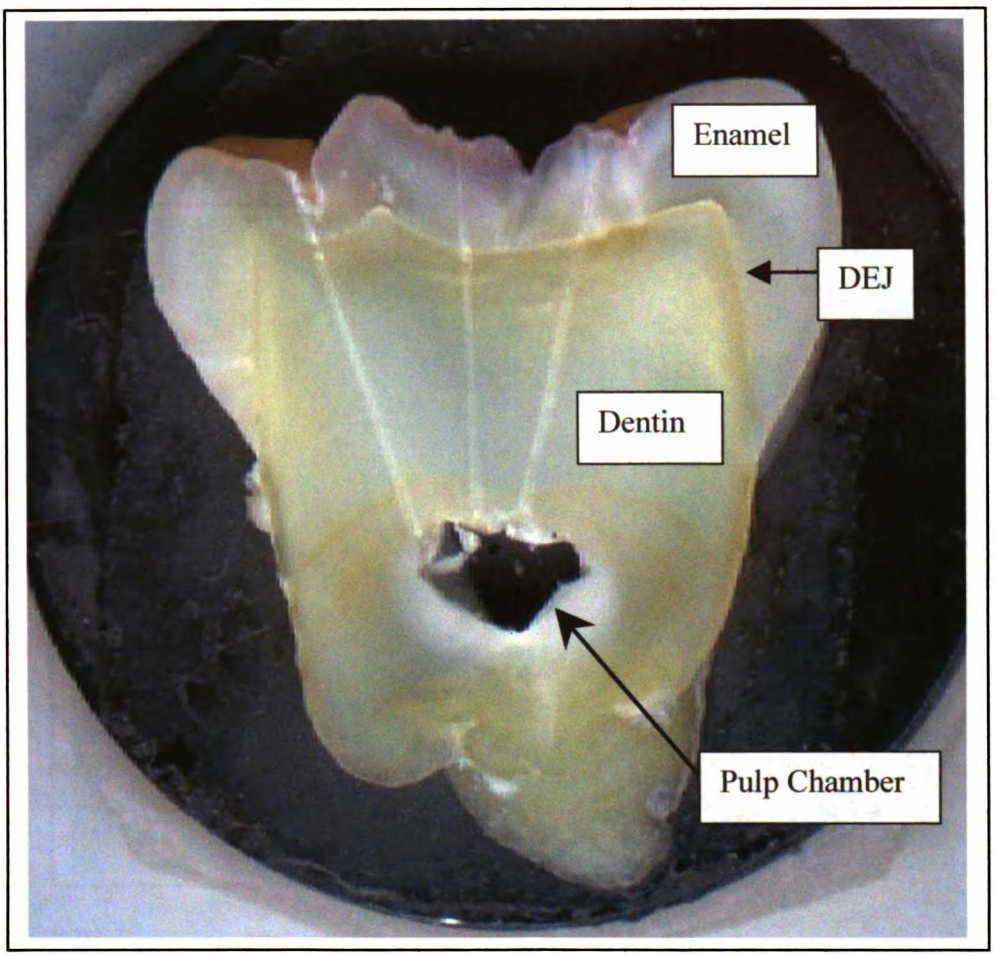

Figure 5.1 Optical light microscope image of a mounted tooth sample prior to AFM imaging and nanomechanical testing. Three optically apparent sample orientation lines were scratched into the surface of the sample prior to imaging in order to facilitate sample placement and orientation.

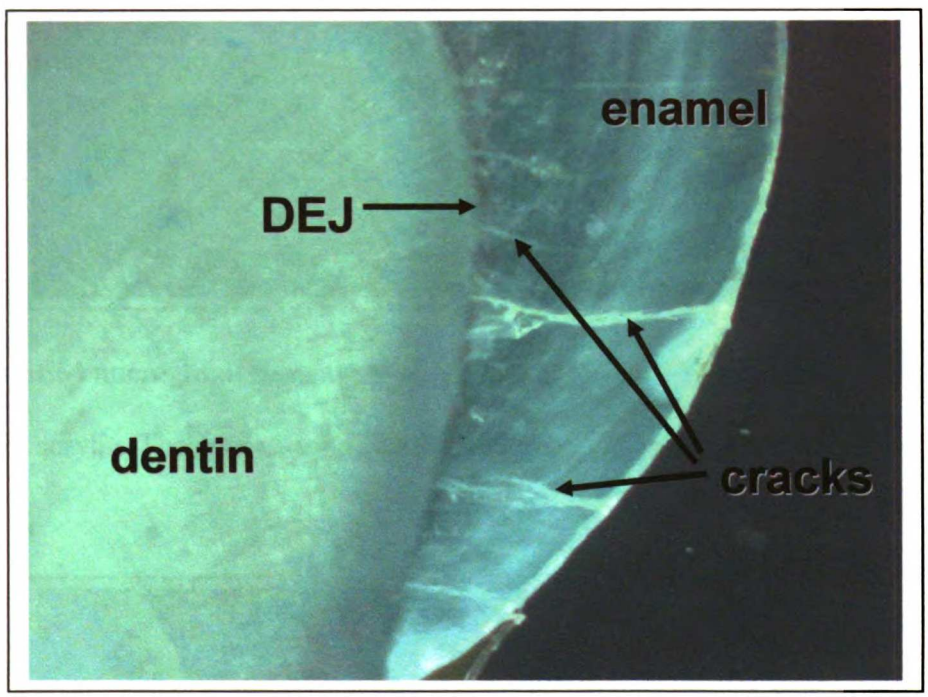

Figure 5.2 Optical light micrograph showing a human third molar in cross-section. Cracks are show that have propagated through the enamel, but that terminate at the DEJ, and are prevented from penetrating into the underlying dentin.

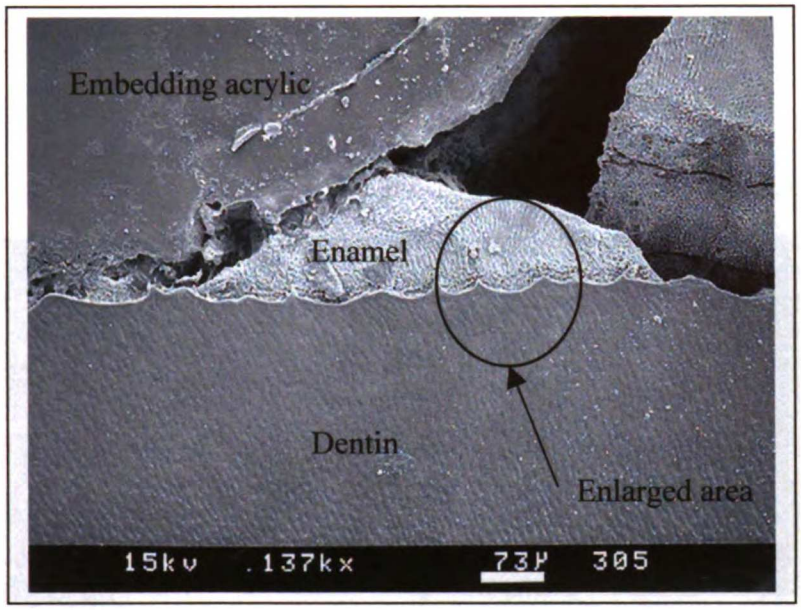

Figure 5.3a SEM micrograph showing a human third molar with a fractured crown that is embedded in acrylic. The area of enlargement contained in Figure 3b is indicated above.

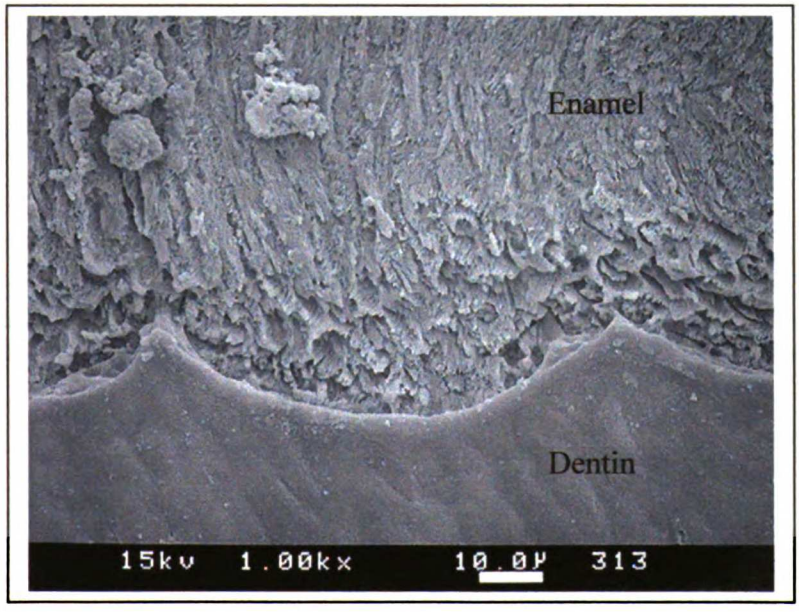

Figure 5.3b Enlargement illustrating the scalloped structure of the DEJ. The scallops are oriented with convexities directed towards dentin and concavities towards enamel.

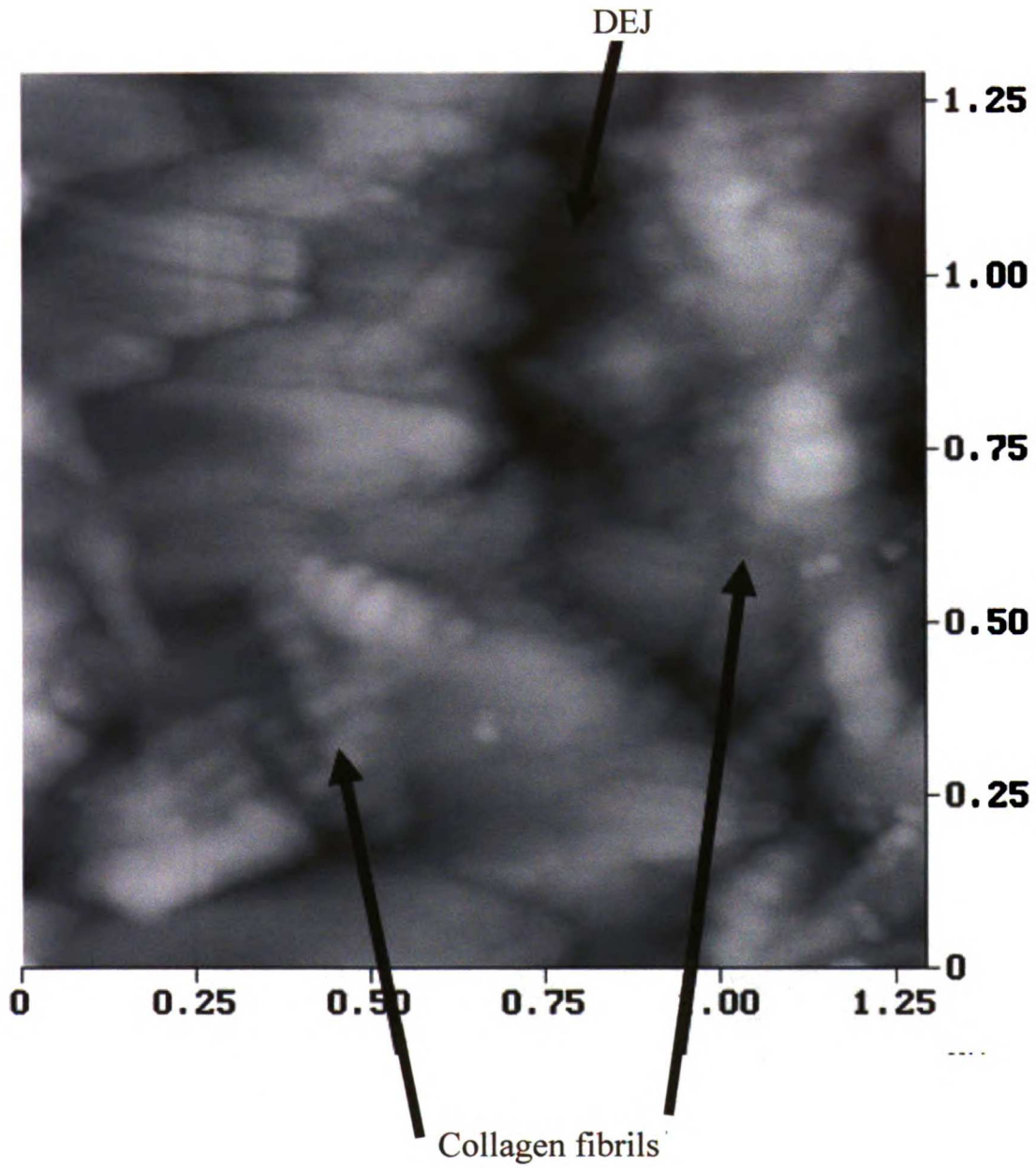

Figure 5.4 AFM high-resolution image of the DEJ showing the extension of collagen fibrils from dentin into enamel.

a)

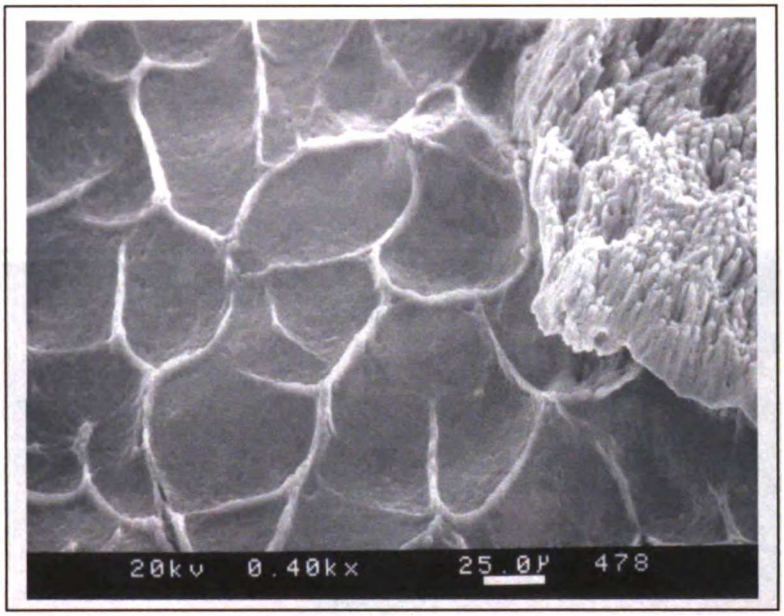

b)

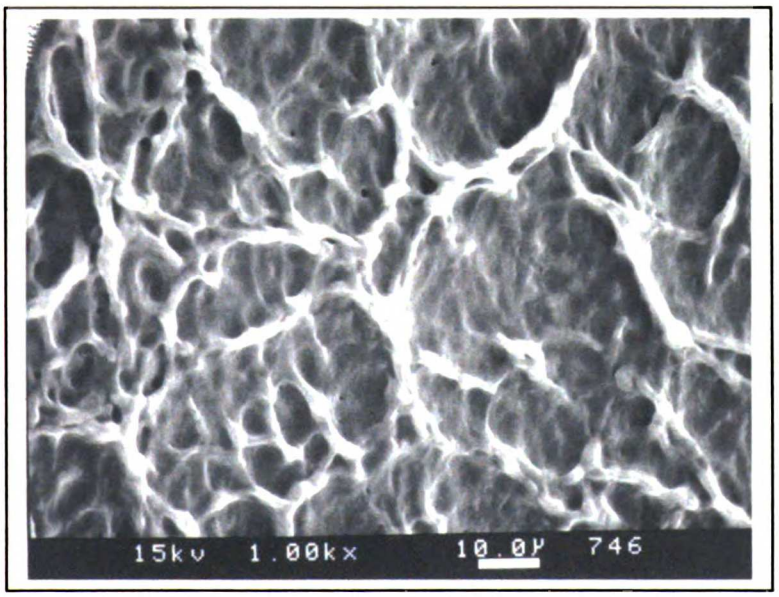

Figure 5.5 a) SEM micrograph showing DEJ scalloping following enamel removal

b) SEM micrograph of DEJ microscalloping

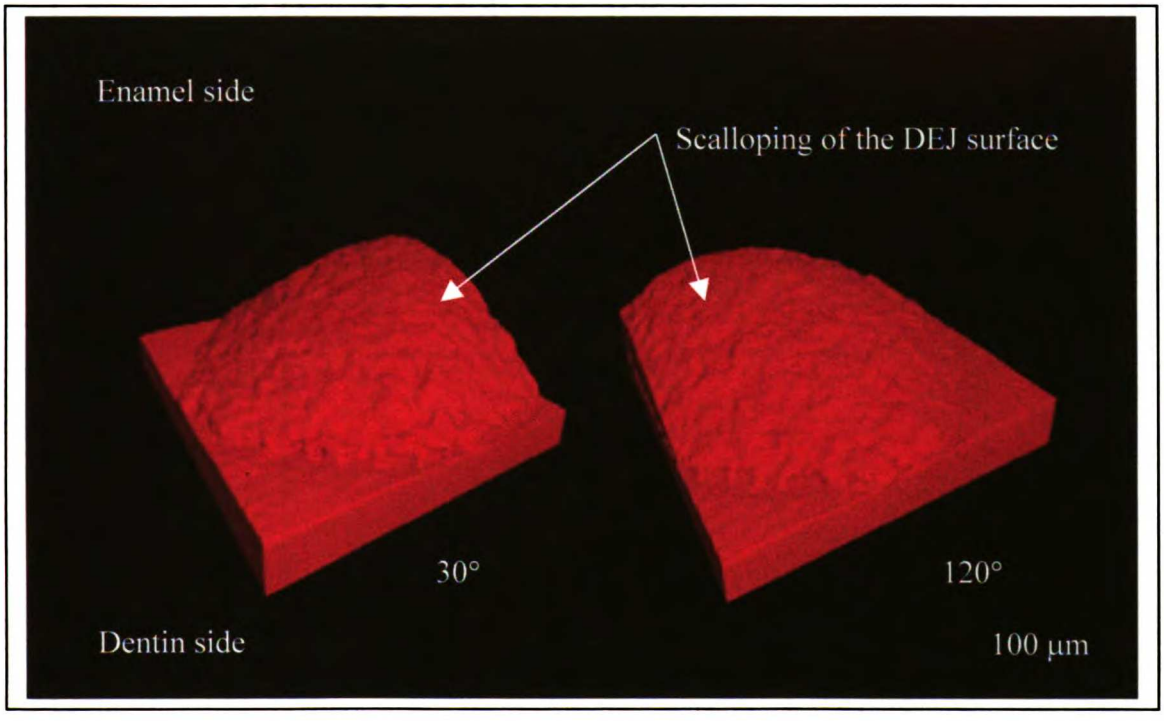

Figure 5.6 **SCRT images of the DEJ from an uncut tooth showing the nature of its scalloping.**

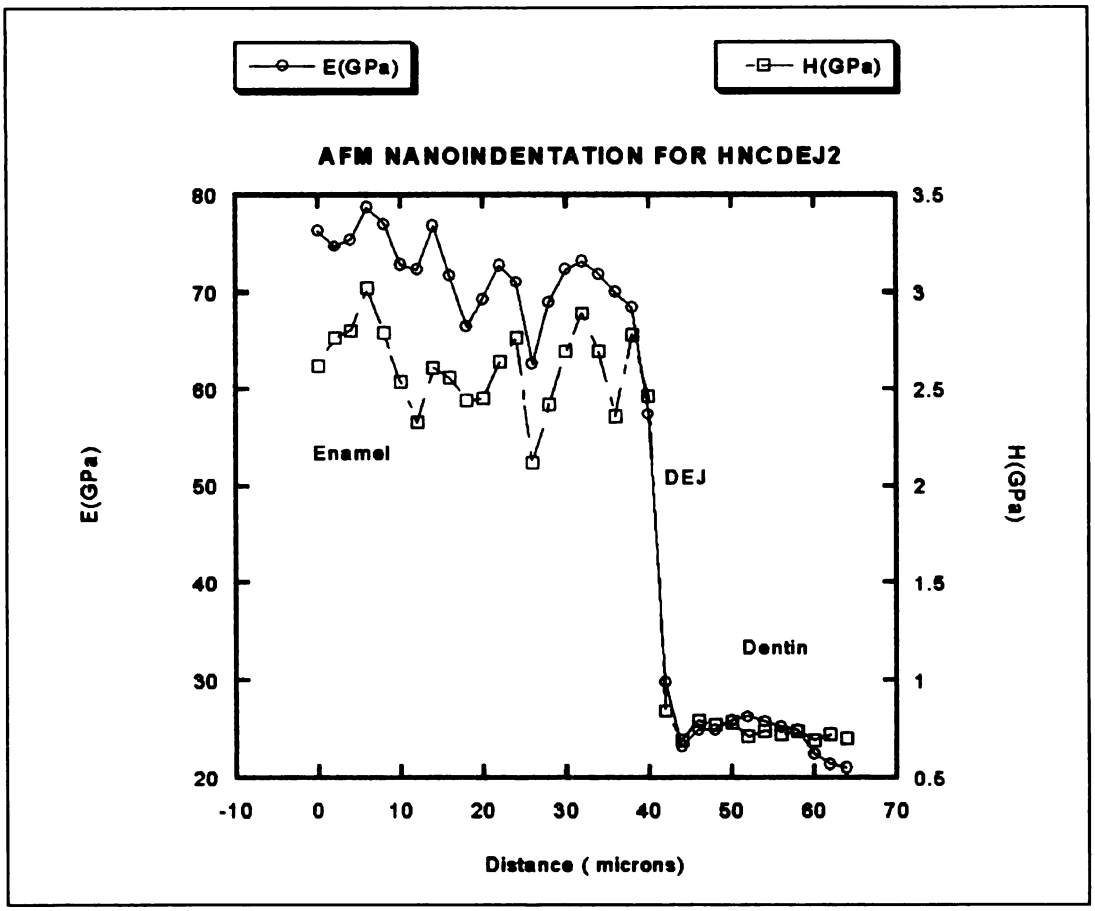

Figure 5.7 Plots of the variation in elastic modulus and hardness across the DEJ obtained using AFM-based nanoindentation testing.

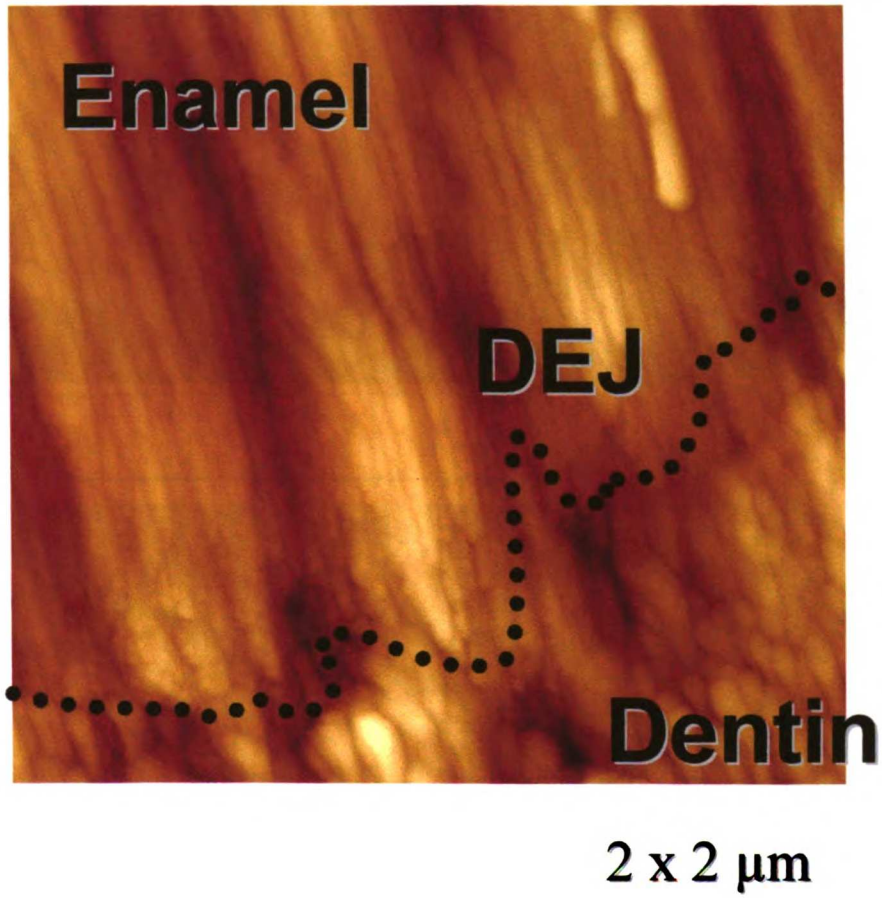

Figure 5.8 High resolution AFM image of the DEJ showing the apatite crystals of enamel and dentin are in close approximation to one another.

a)

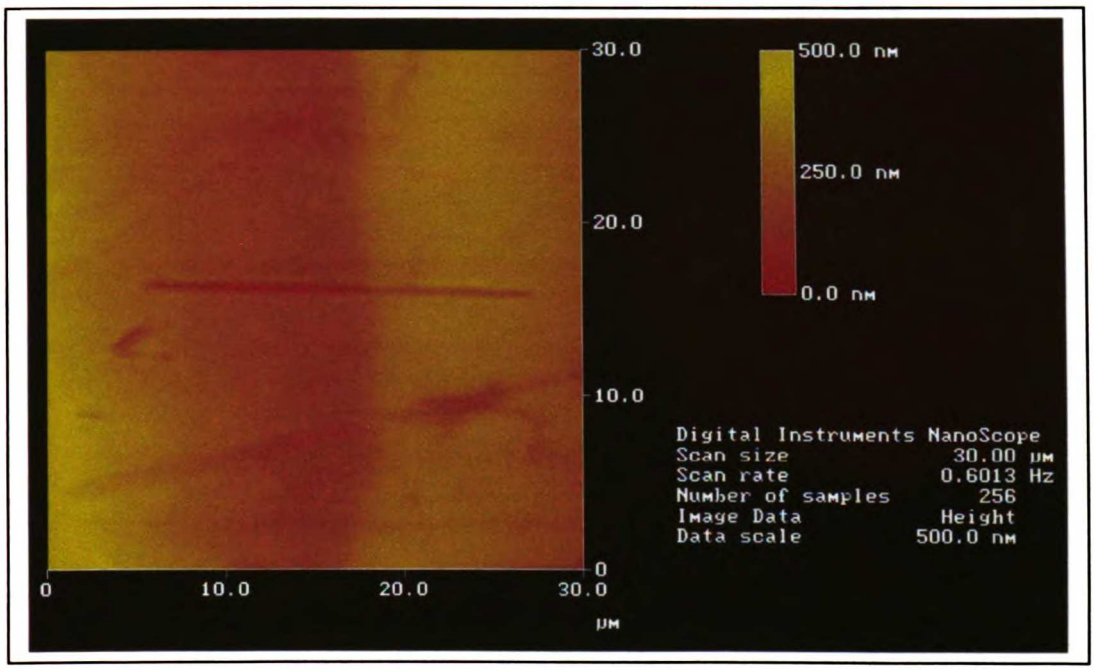

b)

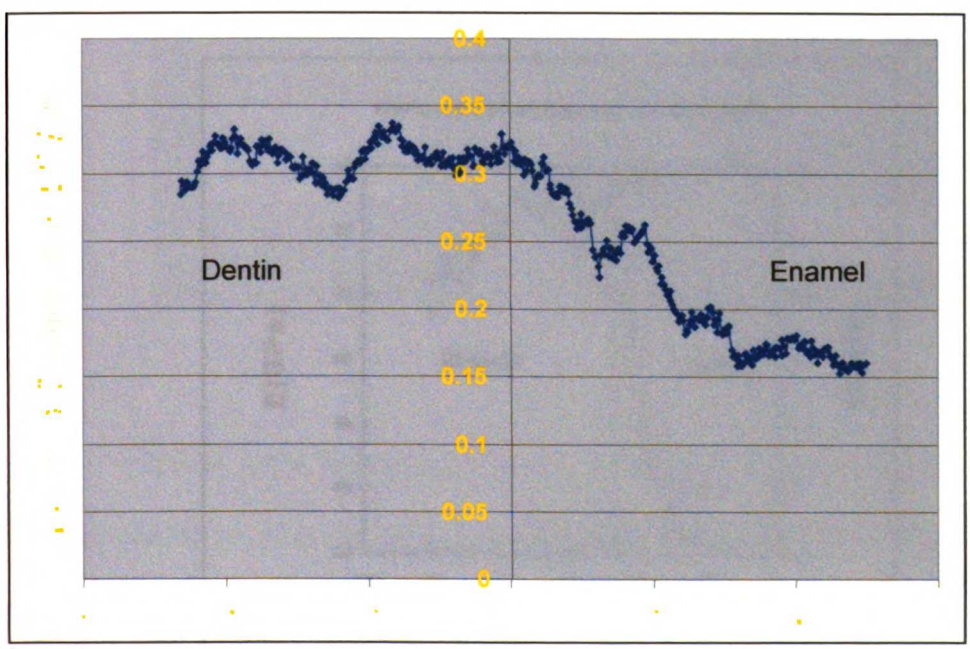

Figure 5.9 a) A single nano-scratch placed across the DEJ. b) Plot of the friction coefficient across the DEJ from AFM-based nanoscratching. Average friction coefficients were 0.31 in dentin and 0.16 in enamel.

a)

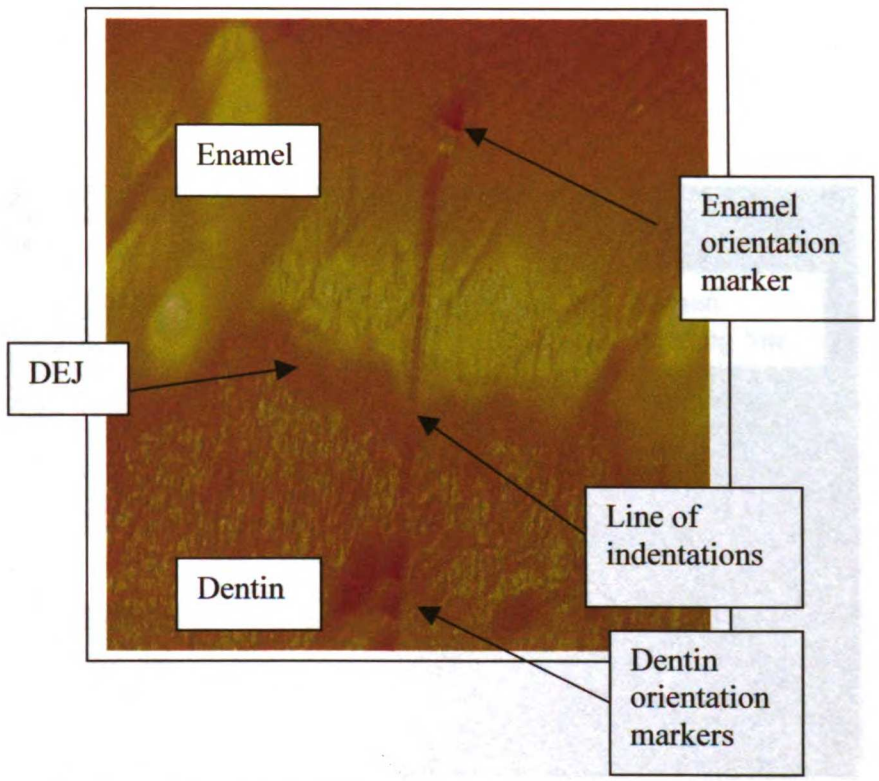

b)

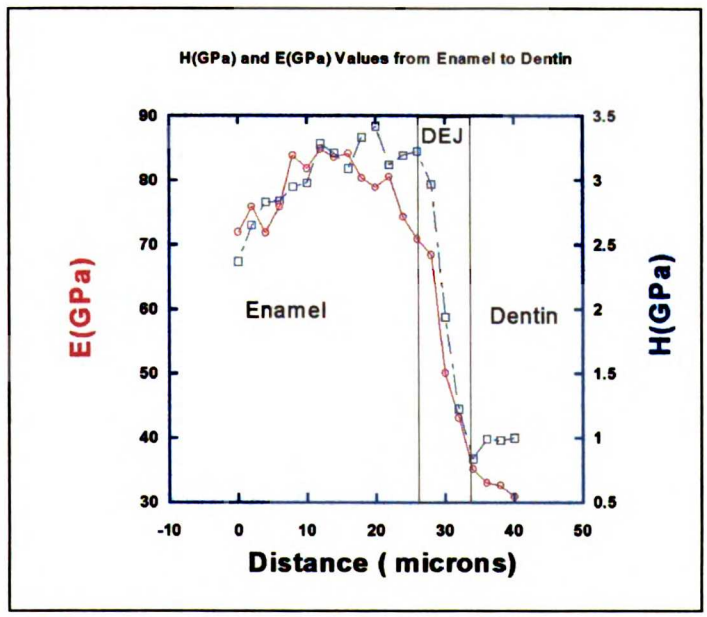

Figure 5.10 a) An AFM image showing a line of nanoindentation points placed across the DEJ. Orientation indentation were placed under maximal loads to make optically visible markers. b) A typical plot of the variation in modulus (E) and hardness (H) across the DEJ.

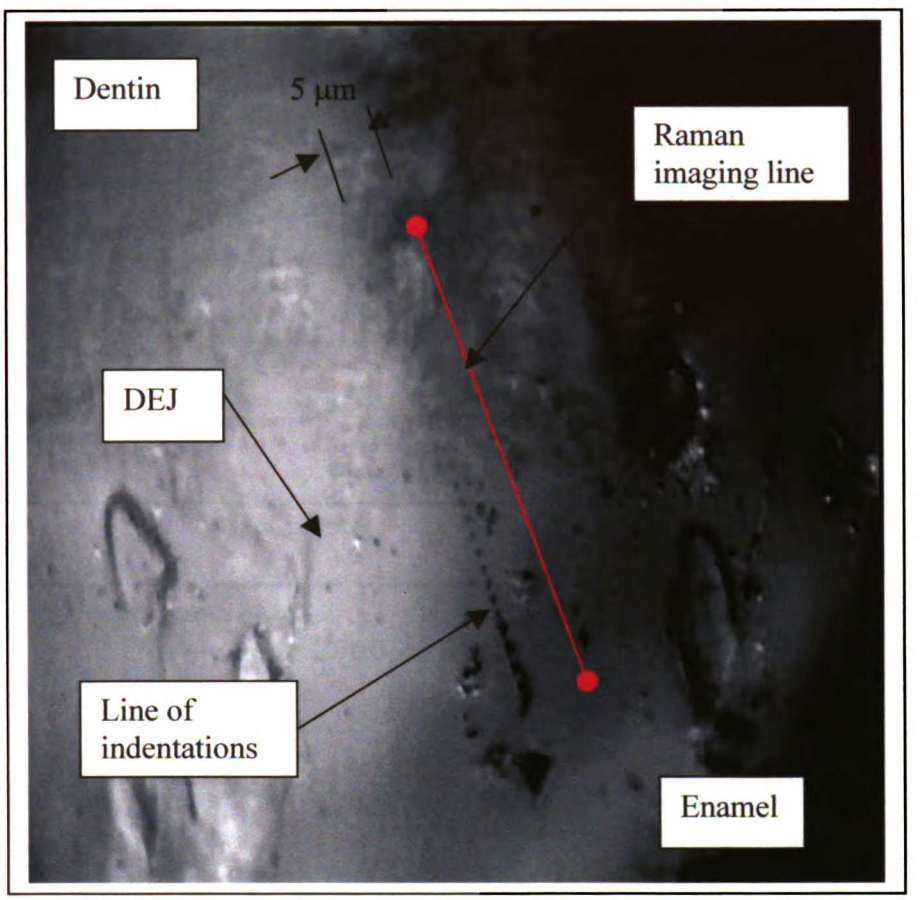

Figure 5.11 Optical light microscope image showing a Raman microspectroscopy imaging line placed to cross the DEJ perpendicularly. The orientation markers allowed orientation of the Raman and nanoindentation instrumentation lines. Note that a single orientation marker was placed into enamel, and several were placed in dentin. The markers denote the starting and termination points of the indentation line. The indenter and Raman lines were laterally offset from one another by approximately 5 μm.

a)

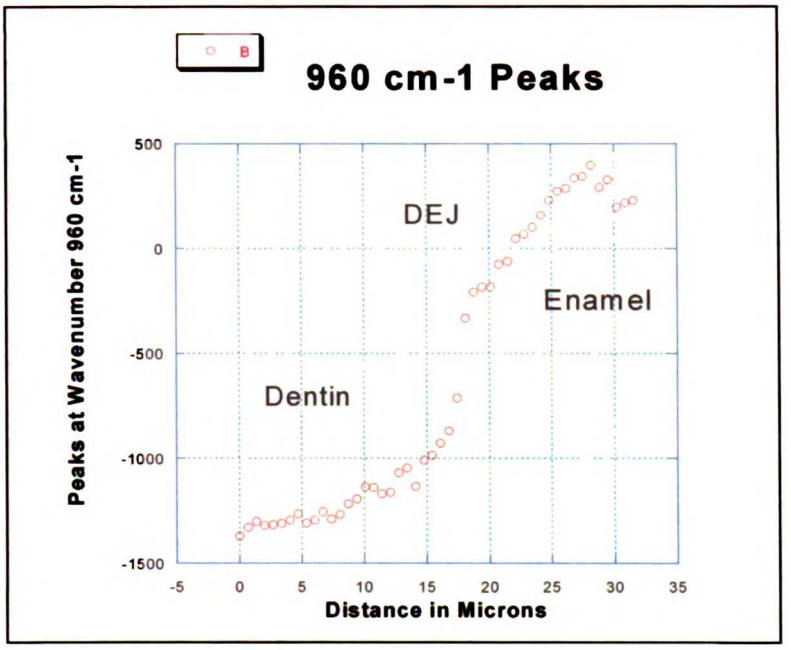

b)

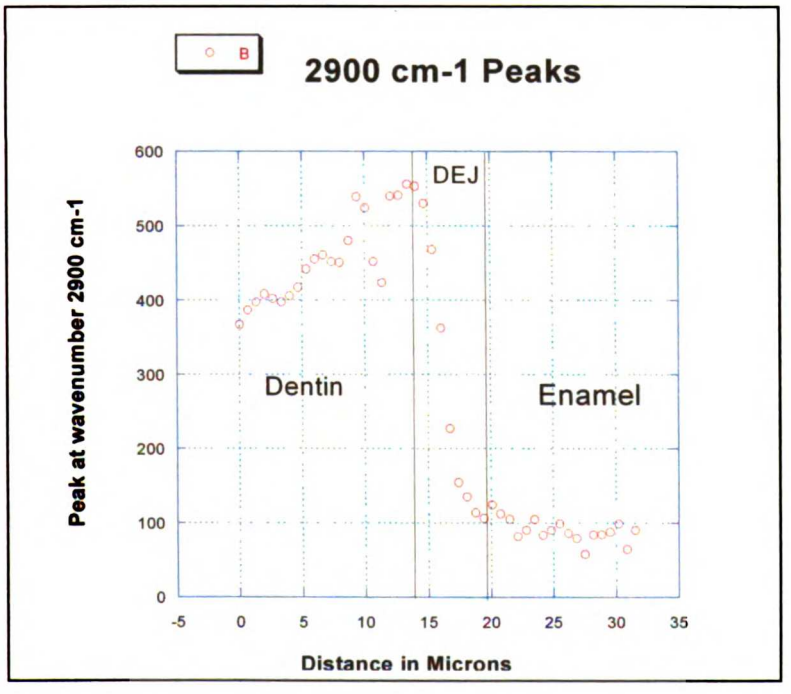

Figure 5.12 a) Plot of the phosphate peak Raman intensity at 960 cm-1. High intensity levels were found in enamel. DEJ width was estimated at 5-7 μm with this method. b) Plot of the C-H stretch peak intensity. High C-H stretch intensities were present in dentin.

a)

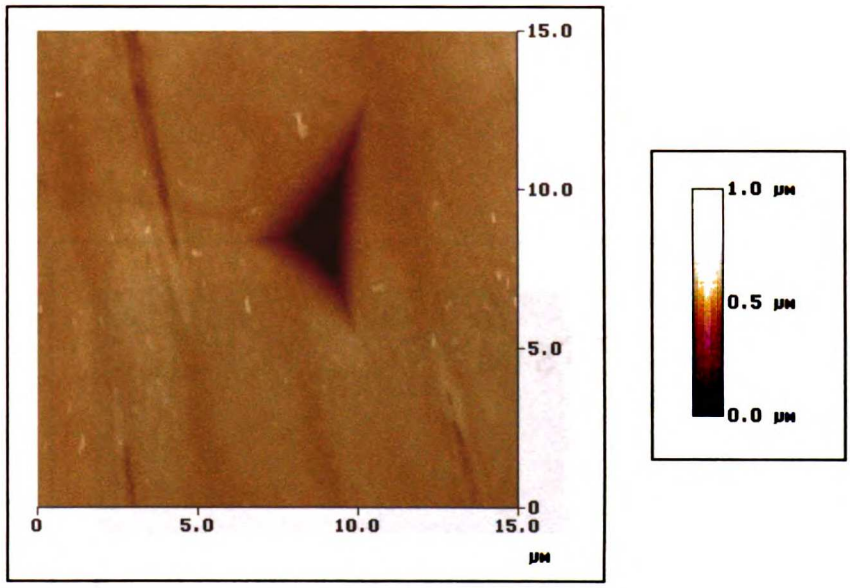

b)

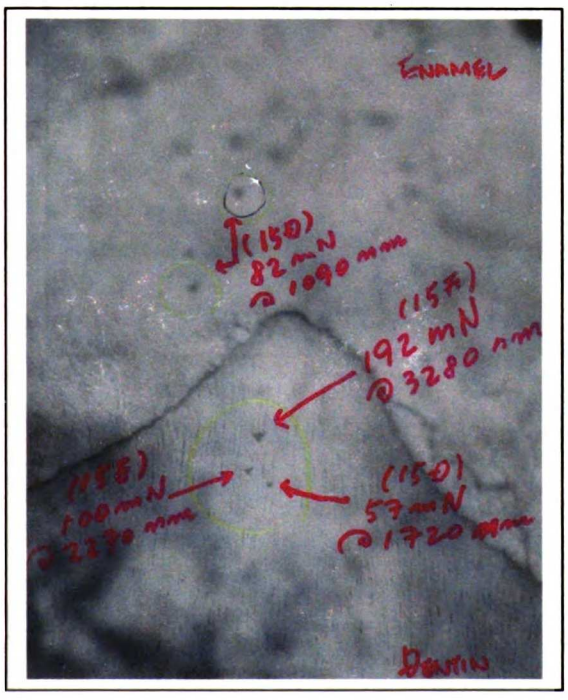

Figure 5.13 a) AFM micrograph of an indent placed into sagittally sectioned dentin under maximal load. b) SEM micrograph of indents placed into sagittally sectioned enamel and dentin. No cracks were generated into sagittal enamel or dentin.

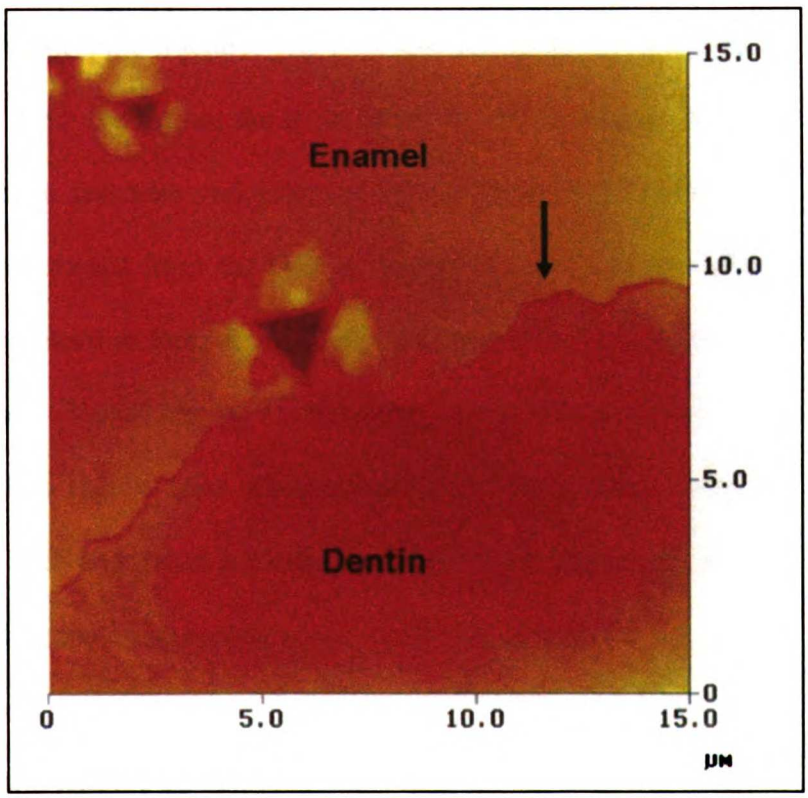

Figure 5.14 AFM image of a nanoindent placed into enamel in the near DEJ region. A crack was generated in enamel that approached the DEJ, but that deflected and propagated into the enamel.

CHAPTER 6 – Conclusion

6.1 Overview

The DEJ is a calcified dental tissue that is sandwiched between enamel and dentin (Figure 5.1). It provides dual critical functions to bind dentin with enamel and to protect the tooth against catastrophic fracture. The DEJ also serves as the initiation site for tooth formation. During tooth formation, the tooth forms in two directions from the DEJ. The calcification of dentin precedes and controls the calcification of enamel and the DEJ. Ameloblasts move outward from the DEJ to form the covering layer of enamel while odontoblasts move inward to form dentin. The existence of the DEJ as a unique tissue has not been confirmed. Variations in architecture, width, composition, properties and characteristics of this region exist. Understanding these variations could increase our knowledge of the DEJ and could provide mechanisms for improving dental restorative materials and bonding materials having widely dissimilar properties.

6.2 Introduction

Enamel is the hardest substance in the human body. It forms a thin shell 1 to 3 mm in thickness covering the coronal portion of the tooth. It is composed of a defective carbonate rich apatite that is arrayed in rods or prisms 4-5 μm in diameter. Characteristic hardness and modulus values for bulk enamel based on nanoindentation testing were found to be 3.5 GPa and 65 GPa, respectively.[1] These properties provide enamel with the ability to protect the tooth from puncture, abrasion and wear during a lifetime of mastication and parafunctional activity. Enamel was found to contain a lower protein content, and a higher mineral content, than either dentin or the DEJ.[1] These characteristics may be responsible for the brittleness, limited fracture resistance and

lower skin friction exhibited by this material. Enamel is formed by ameloblasts during tooth formation, and upon maturity is a non-vital tissue.

Dentin underlies enamel and serves to distribute the masticatory stresses imparted to the thin covering shell of enamel to the underlying and supporting alveolar bone. It is a softer biomaterial than enamel, contains greater amounts of proteins and is less mineralized. Compositionally, dentin is similar to bone and is the most abundant mineralized tissue that is found in the human tooth. It is composed of two types of structures, peritubular dentin and intertubular dentin. These calcified dental tissues make up the characteristic microstructure of dentin. This microstructure has been conceptionalized as consisting of a hydrated intertubular matrix containing type I collagen (Figure 5.4) reinforced with a nano-crystalline, carbonated apatite mineral. Traversing this matrix is peritubular dentin. Peritubular dentin consists of tubules approximately 1 μm in diameter that are surrounded by a 0.5-1 μm thick cylindrical wall containing randomly oriented apatite crystallites.[2] The fluid filled dentinal tubules are surrounded by peritubular dentin which courses radially outward from the pulp chamber to the DEJ.

The mineralized collagen fibrils of the intertubular matrix form a felt-like structure, lying preferentially in the plane perpendicular to the long axis of the dentinal tubules.[3] The mineral occupies two sites within the collagen scaffold: intrafibrillar (within the periodically spaced gap zone in the collagen fibril), and extrafibrillar (located interstitially between collagen fibrils). The intrafibrillar/extrafibrillar mineral distribution is not known. However, it is believed that 70 to 75% of the mineral component is extrafibrillar.[4,5] The shape of the mineral crystallites varies from needle-like crystallites

near the pulp chamber to plate-like crystallites near the DEJ. Crystallite thickness remains constant and invariant of location.[6]

Contained within each dentinal tubule is an odontoblastic cell process. An odontoblast is a living structure that forms dentin. The dentinal tubules represent the formative tracks taken by the odontoblasts during their retreat toward the pulp chamber. Upon tooth maturation the odontoblasts reside lining the pulp chamber. These cells are vital and continue to move inward and make dentin in response to trauma or stimulus. The cylinders of peritubular dentin are embedded within the intertubular dentin. Significant variations exist in the morphology, architecture and the density of peritubular dentin dependent upon location.[7] The mechanical properties of dentin have been defined. Hardness and modulus levels characteristic of bulk, wet intertubular dentin were found to be 0.7 GPa and 20 GPa, respectively. Dry modulus values were slightly higher for dentin at around 25 GPa. Our measurements were made on dry human third molars. They are in line with, but slightly lower than, values reported in the literature. These values and behaviors are also within the range of values reported in the literature for dentin.[31] Contraction of the collagen fibrils upon drying could cause consolidation and reinforcement of the intrafibrillar mineral. We propose that this could limit the amount of deformation that the dentin sees, producing a higher compression modulus value than that for hydrated dentin. This mechanism should also reduce the ultimate tensile strength of this material. Sandwiched between dentin and enamel is the dentin enamel junction (DEJ). The DEJ is a calcified dental tissue interface that serves multiple purposes. It acts to bind two dissimilar calcified dental tissues, enamel and dentin; to one another. It also serves to increase the resistance of a tooth to catastrophic fracture by blunting or turning

the crack tip and limiting its propagation into dentin. Little was known concerning the existence, architecture, width, composition, and properties of this interface. The purpose of this body of research was to improve our ability to answer questions concerning this biomaterial. In order to answer these questions, a number of instruments were employed to address specific questions and improve our knowledge of the DEJ as a whole.

6.3 Discussion

6.3.1 Architecture

Structurally, the DEJ has been described as a scalloped interfacial dental tissue (Figures 5.3a and 5.3b). The scallops are oriented with convexities directed towards dentin and concavities towards enamel. The undulating nature of this interface has usually been described as a series of 25 to 100 μm wide scallops that are further subdivided into a series of smaller 2-5 μm wide micro-scallops containing finer level structures.[9,10,11,12,13,14,15,16] Thus, the DEJ appears to form a three-level architecture: scallops of varying size that may vary with location, micro-scallops contained within each scallop and finer nano-level structures that are located within each micro-scallop. The complex and irregular geometry of this interface has been thought to enhance bonding between enamel and dentin and to increase the resistance of the tooth to catastrophic fracture. Little information on the size and variability of these structures presently exists.

Historically, considerable inter-species inter-tooth and intra-tooth scalloping variability was believed to exist.[14,16,17,18] Whittaker examined 162 deciduous and permanent teeth extracted from humans and monkeys and found considerable inter-

species variability existed.[16] In human teeth the scallop size was found to vary considerably and frequently appeared to be in the range of 25-100 μm.[16] Each scallop also appeared to have a substantial micro-structural range, with the proximal surfaces being more scalloped than either the buccal or lingual surfaces.[16] Increased scalloping in the vicinity of the cusps was reported by Scott and Symons,[14] while Schour suggested increased scalloping occurred in the gingival third of the tooth.[19] Gallagher *et al.*[20] and Le *et al.*[21] found no intra-tooth scalloping differences in human third molars. Le *et al.*[21] noted differences between scalloping in human incisors and molars. The scalloping diameter seen in molars averaged 42.3 ± 8.5 μm, while in incisors it was 29.4 ± 8.5 μm.

To attempt to answer questions regarding the structural variability of the DEJ, a variety of instrumentation assets were employed. Observations with laser induced fluorescence microscopy revealed the presence of 25 to 50 μm scallops with 3 to 5 μm sub-scallops located within the larger scallops (Figure 3.2).[20] Finer nano-level structures were also found to exist lining the surface of each sub-scallop based on SEM and autofluorescence microscopy, confirming the existence of the DEJ's three-level microstructure. Measurements were made on dry, sagittally sectioned human third molar DEJ under the central pit, the pulp horns and the mesial and distal contact points. Laser induced fluorescence microscopy was used to capture and measure back radiated light following sample illumination with a laser source. The laser illumination light passed into the tooth prior to being back radiated. Thus, the light represents an averaging of the character of this interface with respect to depth. No significant intra-tooth scallop size variability was observed for the human third molars tested. Scallop size variability reported in the literature may reflect sample orientation, sample preparation and sample

position when instrumented. We found that scallop size did not exhibit intra-tooth variability, in experiments that were conducted only on human third molars. In contrast, significant inter-tooth scalloping variability was observed between human incisors and molars. The average scallop size noted in the incisors was 29.4 ± 8.5 μm, compared with 42.3 ± 8.5 μm for molars (t-test, $P<0.001$).[18] The larger scallops observed in the molars are likely a geometric requirement to improve interfacial bonding and fracture toughness across this interface since the molars typically must resist significantly increased mastigatory loads, cyclic stresses and loading times as compared to the incisors. Additional studies should be performed to further explore these relationships as well as to define the variability of DEJ width with respect to tooth type.

This research also sought to confirm the existence of a three-level structural model for the DEJ. According to this model, three successively smaller geometric features define the border. Each smaller feature fits inside and lines the surface of the larger feature. The smallest features, the "finer nano-level structures" are much smaller than 1 μm. The three micro-structural feature levels act to increase the surface area of the interface and decrease the stress concentration levels along it. The extremely small size of the smallest micro-structural elements, the "finer nano-level structures", may be so small that they are below the critical flaw size likely to initiate, and allow a crack to propagate through the DEJ until catastrophic fracture occurs. Therefore, the three-level micro-structural model taken together with the mechanical property variations and the compositional distribution suggest that the undulating nature of this interface is responsible for distributing the occlusal stresses across the interface over a much larger area, decreasing the stresses and stress concentrations across the DEJ, and acting to

increase the adhesion properties and the fracture resistance of this interface. Future research should be conducted to test this model and the effect that it has on the adhesion and fracture resistance properties. Finite element modeling to test the three-level model could prove useful in defining the importance of the various structural elements to the performance of this tissue interface and to performance of the tooth as a whole. Advanced three-dimensional imaging assets such as a synchrotron beam line may be required to fully determine the size range and the spatial arrangement of the various structural elements.

6.3.2 DEJ Width

The width or thickness of the DEJ has been investigated by a number of researchers using a variety of instrumentation equipment.[1,20,22,23,24,25] Since the DEJ occupies such an extremely small space, it has proven to be impossible to extract to this point. The variety of testing modalities used to improve our knowledge of the width of this tissue interface measure different characteristics of the material and produce different DEJ width estimates. DEJ width is important because it can confirm the existence of this tissue, it can improve our understanding of its mechanism for binding enamel to dentin, and it can improve our understanding of the manner in which it protects the tooth from catastrophic fracture. Thus, understanding this tissue interface has implications for both improving bonding between materials having dissimilar properties and improving bonded dental restorative materials.

High-resolution imaging of the DEJ suggests close apposition between the apatite crystals of dentin and the larger apatite crystals of enamel.[26] A high resolution AFM image of the DEJ illustrating this approximation is shown in Figure 5.4. TEM studies

indicate that the apatite crystals of enamel and dentin may come into close contact with one another. Optical microscopy, micro-radiodensity profiles[26] and scanning electron microscopy[27,28] suggest that the margins of the DEJ are sharply demarcated and that the interfacial width is extremely narrow, perhaps on the order of 2 μm. Lin[22] and Lin and Douglas[23] characterized the architecture and mechanical properties of bovine DEJ with microindentation and found a functional width of between 50 to 100 μm. White *et al.*[24] reported a functionally graded microhardness width for the DEJ of approximately 100 μm. Berkovich and cube corner nanoindentation suggest functional width estimates of approximately 25 μm and 12 μm, respectively.[1,29] Considerable differences between the DEJ width estimates exist. We propose that the variation in DEJ width is a function of sampling volume, and that a nanoindenter will estimate a narrower functional DEJ width than a microindenter. Since we found that scalloping was intra-tooth independent for teeth of the same type, we also propose that DEJ width is independent of intra-tooth location. However, previous studies using SEM found that scalloping varied between incisors and molars, an indication that additional studies should be performed to determine the variability of DEJ width with respect to tooth type.

To investigate questions relating to sampling volume, the nanoindenter results were compared to reported microindenter results. Microindenter and nanoindenter data indicates that a smooth and relatively linear gradient in mechanical properties exists across the DEJ (Figure 5.7). This functional gradient in mechanical properties runs from those of bulk dentin at the dentin side of the DEJ, to those of bulk enamel on the enamel side of the DEJ.[1,22,23,24,25] This suggests that the stress distribution across this region also follows a similar smooth transition. Raman microspectroscopy that was used to map the

mineral and protein contents found a linear increase in mineral content, and a linear decrease in protein content across the DEJ (Figures 5.12a and 5.12b).[25] This suggests that the composition of the DEJ represents a melding of the bordering constituent tissues.

White *et al.*[24] used a microindenter and determined a functional DEJ width on the order of 100 μm. Lin[22] and Lin and Douglas[23] characterized the hardness of bovine DEJ using a microindenter and determined a graded functional width of between 50 to 100 μm. To determine the functional DEJ width based on nanohardness, an AFM-Tribioscope nanoindenter system was used.[1,25] Bulk properties of dentin and enamel were determined prior to instrumenting the DEJ. Lines of nanoindentation points oriented to intercept the DEJ at a perpendicular angle were placed across the DEJ (Figure 5.10a). The lines of indentation points sampled at 1-2 μm intervals across the DEJ of the human third molars. Hardness and modulus were determined at each indenter point according to methods derived by Doerner and Nix.[30] The mechanical properties were then graphed as shown in Figure 5.10b. Hardness and modulus rose linearly across the interface from dentin to enamel. DEJ width was estimated by local polynomial regression fits for each sample and location using the nanomechanical data, and gave a mean width estimate for the DEJ of 11.8 μm. Comparing the nanoindenter and microindenter results showed a smaller estimated functional DEJ width for the nanoindenter as compared to the microindenter. Since the testing modalities were the same, the important difference between these instruments was their sampling volume. The microindentation sampling volume is an order of magnitude greater than that for the nanoindenter. It is likely that the microindenter sampling volume includes a mixture containing both peritubular and intertubular dentin, while the nanoindenter sampling volume is likely usually limited to

including only either intertubular or peritubular dentin. As a result, the nanoindenter determined narrower functional DEJ width estimates than the microindenter, while the microindenter's results likely include sample mixing.

This dependence on sample mixing is further elucidated by nanoscratching results that yielded even smaller DEJ width estimates than the nanoindenter, on the order of 2 μm since little of the sample is deformed (Figure 5.9b).[7,31] For nanoscratching, the AFM-Triboscope system (Veeco Probes, Santa Barbara, CA) was modified to include an additional, lateral force, transducer. This transducer, a 2D-Tribo-Scanner (Hysitron Inc., Minneapolis, MN), was attached perpendicularly to the standard vertical transducer and recorded horizontal displacement and lateral force that was applied to move the indenter tip across the surface of specimen's surface, producing a plastic "scratch" in the sample surface. The applied normal load could be adjusted to alter the elastic and plastic components of friction while the loads and displacements are continuously recorded. Since the inter-sampling interval is much smaller with nanoscratching than with nanoindentation, a smaller DEJ width estimate was expected and was observed. This estimate is in line with recent AFM-based force modulation and dynamic viscoelastic property mapping that suggested a 2-3 μm functional DEJ width, a result that may be related to improved spatial resolution resulting from continuous sampling.[32]

To investigate the variability of DEJ width estimation based on optical properties, laser induced fluorescence spectroscopy was used.[20] A 351 nm laser excitation source was used to define emission spectra and emission ratios for enamel, dentin and DEJ. Spectral construction required the use of a series of 10 nm wide narrow-band interference filters covering the range from 400 nm to 850 nm. The fluorescence microscope captured the

signal return of the illuminated sample at each narrow pass filter. All images were taken at the same perspective and under the same conditions allowing superimposition of the images. Image intensity maps were constructed for each narrow pass filter. Spectral construction used the image intensity maps to construct the spectrum for each tissue. This allowed these materials to be characterized and enabled chemical composition and mineralization changes to be studied by comparing their spectra.

The emission spectra of enamel, dentin and the DEJ were found to be similar. Image processing operations were performed to accentuate tissue contrast and determine DEJ width (Figures 3.2 and 3.6). No significant difference in DEJ width as noted under the central pit as compared to the pulp horns or the proximal contacts was noted. The margins of the DEJ were clearly visible in all but one of the samples. In the sample where the DEJ margins were not easily identified, standard image processing operations were performed to increase tissue contrast. When the margins were clearly evident, an estimate of the width of the DEJ was made (Figure 3.6). It is interesting to note that spectroscopic and mechanical data imply that the DEJ probably exists as functionally graded interfacial zone containing a relatively linear distribution of the constituents of the bordering tissues. In light of this, viewing the fluorescence images shows that the DEJ has clearly defined margins. Fluorescence spectroscopy merely represents collected emitted radiation following an interaction event with a laser. The laser is oriented to bath the sample in a relatively uniform intensity of incident laser radiation. The laser interacts with the sample and excites phosphors that are present. These back radiate light that is collected and analyzed by the spectroscope. We believe that the "clearly defined" margins of the DEJ represent a sample preparation effect wherein the DEJ, dentin and enamel differentially

absorbed phosphors from the polishing paste. These induce back radiation in relation to the concentration of the phosphors present. The DEJ width estimate, 10 μm, is consistent with the estimate using Raman microspectroscopy. This implies that the compositional variation across the DEJ allows differential absorption of phosphors. Further study of this topic to clarify these points is suggested.

6.3.3 Composition

The extraction of bulk DEJ samples has not yet been accomplished. This is due, in part, to the small size of this tissue interface (Figures 5.5a and 5.5b). The composition of these tissues is also unknown. High resolution AFM imaging indicates that the apatite crystals of dentin and enamel closely approximate one another, a condition implying the DEJ may not exist in a mature tooth.[7,28] Early microindentation testing across the DEJ suggested that a smooth increase in mechanical properties from those of bulk dentin to those of bulk enamel existed.[22,23] Since the mechanical properties of calcified tissues have been shown to be related to their degree of mineralization, we propose that the composition of the DEJ merely represents a mixture of the constituents located on either side of this interface. Further, that the gradation in the observed mechanical properties reflects the precise control of protein expression and biomineralization that occurs during tooth formation.[24,29] We propose that a linear increase in mineral content, and a corresponding linear decrease in protein content occurs as we cross the DEJ from dentin to enamel (Figures 5.12a and 5.12b). We also propose that the observed hardness variation across this interface is an extension of the underlying composition of the interface. Future experiments using discrete protein analytical techniques could provide insight into the types of tissues that are present and help to clarify these results.

Laser induced fluorescence microscopy using a 351 nm excitation source was used to image and characterize the mineral and protein contents of dental tissues in the DEJ region.[20] The first emissive peak was found at 450 nm and was similar in each tissue (Figure 3.4). This is an indication that each tissue contains similar apatite phases and has a similar composition. Differences in the emission spectra were found to be related to the location and character of the second peak. These differences may be explained by differences in the composition of these tissues. Enamel exhibited stronger emission at longer wavelengths that may be attributed to the emission characteristics of the mineral fraction.[20] This produces a broadening of the second spectral band and a second peak shifted to 530 nm. Dentin is more emissive than enamel at lower wavelengths with a "blue shifted" narrow second peak located at 490 nm. The DEJ contains a broad second emission band that extends toward longer wavelengths, similar to enamel. This suggests that the DEJ contains a significant mineral fraction. In DEJ, the second peak is positioned at 490 nm, the same second peak as dentin. This suggests that the DEJ also contains a significant organic fraction, similar to dentin. The laser induced fluorescence microscopy results imply that dentin, DEJ and enamel are composed of similar biomaterials, and that the DEJ may merely represent a mixture of these constituents.

An AFM nano-indenter that was coupled and optically registered to a Raman microspectroscope was used to define the composition and mechanical properties of dry human third molar DEJ.[25] Nano-mechanical testing was performed and determined the elastic modulus and hardness of enamel, dentin and DEJ along lines of indentation points at 2 μm intervals that crossed the DEJ perpendicularly (Figure 5.7). The initial and final two indentation points were placed using maximal loads to act as microscopically visible

sample orientation markers. Lines of Raman spectroscopy points at 1 μm intervals were placed across the DEJ parallel to the nanoindenter points, but with approximately 5 μm of lateral offset. Prior to instrumenting the DEJ, baseline nanoindentation and Raman microspectroscopy testing was performed to characterize bulk enamel and bulk dentin.

Plots of the peak Raman intensity variations across the DEJ for the PO_4^{3-} band and C-H stretching modes are shown in Figures 5.12a and 5.12b, respectively. The peak intensity of the PO_4^{3-} band is an indication of the amount of mineral present in the sample. C-H stretching mode peak intensity is an indication of the organic content present. The C-H stretching mode was chosen to be the indicator for organic content because luminescence at the 2900 cm^{-1} band was much smaller than at other organic band locations such as 1660 cm^{-1}, 1442 cm^{-1} and 1200 cm^{-1}. Mineral content was found to increase monotonically from dentin to enamel (Figure 5.12a), while the organic component decreased monotonically (Figure 5.12b). Plots of the variation in hardness and modulus across this interface are shown in Figure 5.10b. Linear increases in both properties are seen as we cross the DEJ from bulk levels of dentin to those of enamel. This is in accordance with previous microhardness results, although over a narrower width. No characteristic peak intensity was observed for DEJ.

The results indicate a link between composition, in the form of mineral and protein contents, and function in the form of material properties. Previous research established a link between mineral content and mechanical properties.[33,34] The greater the mineral content, the greater the resultant hardness and modulus. The reverse correlation is true concerning protein content. Material composition and function followed linear relationships across this interface. This would indicate that a proportionate change in one

parameter would be expected to have a proportionate change in the other parameters. Future research directions include the use of spectroscopic or protein analysis having greater specificity, sensitivity and sampling volume. Such equipment could be used to produce improved spatial composition maps and assist us with answering questions concerning the uniqueness of the DEJ, its width and the distribution and histology of the tissues present.

6.3.4 Mechanical Properties

The mechanical properties of the DEJ have been explored on a number of instrumentation levels. Microhardness indentation profiles across the DEJ suggest that a broad gradation in mechanical properties exists across this region,[23] and have estimated the functional width of this interface at between 27 and 100 μm based on a relatively linear distribution of hardness values.[24] Discontinuities between the linearly modeled dentin and enamel microhardness values defined the borders of with the DEJ.

To better define the properties of the DEJ, an AFM-Triboscope nanoindenter system was used to define the width and mechanical properties of dry human third molar DEJ along lines of indentation points oriented to cross the DEJ at a perpendicular angle.[1,7,25] Each line of indentation points was centered over the perceived optical midpoint of the DEJ (Figure 5.11). In three of the samples, a single line of nano-indentation points, each having a length of at least 50 μm, was placed across the DEJ. Nano-indentations were made at 2 μm intervals to prevent interference between adjacent indentations. In the remaining two samples, two parallel lines of nano-indentation points, each with a length of at least 50 μm, were placed across the DEJ in opposite directions. Baseline levels of hardness and modulus for enamel and dentin were achieved within 10

μm of the optically perceived center of the DEJ. Typical curves for hardness and modulus are illustrated in Figure 5.10b. The mechanical properties were observed to follow monotonic relationships from those of bulk dentin to those of bulk enamel. The bulk properties of dentin averaged 20 GPa for modulus and 0.7 GPa for hardness. The mean bulk enamel modulus was 65 GPa while its hardness was 3.5 GPa. These measurements compare well with recent resonant ultrasound spectroscopy measurements.[35] Resonant ultrasound microscopy found dry dentin exhibited a slight hexagonal anisotropy, with its stiffest direction perpendicular to the dentinal tubules, in agreement with the planar arrangement of the mineralized collagen fibrils. The anisotropy vanished when the sample was hydrated, as explained by previous work on dry dentin.[36] In those experiments, dry dentin exhibited an isotropic modulus of 28.1 GPa, about 4 GPa greater than that for hydrated dentin.

No unique hardness or modulus values were detected for the DEJ. No sharp discontinuities were detected that would indicate the borders of the interface. The variations in the observed mechanical properties were found to be independent of testing directionality. They are also in line with previous microhardness studies that showed similar relationships, although over a much wider area. The smooth transition and relatively linear progression in mechanical properties suggest that the stress distributions across this interface would also be relatively smooth and uniform. An area of future research would involve the development of coupled resilient modulus, nanoindenter and spectroscopy maps to allow extrapolation of the mechanical properties over a broader range.

To attempt to see if any sharp discontinuities in the mechanical properties occurred while crossing the DEJ, an AFM-Triboscope system was modified by replacing its standard head with a 2D-Tribo-Scanner that incorporated an additional transducer to measure lateral force and horizontal displacement (Figure 5.9b). This nanoscratching machine samples friction coefficients 1000 times over the length of the scratch. Since the scratches were 10 μm long, the sampling interval was on the order of 0.01 μm, much smaller than the nanoindenter sampling interval of 2 μm. The nanoscratches were centered over the optical middle of the DEJ (Figure 5.9a). Baseline enamel and dentin friction levels were observed at each end of the scratch. No discontinuities denoting the margins of the DEJ or a sharp change in mechanical properties were noted.[37]

The distribution of the mechanical properties across the DEJ is important since it may provide insight into the underlying material composition. A sharp demarcation in material properties would infer a sudden change in material type had occurred. This would imply the existence of a unique material and confirm the existence of the DEJ as a distinct tissue. It could also provide improved insight into the fracture characteristics of this region. A well-graded transition in mechanical property measurements across the interface would imply a relatively uniform distribution of stress. The better the stress distribution, the lower the stress concentration and the greater the fracture toughness.

Future research involving mechanical testing equipment having reduced sampling volumes could help elucidate questions related to fracture and DEJ width. Resilient modulus testing with smaller tip sizes may allow cracks to be generated in dentin, affording insight into its fracture characteristics. The development of new techniques or equipment capable of propagating enamel cracks through the DEJ could provide a

method for directly measuring its fracture characteristics. It could also provide insight into interfacial toughening mechanisms for adhesive thin films.

6.4 Summary

The DEJ is a calcified interfacial dental tissue whose architecture, width, composition, mechanical properties and uniqueness have been poorly defined. The architecture of the DEJ was found to follow a three-level model consisting of 25 to 50 μm scallops, 2 to 5 μm micro-scallops and finer level structures. The extremely small size of the finer level structures is likely below the critical flaw size required to initiate and propagate a crack to failure. These flaws could well represent bridging elements. We propose that the arrangement of these structures is responsible for a reduction in stress intensity across the DEJ. The stress reduction across this interface likely resulted in an increased resistance to catastrophic tooth fracture. DEJ width was found to be sampling size and sampling modality dependent. DEJ width estimates suggest that the DEJ does not exist as a unique tissue since the apatite crystals of dentin and enamel likely lie in close approximation to one another. Additional research employing imaging instruments having greater spatial resolution could better describe the observed "finer structures". It may also provide insight into the mechanisms governing enamel cracks termination in the near the DEJ region. Although little intra-tooth variation in scalloping or DEJ width was noted in human third molars, future research may wish to consider differences between different tooth types. Documented inter-species and pathology variations could allow research to investigate disease processes that effect the teeth.

Raman microspectroscopic mapping of the DEJ region uncovered monotonic increases in mineral content and linear decreases in protein content from bulk dentin to

bulk enamel. This was in agreement with other recent work.[38] Characteristic mineral and protein compositions for bulk dentin and bulk enamel were determined. No single mineral or protein composition was found to be characteristic of the DEJ. This indicates that the variation in mineral and protein composition across this interface might simply result from mixtures of dentin and enamel, the constituents located on each side of the DEJ. This finding correlated well with the indexed nanoindenter results. Phosphate concentration, an indicator of mineral content, showed a linear increase across the DEJ from bulk dentin values to bulk enamel values. Indexed hardness and elastic modulus values showed similar increases. Additional research using different spectroscopic peaks characteristic of discrete and characteristic components of dentin and enamel could provide information to better define DEJ width as well as define the mechanism of joining these adjacent tissues. Testing to define the type and size of the mineral crystals could also provide insight into these questions as well.

Elastic modulus and hardness mapping across the DEJ failed to reveal the existence of a characteristic modulus or hardness value for this tissue. Instead, modulus and hardness were found to vary linearly across this region. No sharp variations or discontinuities were found delineating the edges of this interface. The mechanical property values increased monotonically from bulk dentin to bulk enamel. The width over which these parameters varied was used to estimate the functional width of the DEJ. The results obtained were in line with the composition based estimates, although of slightly smaller size. This likely resulted from the smaller specimen volume sampled by the nanoindenter. Characteristic hardness and modulus values were determined for bulk dentin and bulk enamel. They were in line with similar measurements reported in the

literature. However, the mechanical property measurements were obtained using dry samples in order to coordinate work from a variety of instrumentation modalities. It was initially believed that dentin exhibited isotropic material properties. This has been found to be the case for dry dentin. Hydrated dentin exhibits anisotropic behavior oriented along the collagenous framework that is oriented perpendicular to the long axis of the dental tubules. The hydrated and dry properties of dentin, DEJ and enamel are well defined and can be related to one another. The use of dry measurements should have little effect on DEJ width estimates. Future research should be conducted to study the effects of hydration.

The nanoindenter was also used to induce fractures in enamel. We were unable to induce fractures in dentin or the DEJ using the nanoindenter and a sharp cube corner diamond tip even with loads to the maximum operating levels of the equipment. Fractures placed into enamel produced fracture toughness estimates in line with levels published in the literature. Additional materials characterization research using stiffness mapping have provided insight into DEJ width and could provide improved correlations between the spectroscopic and nanomechanical data.[32] The fracture characteristics of dentin and the DEJ are also a future source of research. Recent work in the field of fracture indicates dentin exhibits anisotropic fracture properties.[39,40,41] K_{IC} for hydrated dentin was found to be 1.79 MPa $m^{1/2}$ perpendicular to the tubule axis and 2.72 MPa $m^{1/2}$ parallel to it. Toughening mechanisms include crack bridging and crack tip blunting. Additional work in the field of fracture is required to improve our understanding of the toughening mechanisms and fracture properties of the DEJ. The use of dentin from large mammals including toothed whales and large land animals may allow valid fracture measurements

to be made. Characterization of these materials will be required prior to performing mechanical testing.

This body of research implies that the DEJ likely does not exist as a unique tissue. No characteristic properties or composition for it were noted. Structurally, the interface follows a three-level model that acts to improve bonding between dentin and enamel while also decreasing the tooth's potential for catastrophic fracture. Functional DEJ width was found to depend upon sampling modality and sampling size. Evidence exists that enamel and dentin may approximate one another. Compositionally, this interface may represent a blending of the constituents of the adjacent tissues. Additional research to define the distribution of discrete characteristics of the adjacent tissues could improve our understanding of the mechanism for connecting these tissues, as well as, its performance.

6.4 References

1 Marshall GW, Balooch M, Gallagher RR, Gansky SA, Marshall SJ. Mechanical Properties of the dentinenamel junction: AFM studies of nanohardness, elastic modulus and fracture. *J Biomed Res* 2000;54.1:87-95.

2 Marshall GW. Dentin: Microstructure and characterization. *Quintessence Int* 1993;24:606-617.

3 Jones SJ, Boyde A. Ultrastructure of dentin and dentinogenesis. In: Dentin and dentinogenesis Vol II. Linnde A, Editor. Boca Raton: CRC Press; 1984.

4 Bonar LC, Lees S, Mook HA. Neutron diffraction studies of collagen in fully mineralized bone. *J Molec Biol* 1985;181:265-270.

5 Pidaparti RM, Chandran A, Takano Y, Turner CH. Bone mineral lies mainly outside collagen fibrils: prediction of a composite model for osteonal bone. *J Biomechan* 1996;29:909-916.

6 Kinney JH, Pople JA, Marshall GW, Marshall SJ. Collagen orientation and crystallite size in human dentin: a small angle x-ray scattering study. *Calcif Tiss Int* 2001b;69:31-37.

7 Marshall SJ, Balooch M, Habelitz, S, Balooch G, Gallagher R, Marshall GW. The dentin-enamel junction-a natural multilevel interface. *J Am Ceram Soc* 2003;23:2897-2904.

8 Kinney JH, Habelitz, S, Marshall SJ, Marshall GW. The importance of intrafibrillar mineralization of collagen on the mechanical properties of dentin. *J Dent Res* 2003;82(12):957-961.

9 Ten Cate AR Oral Histology: Development, Structure and Function, 4th ed. Mosby, St. Louis 1994.

10 Arsenault AL, Robinson BW. The dentino-enamel junction: A structural and microanalytical study of early mineralization. *Calcif Tissue Int* 1989;45:111-121.

11 Hayashi Y. High resolution electron microscopy in the dentino-enamel junction. *J Electron Microsc* 1992;41:387-391.

12 Lustman J. Dentinoenamel junction area in primary teeth affected by Morquio's syndrome. *J Dent Res* 1978;57:475-479.

13 Rywkind AW. So-called scalloped appearance of the dentino-enamel junction. *J Am Dent Assoc* 1931;18:1103-1110.

14 Scott JH, Symons NBBB. Introduction to Dental Anatomy, 6th ed. Livingstone, Edinburgh 1971.

15 Sela J, Sela M, Lustman J, Ulmansky M. Dentinoenamel junction area of a resorbing permanent incisor studied by means of scanning electron microscopy. *J Dent Res* 1975;54:110-113.

16 Whittaker DK The enamel-dentine junction of human and Macaca Irus teeth: A light and electron microscope study. *J Anat* 1978;125:323-335.

17 Jones SJ, Boyde A. In: Dentin and dentinogenesis Vol II. Linnde A, Editor. Boca Raton: CRC Press; 1984. p. 5-97.

18 Lingg B, Marshall GW, Watanabe LG, Habelitz, S, Ho SP, Marshall SJ. Incisor and molar DEJ scallop size as a function of intratooth location. *J Dent Res* 2003 82A. Abstract 1700.

19 Schour I. Noyes oral histology and embryology. London: Kimpton; 1960.

20 Gallagher RR, Demos SG, Balooch M, Marshall GW, Marshall SJ. Optical spectroscopy and imaging of the dentin-enamel junction in human third molars, *J Biomed Res* 2003;64A.2:372-377.

21 Le TQ, Habelitz S, Marshall GW, Pugach MK, Marshall SJ. Acid and deproteinization resistance of the DEJ. *J Dent Res* 2001;80,763.

22 Lin CP. Structure-function property relationships in the dentin-enamel complex and tooth restoration interface. PhD thesis, University of Minnesota 1993.

23 Lin CP, Douglas WH. Structure-property relations and crack resistance at the bovine dentin-enamel junction. *J Dent Res* 1994; 73:1072-1078.

24 White SN, Paine ML, Luo W, Sarikaya M, Fong H. The dentino-enamel junction is a broad transitional zone uniting dissimilar bioceramic composites. *J Am Ceram Soc* 2000;83:238-240.

25 Gallagher RR, Balooch M, Balooch G, Wilson RS, Marshall SJ, Marshall GW. A Coupled Nano-Mechanical and Micro Raman Spectroscopic Investigation of Human Third Molar DEJ. *Cal Tiss Int* In press.

26 Elliot JC, Anderson P, Gao XJ, Wong FSL, Davis GR, Dowker SEP. Application of scanning microradiography and X-ray microtomography to studies of teeth and bone. *J X-Ray Sci Technol* 1994;4:102-117.

27 Hayashi Y. High resolution electron microscopy in the dentino-enamel junction. *J Electron Microsc* 1992;41:387-391.

28 Elliot JC, Anderson P, Gao XJ, Wong FSL, Davis GR, Dowker SEP. Application of scanning microradiography and X-ray microtomography to studies of teeth and bone. *J X-Ray Sci Technol* 1994;4:102-117.

29 Fong H, Sarikaya M, White SN, Snead ML. Nano-mechanical properties profiles across dentin-enamel junction of human incisor teeth. *Mater Sci Eng* 2000;C7:119-128.

30 Doerner MF, Nix WD. A method for interpreting the data from depth-sensing indentation instruments. J Mater Res 2004;69A:286-293.

31 Habelitz S, Marshall SJ, Marshall GW, Balooch M. The functional width of the dentino-enamel junction determined by AFM-based nanoscratching. *J Struct Biol* 2001;135:294-301.

32 Balooch G, Marshall GW, Marshall SJ, Warren OL, Asif SAS, Balooch M. Evaluation of a new modulus mapping technique to investigate microstructural features of human teeth. *J Biomech* 2004;37:1223-1232.

33 Kinney JH, Marshall SJ, Marshall GW. The mechanical properties of human dentin: a critical review and re-evaluation of the dental literature. *Crit Rev Oral Biol Med* 2003;14(1):13-29.

34 Featherstone JD, ten Cate JM, Sharlati M, Arends J. Comparison of artificial caries-like lesions by quantitative microradiography and microhardness profiles. *Caries Res* 1983;17:385-391.

35 Kinney JH, Gladden JR, Marshall GW, Marshall SJ, So JH, Maynard JD. Resonant ultrasound spectroscopy measurements of the elastic constants of human dentin. *J Biomech* 2004;37:437-441.

36 Kinney JH, Balooch M, Marshall GW, Marshall SJ. A micromechanics model of the elastic properties of human dentine. *Arch Oral Biol* 1999;44:813-822.